UNIVERSITY OF SOUTHAMPTON

FACULTY OF ENGINEERING AND PHYSICAL SCIENCES

Overcoming the Electricity Grid Capacity and Battery Thermal Limitations of Electric Vehicle Fast Charging using Stationary Energy Storage and Cell Thermal Modelling

by

Thomas Bryden

Thesis for the degree of Doctor of Philosophy

February 2019

UNIVERSITY OF SOUTHAMPTON

ABSTRACT

FACULTY OF ENGINEERING AND PHYSICAL SCIENCES

Thesis for the degree of Doctor of Philosophy

Overcoming the Electricity Grid Capacity and Battery Thermal Limitations of Electric Vehicle Fast Charging using Stationary Energy Storage and Cell Thermal Modelling

Thomas Samuel Bryden

Electric vehicles have the potential to both provide health benefits to the population by reducing air pollution and combat climate change by reducing greenhouse gas emissions. Potential electric vehicle owners currently worry that on long distance journeys they will run out of energy in the vehicle battery and have to wait while their battery is recharged, potentially adding hours to their journey. Fast charging, defined here as a charging power greater than 120 kW, is therefore one of the challenges to overcome before the widespread consumer adoption of electric vehicles. Future advances in battery chemistry may enable the faster charging of electric vehicles, however if these advances are achieved, two challenges will remain and these are the focus of this thesis:

1. Faster charging requires higher power capacity electricity grid connections, which may not be available at the required fast charging station location
2. Faster charging requires the batteries to operate at higher charge rates, which generates more heat meaning the battery may require active thermal management during charging

The solution to the first challenge investigated in this thesis is to use stationary energy storage at fast electric vehicle charging stations. The stationary energy storage buffers the energy between the electricity grid and the electric vehicles using the fast charging station, thereby reducing the maximum power demand required from the grid and meaning installation is possible at more locations on the grid. In this thesis, a novel method is used to predict demand at fast charging stations before a second novel method is proposed to size the required stationary energy storage.

The solution to the second challenge is to use thermal modelling to design thermal management systems to deal with the excess heat generated during fast charging. In this thesis a thermal model that can be used for high rate applications, defined here as a rate that will recharge the battery in less than one hour, is demonstrated and a novel experimental method to determine the parameters required for the model is proposed.

Table of Contents

Table of Tables

Table of Tables

Table of Figures

Table of Figures

Table of Figures

Academic Thesis: Declaration Of Authorship

I, Thomas Bryden declare that this thesis and the work presented in it are my own and has been generated by me as the result of my own original research.

Overcoming the Electricity Grid Capacity and Battery Thermal Limitations of Electric Vehicle Fast Charging using Stationary Energy Storage and Cell Thermal Modelling

I confirm that:

1. This work was done wholly or mainly while in candidature for a research degree at this University;
2. Where any part of this thesis has previously been submitted for a degree or any other qualification at this University or any other institution, this has been clearly stated;
3. Where I have consulted the published work of others, this is always clearly attributed;
4. Where I have quoted from the work of others, the source is always given. With the exception of such quotations, this thesis is entirely my own work;
5. I have acknowledged all main sources of help;
6. Where the thesis is based on work done by myself jointly with others, I have made clear exactly what was done by others and what I have contributed myself;
7. Parts of this work have been published as:
    - Thomas S. Bryden, George Hilton, Andrew Cruden, Tim Holton, Electric vehicle fast charging station usage and power requirements, Energy, Volume 152, 2018, Pages 322-332, 10.1016/j.energy.2018.03.149
    - Thomas S. Bryden, Borislav Dimitrov, George Hilton, Carlos Ponce de León, Peter Bugryniec, Solomon Brown, Denis Cumming, Andrew Cruden, Methodology to determine the heat capacity of lithium-ion cells, Journal of Power Sources, Volume 395, 2018, Pages 369-378, 10.1016/j.jpowsour.2018.05.084
    - Analysis of the current and voltage of the Tesla battery during fast charging, presented at the “HEVC 2016: The 6th Hybrid and Electric Vehicle Conference” along with a conference paper entitled “Off-vehicle energy store selection for high rate EV charging station” doi: 10.1049/cp.2016.0986

Signed: .....

Date: .....

Acknowledgements

I would like to thank my supervisor Andy Cruden for his continuous support and guidance as well as for the opportunities he has given me throughout the PhD. I would also like to thank my second supervisor Carlos Ponce de León for his support. I would also like to thank Borislav Dimitrov for his help in the laboratory and Peter Bugryniec in Sheffield for his help using the calorimeter.

I would also like to thank my family who supported me through the PhD, my mother Mary Bryden, father Harry Bryden and brother Andrew Bryden. A further mention goes to the family members with PhD's who gave me advice relating to the workings of PhDs, namely Harry Bryden, Dan Cornford and Chris Cornford. Also, thank you to Dan Bryden for his enthusiasm and for taking pictures of fast charging stations in the USA.

A further mention goes to the guys in the office, George and Alex, for the discussions. I also appreciate my friend Sam reminding me that there is stuff to do that isn't PhD work.

I would also like to thank Tim and David from Jaguar Land Rover and Peter from Yuasa for the help and advice they gave throughout the PhD.

Finally, I would like to thank the Engineering and Physical Sciences Research Centre for providing funding for the research through two grants "EPSRC Centre for Doctoral Training in Energy Storage and its Applications" EP/L016818/1 and "ELEVATE (ELEctrochemical Vehicle Advanced TEchnology)" EP/M009394/1.

Definitions and Abbreviations

AC	Alternating Current
Ah	Ampere – hour
ARC	Accelerating Rate Calorimeter
CAD	Computer Aided Design
CC – CV	Constant Current – Constant Voltage
CCS	Combined Charging System
CHAdeMO	CHArge de MOve
CO_2	Carbon Dioxide
DC	Direct Current
DCUSA	Distribution Connection and Use of System Agreement
ELEVATE	ELEctrochemical Vehicle Advanced Technology
EPSRC	Engineering and Physical Sciences Research Council
EV	Electric Vehicle
GWh	GigaWatt – hour
GPS	Global Positioning System
HEV	Hybrid Electric Vehicle
IEC	International Electrotechnical Commission
kWh	kiloWatt – hour
LCO	Lithium-ion Cobalt Oxide
LFP	Lithium-ion Iron Phosphate
LMO	Lithium-ion Manganese Oxide
LTO	Lithium-ion Titanate Oxide
MWh	MegaWatt – hour

NCA	Lithium-ion Nickel Cobalt Aluminium
NMC	Lithium-ion Nickel Manganese Cobalt
NREL	National Renewable Energy Laboratory
OCV	Open Circuit Voltage
PHEV	Plug in Hybrid Electric Vehicle
SoC	State of Charge
USABC	United States Advanced Battery Consortium
VA	Volt – Ampere
VAr	Volt – Ampere reactive
Wh	Watt – hour
WLTP	Worldwide Harmonised Light Vehicle Test Procedure

Chapter 1 Introduction

The primary advantage of EVs over conventional gasoline vehicles is that fossil fuels are not combusted in EVs. By not combusting fossil fuels at the point of use, EVs have the potential to help in the fight against climate change and to help reduce air pollution.

The Intergovernmental Panel on Climate Change states that CO_2 is the most important pollutant originating from human activity that causes climate change [1]. Worldwide in 2013 the International Energy Agency estimated that the transport sector accounted for 23% of CO_2 emissions, with road transport accounting for three quarters of these emissions [2]. EVs do not emit CO_2 at point of use and so could potentially reduce the road transport emissions value substantially, currently however the majority of electricity is generated by burning fossil fuels, which produces CO_2. Using EVs to reduce overall CO_2 emissions therefore also requires generating more of the world's electricity from non-fossil fuel based sources, such as renewable electricity generation or using carbon capture and storage at large fossil fuel power stations.

Air pollution from cars is a problem throughout the world, especially in large cities. The World Health Organisation estimates that outdoor air pollution causes 3.7 million deaths worldwide annually, with pollution from transport a major source of the outdoor air pollution [3]. It is hard to directly calculate the health impacts of gasoline vehicles but a Kings College London study estimated that up to 9,416 persons die prematurely in London due to air pollution annually [4]. EVs do not emit air pollution at point of use and so could potentially produce large health benefits.

As well as these advantages, EVs have other advantages over gasoline vehicles, including less noise pollution and the potential for a quieter and smoother ride [5]. Despite these advantages EVs currently make up a small proportion of the number of vehicles on the road, around 0.9% in the USA and 1.4% in the UK in 2016 [6]. The Joint Center for Energy Storage Research in the USA suggests that there are four primary and one secondary challenge to overcome before EVs are widely adopted [7].

- Primary Challenges:
    - Driving range: EVs need to be able to travel further between charges
    - Fast charging: EVs need to be able to recharge faster
    - Inexpensive: EVs need to be comparable cost to gasoline vehicles
    - Safe: Potential EV owners need to be convinced of the safety of the EV batteries
- Secondary Challenges:
    - Charging infrastructure: Local and long distance

The primary challenges listed above are related to the batteries used to store the energy to power the EV. Low driving range and lack of fast charging contribute to what is known as range anxiety, whereby drivers are fearful of fully depleting an EV battery in the middle of a trip and having to wait for hours while their EV recharges [8]. The secondary challenge of charging infrastructure is split into local and long distance. Local charging infrastructure refers to charging points at home or at work. One challenge for local charging infrastructure is that currently some local electricity networks could not cope if everyone on a street had an EV and charged it at the same time [9]. Long distance charging infrastructure refers to fast charging, similar to stopping at a gas station, during journeys where the EV range is exceeded and the EV battery must be recharged quickly.

Automakers are working to overcome these issues and most automakers have plans to sell significant numbers of EVs in the future. The International Energy Agency predicts anywhere from 20 million to 140 million EVs on the road globally in 2030, compared to 2 million EVs in 2016 [6].

This thesis focuses on the challenge of fast charging EVs and the associated secondary challenge of long distance charging infrastructure. The fastest EV charger currently available can provide a power of 120 kW [10], for this thesis fast charging is therefore defined as a charging power greater than 120 kW. A charging power of 120 kW means that fast charging an EV currently takes much longer than refuelling a gasoline vehicle with gasoline, which refuel at a rate of 20 MW [11]. However EVs are more efficient than gasoline vehicles at converting energy to movement, roughly 4 times more efficient, however this still means EVs are 40 times ((20,000 kW / 4) / 120 kW) slower at charging. EVs can however be charged at home and it has been suggested that a charging rate of about 400 kW will be sufficient to encourage the uptake of EVs [12]. Achieving this charging power would enable more travel in EVs and increase the consumer uptake of EVs.

At present, the charging limitation, and therefore the reason EVs charge at 120 kW instead of 400 kW, is the limit of maximum current that can be delivered to the cells in the EV battery pack [13]. To increase the current that EV cells can accept requires research into the materials and chemistry used to make up the cells. Improving the chemistry of cells to enable faster charging is outside the scope of this thesis, however there are many ongoing projects researching this [14-16]. This thesis focuses on other future limits to fast charging of EVs, which will become limiting factors once cell charging current limits are increased. These other future limits to fast charging include [17]:

- Obtaining the required power from the electricity grid
- Dealing with the additional heat generated in the EV battery
- Designing the power electronics in the EV and at the charging station
- Balancing the cells in the EV battery pack

These limits are discussed in more detail in Chapter 2 however the two most important factors, which are the focus of this thesis are:

- Obtaining the required high power connection from the electricity grid, with high power defined as the power required for fast charging of over 120 kW
- Dealing with the additional heat generated in the EV battery during fast charging

These two limits are discussed more in Sections 1.1 and 1.2 below and the research question the thesis is addressing is:

"How can the electricity grid capacity and cell thermal limitations of electric vehicle fast charging be overcome?"

1.1 High Power Grid Connection

The high power, defined here as a power over 120 kW, grid connection is related to the secondary challenge mentioned above of long distance charging infrastructure. Higher power charging requires a high power grid connection and this can cause a problem as there are limited locations on the electricity grid that can accommodate high power connections [18]. If a high power connection is required and the current grid infrastructure cannot support the power required, the grid infrastructure must be upgraded, adding significant cost [19] and hence maximising the utilisation of this connection is important for value for money. High power grid connections also include a standing charge based on the maximum power of the connection [20]. In the future, as charging powers increase, the power required from the grid, and therefore the costs, will increase.

The proposed solution investigated in this thesis is to use a stationary energy store to buffer the power from the grid at a fast charging station, the configuration of which is shown in Figure 1.1. Using stationary energy storage means that the energy required to charge the EVs can be taken from the grid over a longer time period, so the maximum power drawn from the grid is reduced. If the maximum power drawn from the grid is reduced, there will be more locations that can accommodate the connection meaning potentially expensive grid infrastructure upgrade costs can be avoided. The standing charge based on the maximum power of the grid connection will also be reduced.

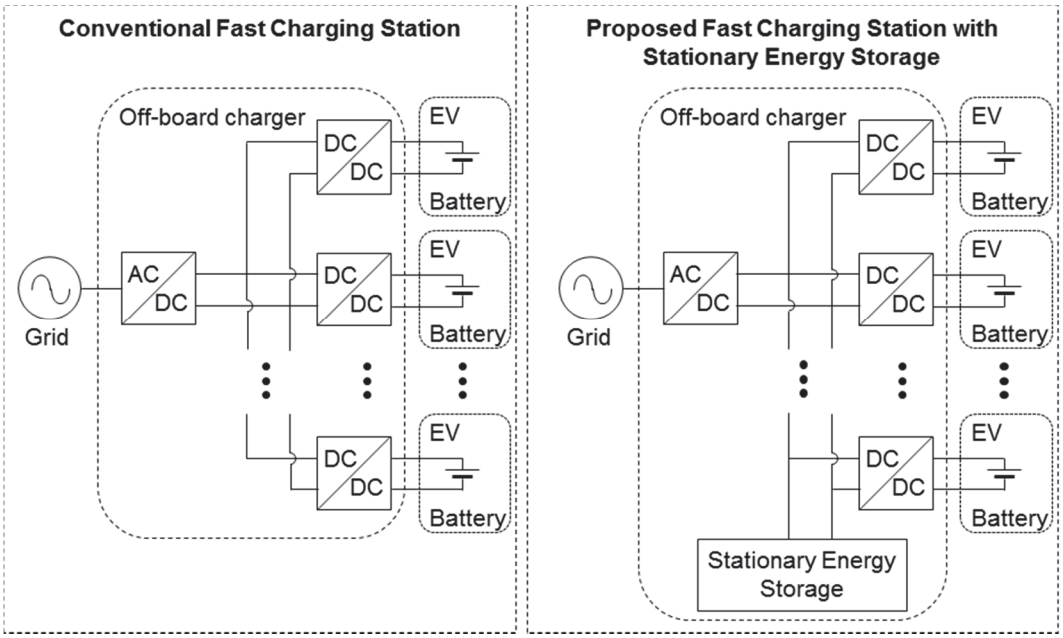

Figure 1.1 Comparison of a conventional fast charging station and the proposed fast charging station with stationary energy storage

The focus of this thesis is on the stationary energy store itself and the aim is to determine the optimum type and capacity of stationary energy store to use at a fast charging station.

The type of stationary energy store is discussed throughout the PhD thesis however from the literature review in Chapter 2 it is determined that the most likely type of energy storage is batteries, specifically lithium-ion batteries. Lithium-ion batteries are chosen as they have many of the likely required characteristics and there is therefore a focus on lithium-ion batteries throughout the thesis. They are suitable for storage capacities from a few kWh to 100's MWh, can operate at a wide variety of rates, fully discharging in seconds to days, can last a long time, up to many years [21], and have rapidly falling costs, with a 14% annual reduction each year between 2007 and 2014 [22].

The capacity of the stationary energy store depends on when and how fast the energy storage will need to charge and discharge and this is directly dictated by the vehicle usage pattern of the fast charging station. When many drivers are using the fast charging station the energy storage will discharge and when few drivers are using the fast charging station the energy storage will charge from the grid. Chapter 3 develops and proposes a novel method to forecast future fast charging station usage, using MATLAB and a forecasting modelling technique with the input of real world GPS driving data collected by researchers in the USA. In this model it is assumed that all gasoline vehicles are replaced with EVs, which can charge overnight. It is then assumed that all the same gasoline journeys are conducted in the EVs and from these journeys the time of day that fast charging stations will be used in the future is estimated.

In Chapter 4 a novel method is proposed for employing this fast charging station usage pattern to determine the required capacity of the stationary energy store at a fast charging station based on vehicle waiting time analysis. Chapter 4 develops a MATLAB model for designing the stationary energy store at the fast charging station with the inputs coming from the model developed in Chapter 3.

The model uses random number generation to assign an arrival time to each EV arriving at the fast charging station, with the randomly generated arrival time being weighted according to the fast charging station usage pattern determined in Chapter 3. The model then steps through each second of the day and determines whether an EV arrives at the fast charging station to charge based on the assigned arrival times. The grid connection power is limited and so if there are lots of EVs charging, some of the EVs may have to wait because there is not sufficient power. The stationary energy store can be used to charge the EVs if the grid connection power is insufficient, however the EVs may still have to wait if the stationary energy store becomes empty. The output of the analysis is therefore the capacity of stationary energy versus the average waiting time of EVs using the fast charging station. An appropriate size stationary energy store can then be chosen based on the chosen acceptable average waiting time.

The methods proposed in this thesis could be used at any location where a fast EV charging station is required. Location specific inputs could be used in the model, which would output the capacity of energy store required for the given location. The model does not include an economic assessment due to the variability of costs of grid connection [23]. An economic assessment could be undertaken using the results of the analysis, comparing the cost of the fast charging station with and without the stationary energy storage.

1.2 Additional Heat Generation within the Electric Vehicle Battery

The heat generated in a battery during charging is dependent on multiple processes, which are discussed in detail in Chapter 2. Faster charging means higher currents, which means the resistive heating in the battery becomes the increasingly dominant heat generation process as the resistive heating is proportional to the battery current squared [24]. This means that if charging rates double the resistive heat generated will quadruple.

This heat must be removed from the battery pack to stop the cells becoming too hot, which can result in reducing the lifetime of the cells or, if the cell exceeds its thermal runaway temperature, catastrophic failure in the form of fire or explosion [25]. The heat is removed from the battery pack by a cooling system, for example passing a coolant in a tube through the battery pack.

Designing cooling systems to deal with this additional heat generation during fast charging is a challenge for battery engineers and to design an effective cooling system a thermal model is required [26]. As the focus of these thermal models will be on the cooling system design the thermal model of the cells needs to be simple to use as well as being accurate.

To address this issue in this thesis a thermal model that is easy to parameterise but accurate at high rates, defined here as rates that will charge a cell in under 1 hour, is developed. The thermal model is of use both to the battery on-board the EV as well as the stationary energy storage, which may also have to operate at high rates although does not suffer from the space and volume constraints that the vehicle energy store must meet.

In Chapter 5 the author's thermal model is demonstrated, which can predict cell temperature at high rates. Novelty is achieved by proposing a new method to obtain the parameters for the thermal model. The thermal modelling in Chapter 5 is conducted using MATLAB and the results are verified using laboratory experiments on commercial cells. The method to parameterise the cells involves charging and discharging the cells using a battery analyser and monitoring the surface temperature response. The method is then repeated and additional cooling applied using a fan. From analysing the results the thermal parameters, including heat capacity and internal thermal resistance, of the cells can be obtained. The method has the advantage that it only uses equipment commonly found in battery laboratories and the cell does not have to be taken apart.

The thermal model and method to obtain the thermal parameters of cells proposed in this thesis can be used to model the temperature of cells during high rate applications similar to those expected by an EV while fast charging. This easy to parameterise model will enable further work, which could use the method and model proposed, to design innovative EV cooling systems to enable the faster charging of EVs.

1.3 Novel Contributions and Associated Publications

The specific major novel contributions claimed by this thesis are detailed in Table 1.1, with reference to supporting chapters of the thesis and evidenced by the corresponding publication.

Table 1.1 Major novel contributions from the PhD, published or submitted to journals

	Novel Contribution	Thesis location	Associated Publication
1	Method to determine the specific heat capacity of lithium-ion cells using common inexpensive laboratory equipment	Section 5.4, Method to Determine the Thermal Parameters, page 118	Thomas S. Bryden, Borislav Dimitrov, George Hilton, Carlos Ponce de León, Peter Bugryniec, Solomon Brown, Denis Cumming, Andrew Cruden, Methodology to determine the heat capacity of lithium-ion cells, Journal of Power Sources, Volume 395, August 2018, Pages 369-378, 10.1016/j.jpowsour.2018.05.084 [27]
2	Method to predict time of day use of fast EV charging stations	Section 3.3, Method for Predicting Usage, page 58	Thomas S. Bryden, George Hilton, Andrew Cruden, Tim Holton, Electric vehicle fast charging station usage and power requirements, Energy, Volume 152, June 2018, Pages 322-332, 10.1016/j.energy.2018.03.149 [28]
3	Method to determine the size of stationary energy storage at a fast EV charging station	Section 4.1, Description of Model, page 76	Submitted and under review, Thomas S. Bryden, George Hilton, Borislav Dimitrov, Carlos Ponce de León, Andrew Cruden, Rating a Stationary Energy Storage System within a Fast Electric Vehicle Charging Station Considering User Waiting Times

Additional novel contributions and associated conference and co-author papers are included in Appendix A.

Chapter 2 Literature Review

This chapter presents a detailed literature review of the topics covered in this thesis. Lithium-ion batteries form a large part of the thesis as they will make up the EV battery and may make up the stationary energy storage, therefore the chapter starts with a brief introduction to lithium-ion batteries in Section 2.1.

In Section 2.2 a background to EVs is given, including current and future EV capabilities and costs and details on how fast charging is currently achieved. From the literature review in this section the limitations of fast charging are detailed and it is shown how there are three critical limitations to increasing charging rates in the future: cell current limits, obtaining the high power required from the grid and dealing with the additional heat generation associated with fast charging. It is described how increasing the cell current limits is currently the focus of many research projects and requires changes in the cell chemistry. Such fundamental chemistry work was not the subject of this thesis, therefore this limitation is not investigated further in this thesis.

The subsequent two sections therefore investigate the other two limitations. In Section 2.3 background information regarding obtaining the high power grid connection required for fast charging is given. The solution investigated in this thesis is to use stationary energy storage at the fast charging station and so topics related to this are covered, including the electricity grid connection costs, potential types of stationary energy storage, and a review of research already conducted into stationary energy storage at fast charging stations. In Section 2.4 background information regarding dealing with the additional heat generation during fast charging is given. The solution investigated in this thesis is to use thermal modelling so topics related to this are covered, including the theory and a review of research already conducted into battery thermal models as well as details of EV cooling systems.

The chapter ends with a summary of the literature review and the research objectives of the following chapters.

2.1 Introduction to Lithium-ion Batteries

In this section, the important aspects of lithium-ion batteries that are required for understanding of the thesis are detailed.

A battery is combination of one or more cells, with a cell being a device that converts stored chemical energy into electric energy by means of an electrochemical reaction. Lithium-ion cells

are rechargeable and so the process is reversed to recharge the cell [29]. A cell consists of three major components: the negative electrode, the positive electrode and the electrolyte. These components can be made of different combinations of materials to make different types of cells. Lithium-ion cells also include a separator to stop the electrodes touching each other and negative and positive current collectors, which are required because the electrodes are normally not very electrically conductive. An overview of a lithium-ion cell can be seen in Figure 2.1.

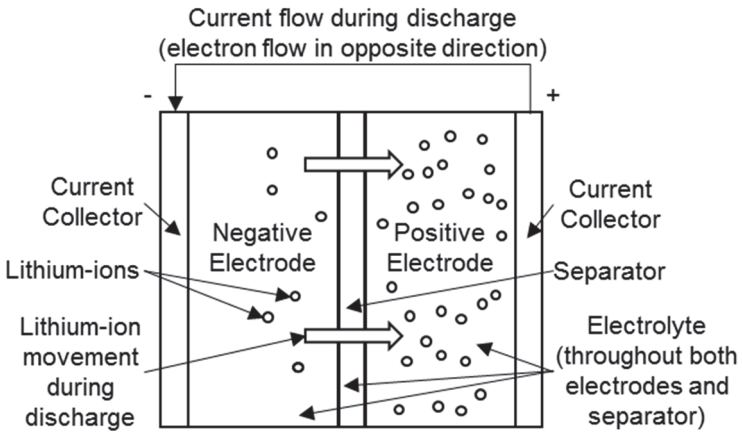

Figure 2.1 Overview of inside of a lithium-ion cell

Figure created by adapting data from [29, 30]

Multiple cells are combined to create a battery module and multiple modules are then combined to create a battery pack, as seen in Figure 2.2. Battery packs can contain many thousands of cells, for example Tesla EVs contain over 7,000 cells [31]. A battery management system is used in battery packs to ensure that all the cells are operating within acceptable voltage, current and temperature ranges. Differences in voltage, current and temperature can arise as a result of differences in the manufacture of the cells as well as the location of the cell within the pack.

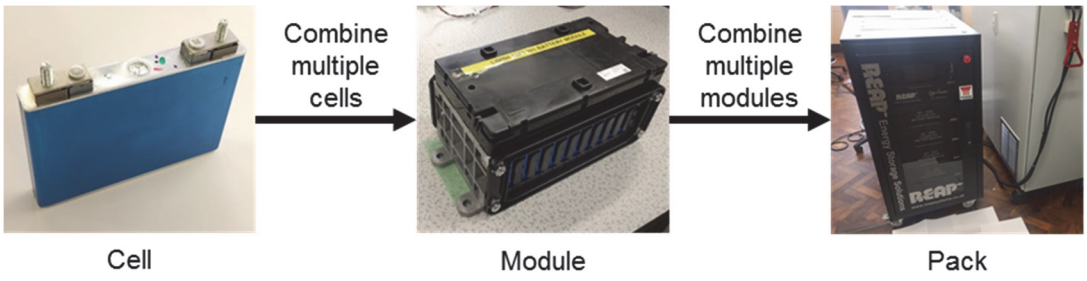

Figure 2.2 Constituents of a battery pack

There are three geometries of cells that are commonly used in battery packs: cylindrical cells, prismatic cells and pouch cells, seen in Figure 2.3. The geometries have different advantages and disadvantages, such as ease of manufacturer and packing density [32]. When designing the cell, as well as the geometry of cell, it must also be decided if the cell is to be used for applications where

energy or power is more important. For the same size cell, a cell designed for high energy applications will have a higher energy density but lower power density than a cell designed for high power applications, for which the opposite is true. In terms of the components seen in Figure 2.1, a cell designed for high energy will have thicker electrodes than a cell designed for higher power, while a cell designed for higher power will have thinner electrodes.

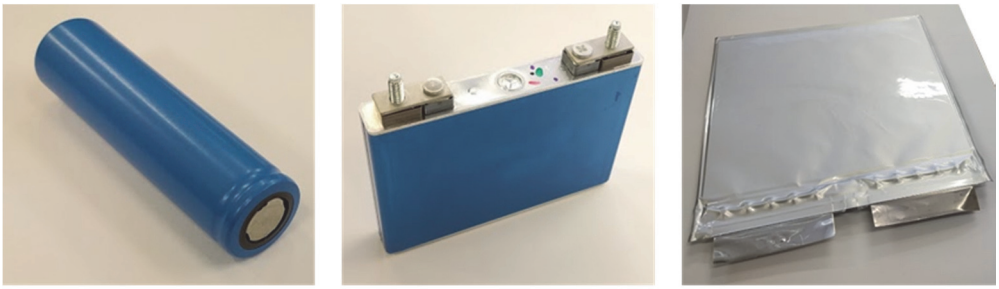

Figure 2.3 Three geometries of lithium-ion cells that can be used in a battery pack

As well as the geometry, lithium-ion cells also vary depending on the exact chemistry used for each of the components. The negative electrode is generally graphite, however some manufacturers add other chemicals, such as silicon [33], to the negative electrode to increase the energy density. The biggest difference between types of lithium-ion batteries is the chemistry of the positive electrode where there are six commonly referred to chemistries of lithium-ion battery [34]: LCO, LFP, NMC, NCA, LMO and LTO. The name refers to the chemistry of the positive electrode except for the LTO chemistry, where the negative electrode is lithium titanate and the positive electrode can be any of the other types of lithium-ion battery. Each type has its own advantages and disadvantages and these are discussed more in Section 2.3.2 and a comparison between the types of lithium-ion battery are seen in Table 2.7.

When characterising batteries, the most common technique is to charge the battery with a constant current followed by a constant voltage and to discharge the battery with a constant current. The CC – CV charging technique involves applying a constant current, with a maximum value specified by the manufacturer, to the battery until a set voltage is reached and then applying a constant voltage until the current drops below a set value. The constant current discharging technique involves applying a constant current, with a maximum value specified by the manufacturer, until a set voltage is reached. These techniques can be seen in Figure 2.4, the exact shape of the graphs in Figure 2.4 vary depending on many aspects, including the cell chemistry, the capacity, the current applied and temperature of the battery. The battery does not have to be charged and discharged using these techniques described and any charging or discharging mechanism can be used as long as the battery is kept within voltage, current and temperature limits. One battery cycle is equal to a full charge and a full discharge.

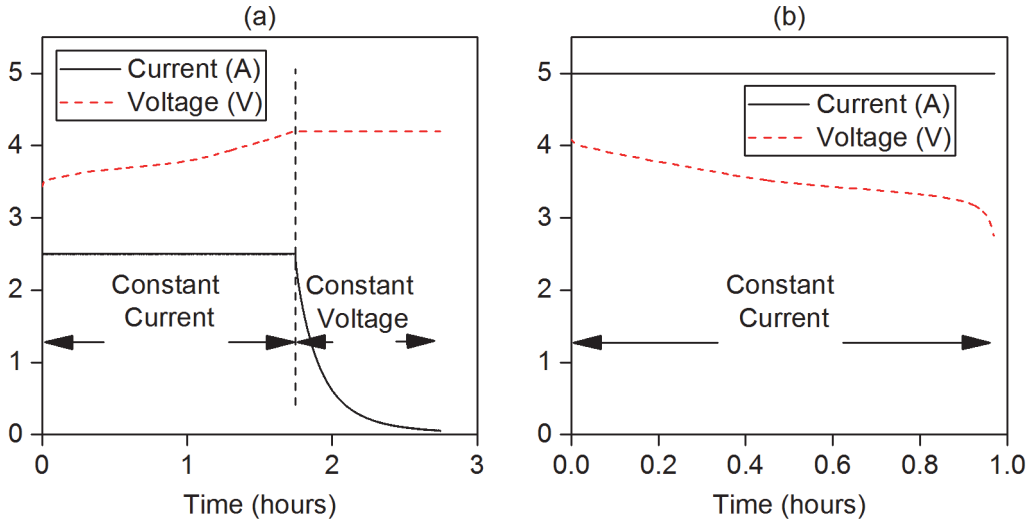

Figure 2.4 Typical lithium-ion charge and discharge current and voltage profiles

CC – CV charge (left), constant current discharge (right)

The most commonly compared battery characteristics are the energy and power characteristics of the battery. The capacity of a battery is expressed in ampere hours (Ah), the rated capacity of the battery is found by charging the battery fully and then discharging using the constant current technique, normally the current used is a current that should discharge the battery in 5 hours. The capacity is then found by multiplying the constant current value in amperes by the number of hours the battery discharged for. The energy stored in a battery is expressed in watt hours (Wh) and is found by multiplying the capacity by the voltage. As seen in Figure 2.4, the voltage is continually changing as the battery is discharged, if a constant current is used to discharge the battery the average voltage value can be used to find the energy. The energy can be divided by the volume of the battery to obtain the energy density (Wh L^{-1}) or by the mass of battery to obtain the specific energy (Wh kg^{-1}) [30].

The energy efficiency of the battery is made up of the coulombic efficiency multiplied by the voltage efficiency. The coulombic efficiency is the difference between the charge and discharge capacities, for example when charging a cell it may use 5.1 Ah and when discharging the cell only 5.05 Ah is obtained. This difference occurs due to irreversible chemical reactions in the cells that may occur during charge and discharge. It should be noted that to obtain accurate coulombic efficiency results a constant voltage step should be added to the test procedure seen in Figure 2.4 during the discharge after the constant current discharge step to ensure the battery is fully discharged [35]. The voltage efficiency is the difference between the charge voltage and the discharge voltage, for example while charging the cell may have an average voltage of 3.75 V but while discharging the average voltage may be 3.65 V, note that to take account of current variations the average voltage is taken over the SoC rather than time. Another method to

calculate the energy efficiency of the battery can be found by summing the voltage multiplied by the current at all times during discharge and charge and dividing the discharge value by the charge value.

The rate at which a battery can be charged or discharged is normally defined as a maximum current. To convert the current into a power it must be multiplied by the voltage of the battery however, as seen in Figure 2.4, the voltage varies while the battery is being charged and discharged and so the power also varies. The C-rate (C_{rate}) is a method of comparing the current (*I (A)*) rate ability of batteries of different sizes and is defined as per Equation 2.1. The capacity (*Cap (Ah)*) is usually taken as the manufacturer's rated capacity. A fully charged battery discharged at a C-Rate of 1C will take around one hour to fully discharge, at 2C the battery would discharge in around half an hour, and so on.

$$C_{rate} = \frac{I}{Cap}$$

Equation 2.1

Other parameters that may be used for comparison between types of lithium-ion battery include [21]: cost, lifetime, both in calendar years and in the number of times the battery can be cycled, safety, recyclability and self-discharge, i.e. if the battery is not being used how fast will the energy dissipate from the battery.

2.2 Background to Electric Vehicles

This section gives an overview of EVs, including the current state of EVs and fast charging along with the current and future fast charging limitations. When discussing EVs there are three types of vehicles with batteries that can be used to drive the vehicle seen in Table 2.1 [17]. There are other differences between the vehicles regarding the layout of the drive train, such as whether the wheels are powered by only electric motors or by electric and gasoline motors, however all battery vehicles could be classed into one of the 3 categories in Table 2.1.

Table 2.1 Types of vehicles that use a battery to drive the vehicle

Type	Drivetrain	Recharge	UK best selling vehicle example [36]
HEV	Gasoline Engine + Battery	Regenerative Braking	-
PHEV	Gasoline Engine + Battery	Regenerative Braking + Plug in	Mitsubishi Outlander
EV	Battery	Regenerative Braking + Plug in	Nissan Leaf

Moving from top to bottom of Table 2.1 the vehicles become more environmentally friendly and less polluting. An HEV can be thought of simply as a more efficient conventional gasoline vehicle as the battery can only be used in conjunction with gasoline. In a PHEV shorter journeys can be completed using only the battery but long journeys, or if the PHEV is not plugged in between journeys, will result in the use of gasoline. In an EV there is not a combustion engine and the distance one can travel before recharging depends on how large the EV battery is, EVs therefore have larger batteries than HEVs and PHEVs.

2.2.1 Current Electric Vehicles and Research Challenges

The ideal scenario therefore is to replace gasoline vehicles with EVs, as stated in the introduction, there are however four primary challenges to overcome before people will purchase EVs [7]: range, fast charging, cost and safety, as well as the secondary challenges of providing sufficient slow and fast charging infrastructure for the EVs. These challenges are described in detail in the sections below with fast charging and fast charging infrastructure given its own section due to its importance to the thesis.

2.2.1.1 Range and Cost

The range and costs of EVs are directly related to the battery in the EV. The range of an EV is equal to the efficiency of the EV at converting the energy in the battery into movement multiplied by the capacity of the EV battery, the larger the battery the greater the range of the EV. The cost of the EV is also highly dependent on the cost of the battery, for the Chevrolet Bolt EV the battery pack is the largest cost item in the vehicle [37].

In current EVs the range and cost of EVs go hand in hand, with EVs having longer range costing more. At one end of the spectrum the Citroen C-Zero is marketed as a city car and has a range of

93 miles and costs £20,000 [38]. At the other end of the spectrum the Tesla Model S 100D has a range of 424 miles and costs £83,000 [39]. Of the EVs that are available for purchase now there are two EVs with a relatively low cost that have ranges of over 200 miles. These are the Chevrolet Bolt with a battery capacity of 60kWh, a range of 238 miles and costing $38,000 [40] and the Tesla Model 3 with a range of 220 mile range and costing $35,000 [39].

The current trend is for the capacities of the batteries used in EVs to increase. The capacities of the Nissan Leaf [41] and Tesla Model S [39] have increased from 24 kWh and 65 kWh respectively at their introduction to 40 kWh and 100 kWh now. The costs of the batteries is also decreasing, it is however hard to find good references on how much lithium-ion batteries currently cost. One study estimated the cost at battery pack level has decreased from over 1,000 $ $(kWh)^{-1}$ to 410 $ $(kWh)^{-1}$ between 2009 and 2014 [22]. Chevrolet has also stated that on a cell level, the cost is 145 $ $(kWh)^{-1}$ in 2017 [42].

Increases in range and decreases in cost can be made by modifying the lithium-ion battery chemistry, improving the battery pack design, increasing the efficiency of the EV or improving manufacturing techniques. These improvements however can only have limited impacts as the energy density of lithium-ion batteries can only increase by a small amount, currently the most energy dense lithium-ion batteries have an energy density of 650 Wh L^{-1}, while the maximum energy density of future lithium-ion batteries is 850 Wh L^{-1} [34]. To achieve a step change in energy density, research is being conducted into using chemistries other than lithium-ion, such as Aluminium-air [43] or Lithium-air [44]. These chemistries have theoretical energy densities an order of magnitude higher than lithium-ion however currently problems with these chemistries include practically achieving the energy density, overcoming low efficiencies and short cycle lives.

In terms of the cell chemistries used, comparisons of which can be seen in Table 2.7, the majority of EVs use NMC type lithium-ion batteries, with the Society of Automotive Engineers [45] stating “several companies that started with the lower cost, very safe lithium-manganese oxide (LMO), including Hitachi and GS Yuasa, migrated to LMO/NMC blends and are now moving to NMC to achieve greater energy density”. Jaguar Land Rover [46], Chevrolet [47], Nissan [48] and Kia [49] all use NMC batteries. The main reasons for using NMC batteries are the high energy density and the low cost, the downsides of the battery are the safety concerns. Despite the majority of automakers opting for NMC batteries the largest current EV manufacturer, Tesla, use NCA batteries [50]. The NCA chemistry generally has similar advantages and disadvantages to the NMC chemistry. One further exception to the rule is Mitsubshi, who use LTO batteries [51]. The geometry of the cells is also varied with cylindrical, prismatic and pouch cells all used by different automakers.

2.2.1.2 Safety

There are concerns regarding the safety of lithium-ion batteries as if a battery pack is damaged there is the potential for thermal runaway, fire and explosion [52]. This will be amplified in the future, as EV battery capacities increase, battery accidents may become more violent. It should however be noted that this can also occur in gasoline vehicles if the gasoline tank is damaged and catches fire [53].

In current EVs, common methods to improve the safety of the battery include choosing a safer lithium-ion chemistry or encasing the cell or battery in a more crash resistant enclosure. Research into safer batteries therefore spans multiple length scales, from the chemicals that make up the cell using safer electrolytes [54], through to the cell design using materials that become non conductive if they get too hot before thermal runaway [55] to the battery pack design looking at the way the battery pack will respond in an accident.

2.2.1.3 Charging Speeds and Slow Charging Infrastructure

When charging an EV, either AC or DC charging can be used, where AC or DC refers to the current state (AC or DC) that the current is in when the power is transmitted to the EV [56]. An overview of AC and DC charging systems is shown in Figure 2.5, where it is clear the components for AC and DC charging systems are quite similar. The main difference is that for AC charging systems the charger is located on-board the EV while for DC charging systems the charger is located off-board the EV. Using an off-board charger means that communication must be established between the EV and the charger. When using an off-board charger the EV typically monitors the battery and transmits requests to the charger for the voltage and current to be delivered to the EV.

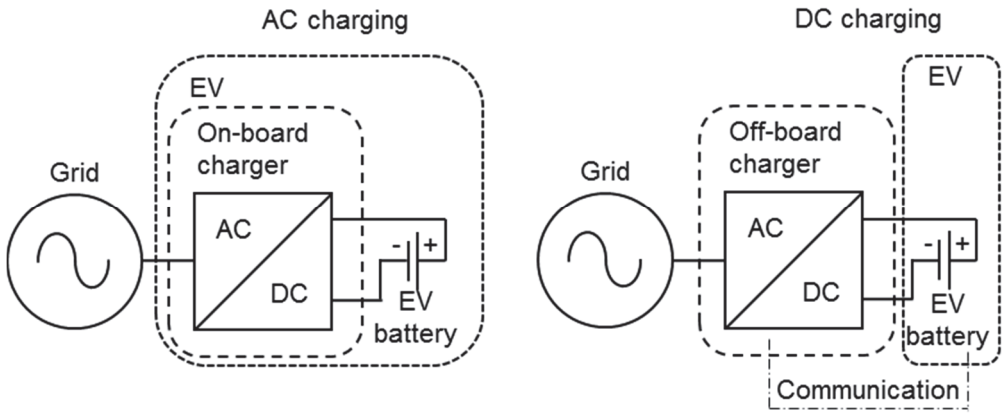

Figure 2.5 Overview of AC and DC EV charging

In terms of the charging of EVs, the IEC defines four modes of EV charging (IEC61851-1) [57], shown in Table 2.2. The power levels for slow and fast charging are not well defined by the

standard. Zap Map [58] defines three charging levels, slow up to 3 kW, fast up to 22 kW and rapid up to 120 kW. Due to the low power, slow charging is conducted in locations where the EV is typically parked for many hours, such as at home or work. If the Nissan Leaf mentioned above with a 40 kWh battery was fully discharged and was then charged using a slow charger it would take over 13 hours to fully charge.

Slow charging has challenges associated on both the local and national grid level. On a local level if everyone on a street had an EV and charged at the same time local transformers may become overloaded [59]. This overloading is possible as in the UK the grid is typically designed for an after diversity maximum demand of 2 kW while the slow charging described above is up to 3 kW. On a national level it is likely that people will start slow charging their EV around 5 pm at night as they arrive home for the evening, this is the same time as the peak load on the grid and so additional electricity generation may be required, grid challenges are discussed more in section 2.3.1. One of the ideas to mitigate these issues is to use smart charging [60], which shifts the charging to off-peak electricity usage times. For example if an EV owner arrives home at 5 pm, plugs in their EV and does not need the EV again until the morning, the charging can be delayed from 5 pm to start at midnight when electricity grid usage is less and the price may be reduced.

Table 2.2 Four modes of EV charging

Adapted from IEC61851-1 [57, 61]

Mode	AC or DC	Charging Speed	Description	Current / Voltage
Mode 1	AC	Slow	Household type socket outlet	16A, 250V single-phase 16A, 480V three-phase
Mode 2	AC	Slow	Household type socket outlet with an in cable protection device	32A, 250V single-phase 32A, 480V three-phase
Mode 3	AC	Slow or Fast	Specific EV socket outlet with control and protection function	-
Mode 4	DC	Fast	External charger	-

2.2.2 Fast Charging and Fast Charging Infrastructure

Currently, the fastest chargers all use DC off-board charging. AC high power charging has the problem that an on-board charger is required in the vehicle and to accommodate the high powers required for high power charging an on-board charger would likely weigh too much and take up

too much space in the vehicle. There are currently 4 types of DC chargers and an EV capable of fast charging will typically have a plug capable of using one of the following charging standards [62]:

- CCS
- CHAdeMO
- Tesla Supercharger
- GB/T

A summary of key information regarding these four fast chargers is presented in Table 2.3. Key differences between the chargers include different powers, different charging procedures and communication protocols. The CCS and Tesla chargers accommodate AC and DC charging in one plug while the CHAdeMO chargers require separate plugs for AC and DC charging.

CHAdeMO and CCS are often installed together [63]. Although it is complicated having different types of chargers, it is estimated that it only costs 5% extra to install a charging station with both CHAdeMO and CCS charging points compared with a charging station with a single charging point [64]. Tesla charging points are installed separately and the GB/T standards are not used outside China. The CHAdeMO charging plug has been the most popular plug standard in the past, it should be noted however that EVs with CCS charge capability have only been on the road since 2013. It is predicted that in the future as more EVs with the CCS standard are sold there will gradually be a more even split between the CHAdeMO and CCS standards [65].

Currently the majority of fast charging stations installed worldwide are 50 kW. EVs that can support rapid charging currently will charge at a maximum of 50 kW, except for the Tesla EVs which can charge at up to 120 kW using the Tesla Supercharger network [62]. Several projects have however recently been announced to install fast charging stations between 350 kW [66] and 400 kW [67].

Table 2.3 DC fast EV charging protocols

	CCS	CHAdeMO	Tesla Supercharger	GB/T
Proposed by	Europe/USA	Japan	Tesla	China
Chargers installed in the UK	✓	✓	✓	✖
Defined in IEC IEC61851-23 [68]	✓	✓	✖	✓
Current maximum power [62]	60 kW	50 kW	120 kW	50 kW
Current theoretical maximum power [62]	100 kW	62.5 kW	145 kW	180 kW
Future perspective power	350 kW	350 kW	Unknown	Unknown
Charger	 Europe  USA		 Europe  USA	-
Car manufacturers [69-71]	Audi, BMW, Daimler, Jaguar Land Rover, Porsche, Volkswagen, Chrysler, Ford, GM	Toyota, Nissan, Mitsubishi	Tesla	BAIC, BYD, Dongfeng

2.2.2.1 Limitations of Fast Charging

This section details all the potential limitations of fast charging and discusses which limitations are most likely to limit charging speeds in the future. The conclusion from the literature review in this section and discussions with industry is that it is thought that the fast charging limitation of current EVs is the cell current limit, this is discussed in detail below. Breaking this down even further the current is likely limited by the current which can be applied before lithium plating

occurs [13]. The limitations of fast charge are shown in Figure 2.6, and if the current limit is overcome any of the other limitations could become the limiting factor and these are described in more detail in the sections below.

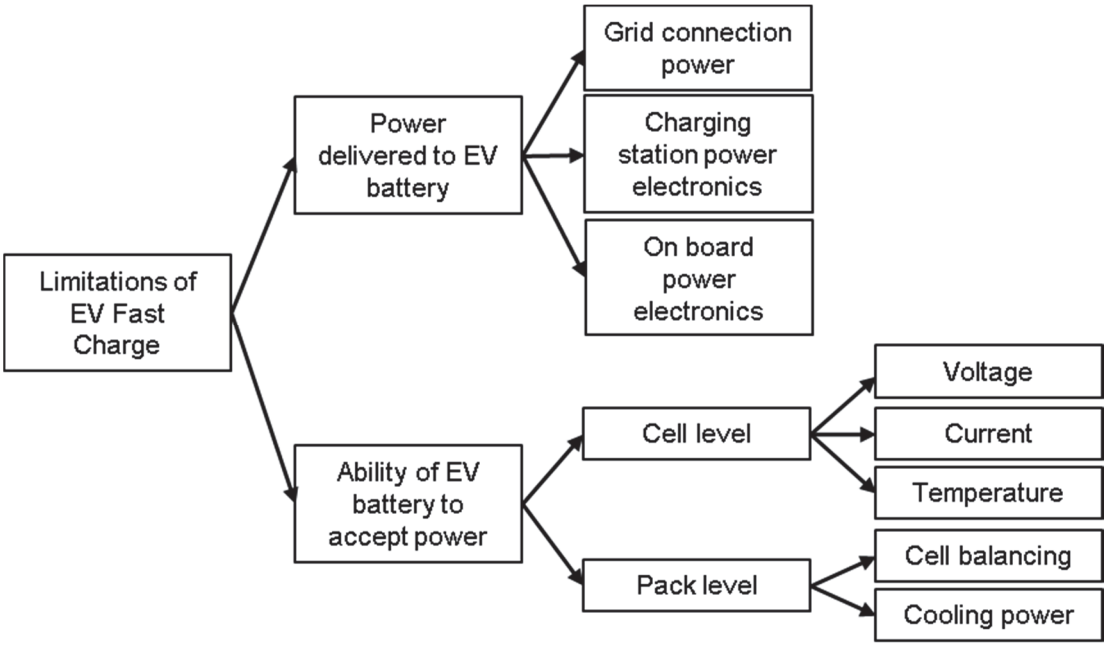

Figure 2.6 Potential limitations of fast EV charging

Power Delivered to Electric Vehicle Battery

As shown in Figure 2.6, the power delivered to the EV battery is reliant on having a sufficient electricity grid connection and having the power electronics able to handle the required voltages and currents both in the charging station and on-board the EV.

A sufficient grid connection capacity is related to constraints on the electricity grid. If a high power connection is required at a specific location and the current grid infrastructure cannot support the power level, the grid infrastructure must be upgraded [19]. Faster charging and therefore higher powers will amplify this problem. The grid connection is therefore one of the focuses of this thesis and along with the proposed solution of using stationary energy storage at the fast charging station is described in detail in Section 2.3.

It is assumed that the power electronics in the charging station will not be the limiting factor as, although it is complicated to design systems for such high powers, charging stations up to 400kW are currently available commercially [67].

The on-board power electronics are also not considered a limiting factor as for DC charging the charger power electronics are located off-board the EV. There are therefore few power electronic devices on-board the vehicle for fast charging as on-board the vehicle consists of one positive and

one negative conductor linking the charging connector to the EV battery. These conductors could be made larger to accommodate higher powers. The power electronic converters required for fast charging are therefore not researched further in this thesis.

Ability of Electric Vehicle Battery to Accept Power

For the EV battery the limitations are broken down into cell level limitations and pack level limitations.

Cell Level

On a cell level, there are three potential battery limitations of fast charge: voltage, current or temperature. Charging or discharging the cell outside the specified limits can cause accelerated degradation and so for fast charging, maximum values for the cell voltage, current and temperature are set by cell manufacturers. The reasons for the voltage, current and temperature limits are down to the electrochemistry of the cells and hence a brief overview of the chemical explanation of each limit is now presented.

The cell voltage upper and lower limits are determined by the voltage window where the electrolyte will not break down. Applying a voltage above the upper limit or below the lower limit causes the cell electrolyte to break down, which causes significant degradation to the cell. NMC, NCA, LCO and LMO cells generally operate between 2.5 V to 4.2 V, however the lower and upper limits can vary slightly, while LFP and LTO cells operate at lower voltages. In addition to electrolyte break down, at too low cell voltages the negative current collector can dissolve while at too high cell voltages lithium deposits can form, consuming lithium and putting the cell in danger of short circuiting [72]. The cell voltage can become a limit to the fast charging if, when a current is applied to the cell, the voltage reaches the limit too soon after the start of charging. An example of two cells being charged at the same rate (2C) but reaching the voltage limit after different times after the start of charging can be seen in Figure 2.7, in this figure cell 2 takes longer to reach the voltage limit than cell 1 meaning the higher current can be applied for longer to cell 2 and cell 2 charges faster than cell 1. The time after start of charging that the voltage limit is reached is related to the materials and chemistry make up of the cell and therefore out of the scope of this thesis and is not researched further in this thesis.

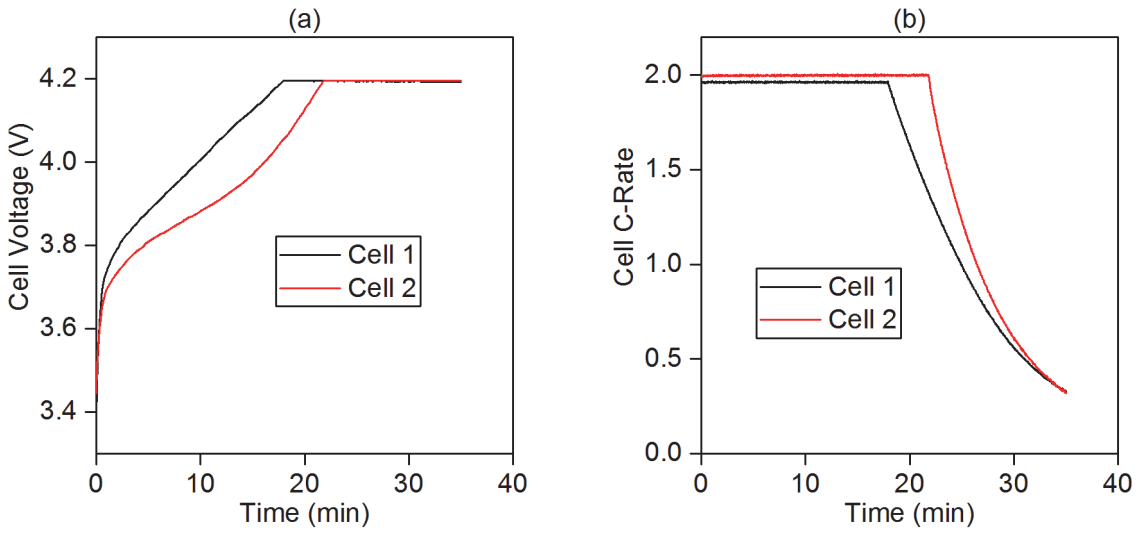

Figure 2.7 Voltage response of two different cells charged at 2C from 0% SoC

The cell current limit is dependent on many factors, one of the most important is the lithium plating limit [73]. Lithium plating occurs as the electrolyte breaks down and the lithium is plated on the negative electrode during charging at too high current [74]. At lower states of charge lithium plating is less likely to occur and so higher currents can be applied at lower states of charge [75]. Most chargers for batteries use a simple method of either applying constant current or constant voltage, therefore most charging regimes use the CC – CV charging regime described in Section 2.1. Figure 2.8 shows a comparison between this CC – CV charging profile and a dynamic charging profile that has been optimised to prevent lithium plating. The dynamic profile involves applying higher currents at lower states of charge and it can be seen to charge the cell significantly quicker than the CC – CV profile.

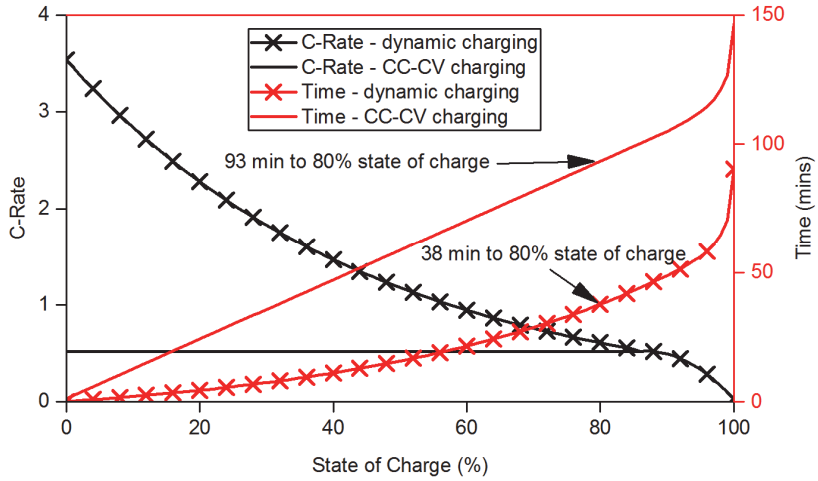

Figure 2.8 Dynamic battery charging profile versus standard CC-CV charging profile

Graph created by adapting data from [76]

In addition to lithium plating, other potential limitations of current include atomic rearrangement and particle cracking, where lithium-ion insertion and extraction to the electrode causes volume expansion and contraction, which is accelerated at higher rates [77]. As the current limit is related to the materials and chemistry make up of the cell it is not researched further in this thesis.

The temperature limit is linked to the pack level cooling system limit, described below, as a larger cooling system can prevent the cells heating up too much during charge. Too high temperature can accelerate the electrolyte degradation and decomposition of the binder, which is used to bind the electrode to the current collector [78]. As well as degradation, the temperature limit may also be specified to stop thermal runaway, where the cell fails catastrophically resulting in a fire or explosion. As stated in the previous section, the EV cooling and the cell temperature is a potential limit to future fast charging and therefore one of the focuses of this thesis, which is described in detail in Section 2.4.

With all limits there is a trade off between degradation and cell ability. The manufacturer could specify a current limit of 0.01C, a voltage window of 3.6 – 3.8 V, a temperature range of 24 – 26°C and claim their cells could last many thousands of cycles however the cells would not meet many applications. Cell manufacturers generally specify limits and then guarantee that if operated within these limits the cells will last for at least a minimum number of cycles.

Pack Level

At the pack level, cell balancing and the battery cooling system could limit the maximum EV charging rate. As stated in Section 2.1, batteries are manufactured as cells with capacities much lower than that required for an EV battery, a breakdown of a Tesla battery pack is given in Section 2.2.2.2. Many cells must therefore be connected to create a battery with a large enough capacity, which creates the challenge of cell balancing [79]. Cell balancing is the process of ensuring that all cells in a battery pack are at the same voltage, SoC and temperature. Cells may become unbalanced due to manufacturing tolerances and material impurities and cell imbalance in a battery pack can reduce the cycle life of the battery pack as some cells are overcharged.

Cell balancing systems can generally be classed as either active or passive [79]. Passive balancing involves discharging the cells at high states of charge though resistors whilst continuing to charge cells at low states of charge until balance is achieved. Passive balancing is relatively simple and cheap but wastes energy. Active balancing involves transferring energy from the cells at high states of charge to cells at low states of charge using power electronic converters and inductive or capacitive charge storage. Active balancing wastes less energy but is more complex and expensive

than passive balancing. In current EVs, passive cell balancing is the norm due to the lower cost [24].

To enable fast charging, EV battery voltages will increase as for the same pack power a higher voltage means a lower current, which in turn means smaller current carrying cables, both in the EV and at the charging station. 1000 V is suggested as a future voltage for EVs because above 1000 V requires increased insulation requirements [12]. These higher voltage battery packs will require modified cell balancing circuit design as more cells are connected in series. Research is being conducted on cell balancing to try and encourage the use of active cell balancing [80]. However, as the majority of current EVs use passive balancing, which can be adapted for higher voltages and faster charging, cell balancing is not a research focus of this thesis.

EV cooling systems are required to remove the heat generated in a battery pack as the battery charges or discharges. The heat generated by the cells is affected by many different processes as described in Section 2.4.2.1. One of the main heat generation mechanisms is ohmic heating, which is equal to the current squared multiplied by the resistance of the cell. At the higher currents required for fast charging the heat generation and therefore the EV cooling system is likely to be an issue because the heat generation is proportional to the current squared. The EV cooling is therefore one of the main areas of study of this thesis and is described in detail in Section 2.4.

2.2.2.2 Example Fast Charging Profiles

For fast charging, the majority of current EVs use a CC – CV charging regime, similar to that shown in Figure 2.4a. The battery energies and C-Rates of a select few EVs that use the CC – CV technique are as follows:

- BMW i3 (33 kWh, ~1.5C) [81]
- Nissan Leaf (24 kWh, ~2.2C) [82]
- Mitsubishi i-MiEV (16 kWh, ~3.1C) [82]
- Citroen C-Zero (16 kWh, ~2.8C) [83]

Tesla EVs however use a more complicated three stage charging process, as shown in Figure 2.9. The first stage is constant power where charging is limited by the power delivered to the EV battery and this stage lasts until roughly 25% SoC. The second stage does not involve constant current, power or voltage and it is thought that during this stage the EV may be charging using the dynamic charging profile similar to that shown in Figure 2.8 however it could also be limited by the cooling system and the temperature of the cells, this stage lasts until around 90% SoC. The final stage is constant voltage. Although Tesla EVs use a more complicated fast charging regime at

higher powers the C-Rate is actually lower than other EVs as the energy in a Tesla EV is 85 kWh. The Tesla battery consists of 7104, 3.1 Ah cells, with 74 cells in parallel and 96 in series [84], giving a total capacity of 230 Ah. As can be seen in Figure 2.9a the maximum current is 320 A, giving a maximum C-Rate of 1.4C.

In the future, as EV battery capacities increase and charging powers increase, more charging profiles will look like the Tesla charging profile. This analysis of the Tesla charging profile was presented at "HEVC 2016: The 6th Hybrid and Electric Vehicle Conference" along with a conference paper entitled "Off-vehicle energy store selection for high rate EV charging station" doi: 10.1049/cp.2016.0986 [85].

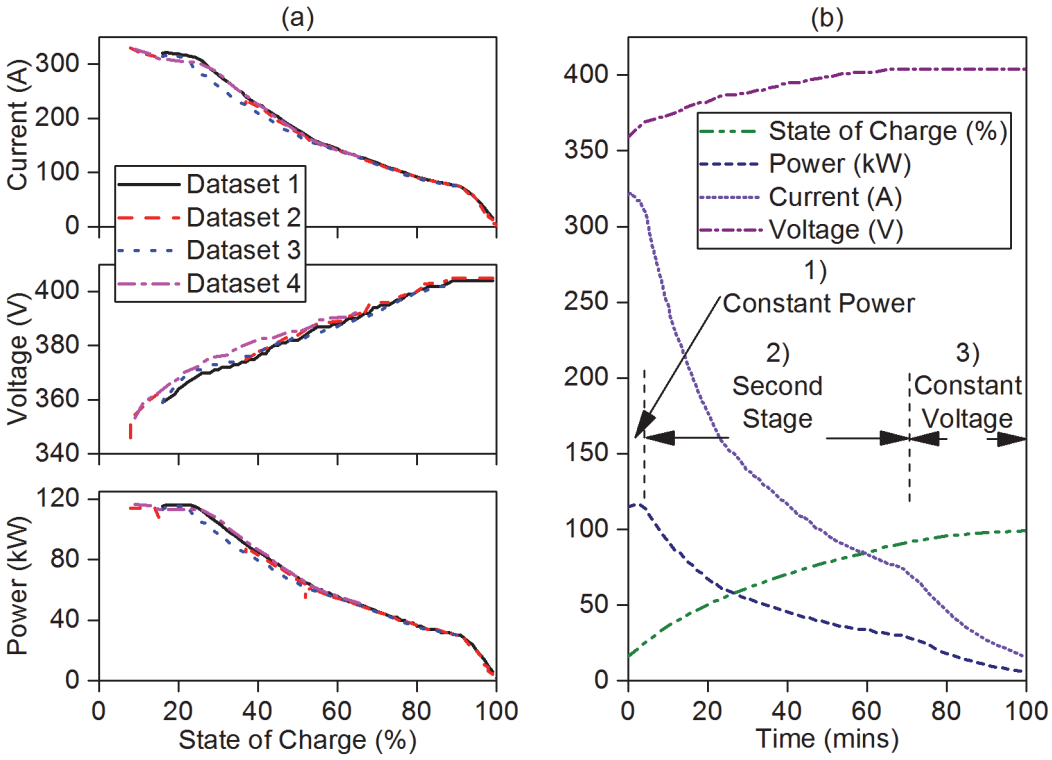

Figure 2.9 Tesla Supercharger charging details

Four Tesla Supercharger profiles versus SoC (left) and the Tesla Supercharger Dataset 1 versus time (right) [76]

2.2.3 Conclusions from Electric Vehicles

EVs, as opposed to HEVs or PHEVs, are needed in order to address, in particular, urban transport emissions and related health impacts. EVs have four main challenges: range, fast charging, cost and safety, as well as related infrastructure challenges associated with providing sufficient slow and fast charging points. Every year the number of EVs on the road is increasing and the capabilities of these EVs, including the range, charging speeds and costs are all improving.

In terms of fast charging, the majority of current, and all predicted future, fast charging will be enabled using DC fast charging. Cell current limits due to chemical limitations, such as lithium plating, are currently thought to be limiting factors. These current limits are not investigated in the thesis as the thesis is not looking at changing the chemistry of lithium-ion cells. An overview of potential limitations are shown in Table 2.4.

If the current limit is increased, obtaining the high power grid connection and overcoming thermal constraints will be the most important challenges to overcome to achieve fast charging. The following two sections therefore provide background information to these two potential fast charging limitations.

Table 2.4 Fast EV charging constraints, in order from most to least important

Related to constraints presented in Figure 2.6

Limit	Constraint	Category	Investigated more in thesis?	
Current	Cell current limit is not high enough to allow fast charging	Chemistry	×	Increasing current limits requires advances in cell chemistry, which is outside the scope of this thesis, it is however critical to achieving fast charging
Voltage	At high currents cells reach the voltage limit, slowing the charging	Chemistry	×	Linked to the current limit above and depends on the cell chemistry, which is outside the scope of this thesis
Temperature	Cells become too hot while charging, linked to 'Cooling power'	Chemistry / Engineering	✓	Section 2.4
Cooling power	Excess heat with fast charging requires large cooling system	Engineering	✓	Section 2.4
Grid Connection Power	Grid constraints restrict available charging power from grid	Economic	✓	Section 2.3
Charging station power electronics	Power electronic devices in charging station cannot handle high power required	Engineering / Economic	×	Fast charging stations are currently available with charging powers up to 400 kW and so this is not thought to be a limiting factor
On-board power electronics	Power electronic devices on-board EV cannot handle high power required	Engineering	×	DC charging and communication mean the on-board power electronics are two conducting rods and so this is not thought to be a limiting factor
Cell balancing	High power charging results in cells in EV becoming unbalanced	Engineering	×	Currently EVs use passive cell balancing and this can be scaled to larger battery packs at higher voltages and so this is not a limiting factor

2.3 Background to Stationary Energy Storage at Fast Charging Station

This section looks at the fast charging limit of grid connection power in more detail, with a focus on the solution investigated in this thesis of using a stationary energy store as part of the fast charger to reduce the grid connection power. The section provides details of the electricity grid and the costs associated with connecting a high power connection to the grid before conducting a review of potential energy storage devices that could be used as the stationary energy storage. The section ends with a review of research already conducted into using stationary energy storage at fast charging stations.

2.3.1 Electricity Grid

It is important to understand the costs of connecting a fast charging station to the electricity grid and therefore the potential benefits of using stationary energy storage at fast charging stations. The future of the electricity grid is also discussed and future potential benefits of the stationary energy storage are highlighted. The electricity grid is currently in a period of great change with demand magnitudes and usage patterns changing with the introduction of EVs and generation becoming more distributed and intermittent with the introduction of renewable electricity generation [86].

The electricity demand variation throughout the day for a typical day is illustrated in Figure 2.10. The demand is lowest throughout the night when most people are asleep and the demand peaks around 6pm as people arrive home from work but offices and factories are still in use. As well as these large changes in demand over time scales of hours, the demand fluctuates every second as people turn on and off devices randomly. In the future, with more EVs on the road the electricity demand is likely to change, both in terms usage patterns and increasing demand magnitude. The UK National Grid predicts many future scenarios, the scenario with the largest increase in EVs causes a peak demand increase of 40% between 2015 and 2050 [87].

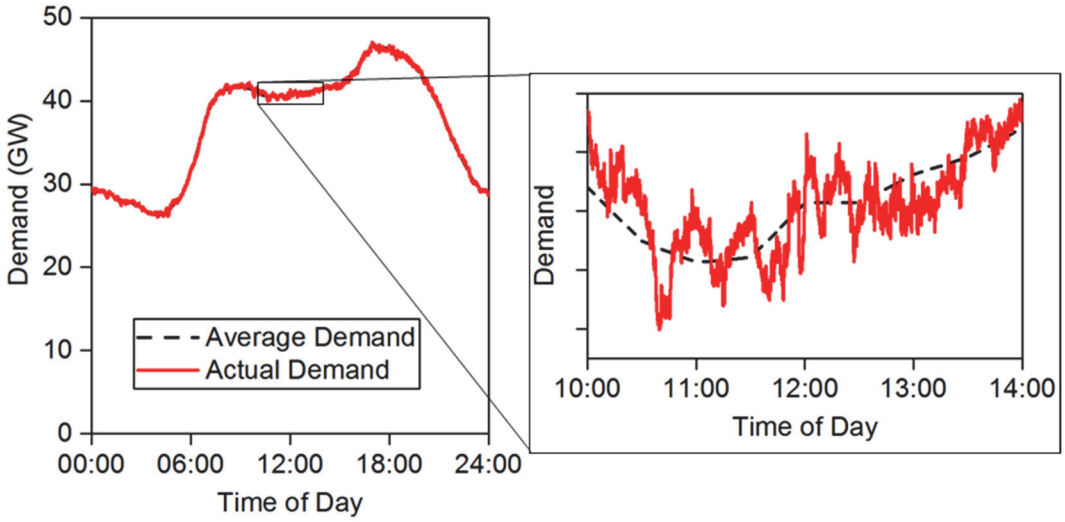

Figure 2.10 Typical winters day electricity demand in the UK

Graph created by adapting data from [88, 89]

Figure 2.11 illustrates that UK electricity is traditionally generated using coal, gas, nuclear and, in the past, oil. These generation types are controllable, meaning the generation output can be regulated up or down on demand. Although all are controllable it is easier to vary the generation from a gas power station than coal or nuclear, with the start up times for gas, coal and nuclear power stations being 10 minutes, 3 hours and 24 hours respectively [90]. As seen in Figure 2.11 the amount of electricity generation from renewables has increased rapidly since 2010 and is predicted to increase in the future, with the future predicted to include significantly more wind and solar generation. A problem with wind and solar electricity generation is that they are uncontrollable, i.e. they only generate electricity when the wind is blowing or sun is shining.

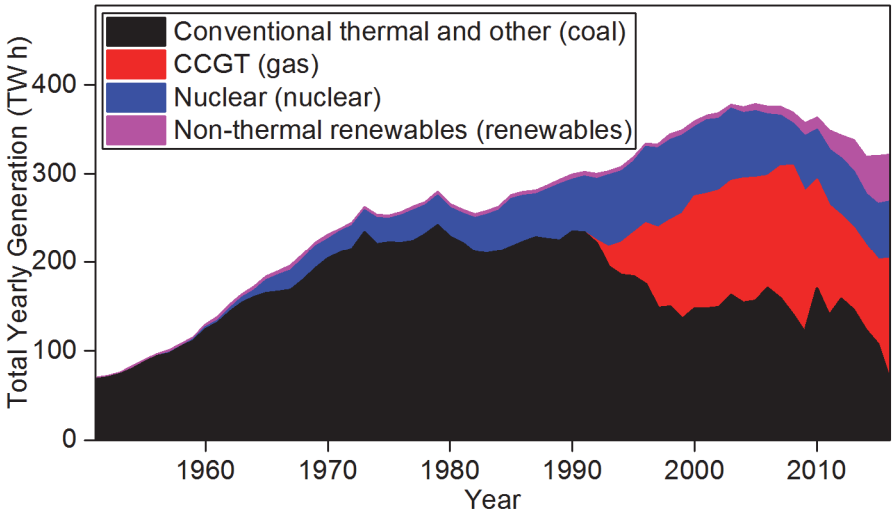

Figure 2.11 Electricity generation mix in the UK between 1951 and 2016

In brackets are the main generation source [91]

There is currently around 2 GWh of electricity storage on the UK electricity grid [92]. This is enough to store some energy for the grid peak demand period and also deal with some of the short term fluctuations in generation and demand. However if the UK was powered entirely by solar and wind and these suddenly stopped generating, at the current peak demand of 62 GW, this 2 GWh of storage would be used up within 2 minutes. In the traditional grid the controllable generation is ramped up or down to match the demand, the large jumps or falls in demand are dealt with by changing the output from power stations or taking the power stations on or offline. The smaller fluctuations shown on the right of Figure 2.10 are dealt with by changes in frequency. The frequency of the grid is a measure of how well the supply and demand of electricity on the grid are balanced, if there is more demand than generation the frequency decreases while more generation than demand results in the frequency increasing, in the UK the grid operates at a frequency of 50 Hz, with limits of ±0.5 Hz and operational limits of ±0.1 Hz [93].

With more uncontrollable renewable electricity generation and larger changes in demand from the increased number of EVs it is predicted in the future that it will become harder to match the generation to the demand. The National Grid in the UK has a range of options to balance supply and demand. Examples include, allowing the frequency to change by ±1%, telling generators to reduce or increase their generation, telling big users to reduce their demand, changing the voltage of the grid by a few percent (in the UK maximum values are minus 6% and plus 10% [94]). In the future, energy storage may play a larger role in balancing electricity supply and demand. It has been suggested [95] that there are 15 potential ways for energy storage to be used on the electricity grid, ranging from storing energy from excess wind and solar generation to be used when there is insufficient wind and solar generation to storing energy for frequency regulation to cope with the short term power fluctuations.

Fast charging stations will contribute to more demand fluctuations, however looking at the system from the perspective of the person installing the fast charging station there is currently no penalty for installing equipment with demand fluctuations, as these demand fluctuations are dealt with at a national level using the balancing mechanisms described above. The only aspect the developer of the fast charging station has to worry about when connecting to the grid is the maximum power required by the fast charging station. In this thesis the current costs that a developer may need to cover are described but in the future there may be other ways a stationary energy storage could be valuable to a developer, such as providing some of the services mentioned above to the grid.

The cost of connecting a fast charging station to the grid could come from two sources and these are described in the sections below:

- Standard electricity and connection charges
- Grid infrastructure upgrade costs

2.3.1.1 Standard Electricity and Connection Charges

An electricity bill for a high power connection can consist of four parts as per Table 2.5. The unit rates are the actual electricity used by the consumer. The one, two or three refers to electricity costing different amounts at different times during the day. For example the cost of electricity will be greatest around 6 pm when demand is highest and lowest in the night when demand is lowest, in the UK the most well known example of this is Economy 7 [96]. The fixed charge is simply a charge each day for having an electricity connection. The capacity charge is also a fixed daily charge however it varies depending on the maximum power rating of the connection. Reactive power occurs in AC systems when the current and voltage are not in phase because the consumer is using devices with significant capacitance or inductance. The reactive power is not useful power but must still be generated, as such large consumers are charged per unit of reactive power.

Table 2.5 Electricity tariff components

Taken from the DCUSA [20]

Tariff component	Unit
One, two or three unit rates	p $(kWh)^{-1}$
Fixed charge	p day^{-1}
Capacity charge	p $(kVA\ day)^{-1}$
Reactive power charge	p $(kVAr\ h)^{-1}$

The reactive power charge of a fast EV charging station can be minimised by the design of the power electronics. The two important tariff components for a fast EV charging station are unit rates and capacity charge and these are discussed in more detail below.

The unit rates are currently very simple. On a household electricity bill in the UK, consumers may be used to an Economy 7 rate. For a standard household from British Gas [96] the day unit rate is 17.93 p $(kWh)^{-1}$ compared to a night rate of 7.4 p $(kWh)^{-1}$. This simple pricing structure may change in the future if more variable pricing is introduced. If pricing of electricity became fully variable the price would vary continuously throughout the day, with the price increasing when

demand is high and renewable electricity generation low and decreasing with low demand and high renewable electricity generation [97].

The method for calculating the fixed capacity charge varies for each electricity user. From a UK Power Networks report [98], this charge varies between 0.3-5.9 p $(kVA\ day)^{-1}$ with a mean value of 1.7 p $(kVA\ day)^{-1}$. A McKinsey & Company report [23] suggests the demand charge is highly variable in the United states, between \$2 kW^{-1} and \$90 kW^{-1} per month and the demand charges can make up over 90% of the cost of a fast charging station.

2.3.1.2 Grid Infrastructure Upgrade Costs

The electricity grid historically has operated with electricity transferred primarily in one direction from large generation power plants through power lines to electricity consumers. Once the electricity is generated at a large coal, gas or nuclear plant, the electricity is transferred through a transformer to step up the voltage to the high voltage required for transmission. Transmission lines are high voltage to reduce losses when transferring electricity in bulk over long distances. From the transmission lines the electricity is transferred through a transformer to step down the voltage for distribution for customer use. In the UK, transmission lines operate at 400 kV and 275 kV and are the responsibility of the National Grid while distribution lines operate between 230 V and 132 kV and are the responsibility of local distribution companies, such as Scottish and Southern Energy [99].

Each power line and the associated equipment on both the transmission and distribution network are rated at a certain power. If a new electricity load, such as a fast charging station, wants to connect to the electricity grid at a specific location it must be checked whether all lines between the new load and the generation have spare capacity to supply the required electricity. If a line does not have sufficient capacity the line must be upgraded. The costs of grid infrastructure upgrades vary greatly depending on location, one estimation puts the upgrade costs in the range \$25-250 kW^{-1} [19].

Distributed generation is small scale electricity generation that is connected to the distribution network. The National Grid, who are responsible for balancing the grid, do not see the distributed generation as generation, instead they see a drop in a demand while the distributed generation is generating. Similarly to installing a new load on the grid, installing new distributed generation also requires a check to see if there is spare capacity to accommodate the new generation [100] and if there is not, expensive grid infrastructure upgrades are required. This leads to a further idea of combining fast charging stations with stationary energy storage using distributed electricity

generation. If combined this could enable both fast charging stations and distributed generation to connect to the grid in locations that they previously could not.

2.3.2 Energy Storage Types and Characteristics

The requirements, such as capacity and power rate, of the stationary energy storage are determined later in the thesis in Chapter 4. These requirements will influence the choice of energy storage technology to use at the fast charging station as different energy storage technologies have different advantages and disadvantages. In this section an overview of energy storage technologies and comparators is given to ensure the correct energy storage technology is chosen for use as the stationary energy storage.

An energy storage device is a device that captures energy to be used at a later time. There are many different types of energy storage technologies and the different technologies are described below. To determine the optimum energy store for certain applications, comparators must be defined, these comparators commonly include [21]:

1. Power, how much power can the energy store provide? (kW) The power of the energy store for the fast charging station is a critical parameter when deciding the type of energy store to select and is seen in Ragone plot in Figure 2.12.
2. Size/capacity, how much energy can the energy store hold? (kWh) The energy of the energy store for the fast charging station is also a critical parameter when deciding the type of energy store to select.
3. Density, what is the density of the energy store in terms of both power and energy per unit mass and per unit volume? (W kg^{-1}, Wh kg^{-1}, W l^{-3}, Wh l^{-3}) The density of the energy store for the fast charging station is less critical as the energy store is stationary meaning size and weight of the energy store are less important.
4. Self-discharge, if left idle, how much energy will be lost to the environment from the energy store? (% day^{-1}) The self-discharge of the energy store for the fast charging station may be important depending on the determined length of time that the energy must be stored.
5. Lifetime, how long will the energy store last, in terms of both number of cycles and calendar life? (% $cycle^{-1}$, % $year^{-1}$) The lifetime of the energy store for the fast charging station is likely to be a critical parameter in determining whether the system is economically viable.
6. Efficiency, how much energy is lost when charging and discharging the energy store? (%) The efficiency of the energy store for the fast charging station is likely to be an important

parameter when selecting the type energy store and must be considered along with the economics of the system.

7. Response time, when requested, how quickly can the energy store provide energy? (s) The response time of the energy store for the fast charging station must be within a few seconds, as long as this criteria is met it will not be a critical parameter when deciding the type of energy store.
8. Suitable storage duration, how long can energy be stored in the energy store? (s) The suitable storage duration is similar to the self-discharge in that it may be important depending on the determined length of time that the energy must be stored.
9. Discharge time at power rating, if discharged at the power rating, how long will it take the energy store to fully discharge? (s) The discharge time of the energy store for the fast charging station is a key parameter used to make a decision regarding the energy store type and is seen in Ragone plot in Figure 2.12.
10. Costs, how much does the energy store cost, in terms of both capital costs and maintenance costs? ($) The costs of the energy store for the fast charging station is likely to be a critical parameter in determining whether the system is economically viable.
11. Maturity, are there multiple operating examples of the energy store or has the energy store not left the research laboratory? The maturity of the energy store for the fast charging station must be considered as the risk of using an immature type of energy store will effect whether the system will receive investment.
12. Safety, if the energy store fails is there a danger to humans or the environment? The safety of the energy store for fast charging station must be considered as members of the public will be using the fast charging station however as the energy store is stationary safety measures, such as containment, should be easier to construct.
13. Recyclability, once the energy store reaches the end of its life, what percentage of it can be recycled? As one of the benefits of EVs is the environmental benefit of combating climate change, the recyclability of the energy store for the fast charging station must also be considered.
14. Site availability, if the energy store requires many acres of land or specific geography, is this available at the desired location? The site availability of the energy store for the fast charging station will need to be considered to determine if it is feasible to use a certain type of technology at the fast charging station location.

There is no one energy storage technology that is best for all comparators, for each application it must be decided which capabilities are most important and trade-offs made. A Ragone plot of some of the most common types of energy storage can be seen in Figure 2.12. The energy storage

ratings have been taken from the reference given. Three stationary energy stores at fast charging stations have also been included in the Ragone plot, these have been taken from three papers detailed in the literature review in Section 2.3.3. These three examples have been chosen as they cover a wide range of energy and power requirements.

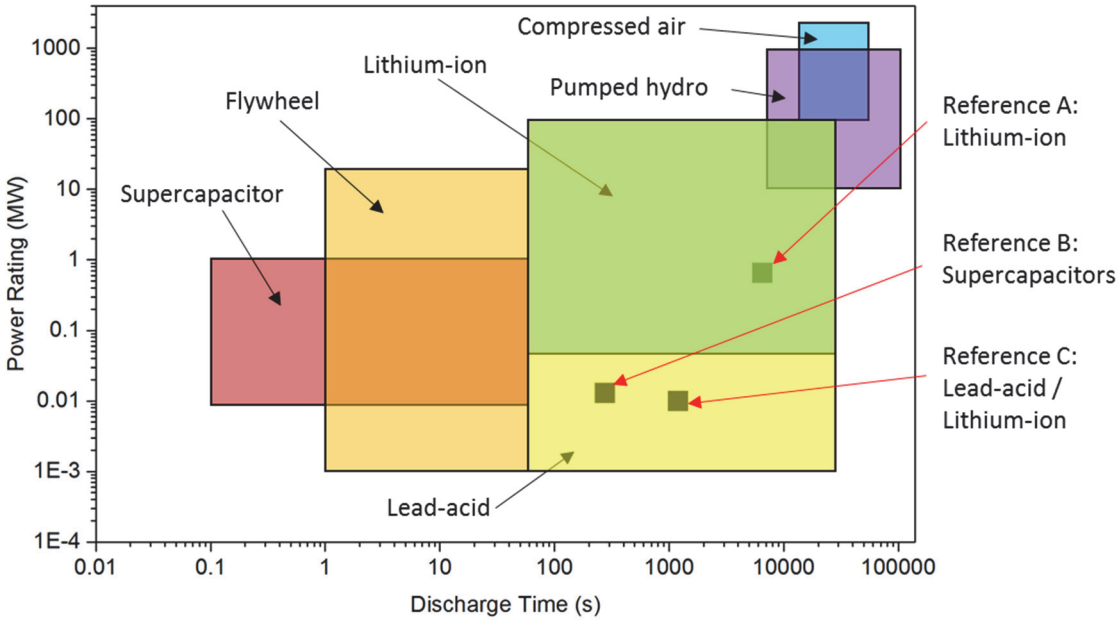

Figure 2.12 Ragone plot of energy storage technologies and energy stores for fast charging stations along with the stationary energy stores chosen

Energy storage parameters are taken from [101] and energy stores for fast charging stations are taken from: Reference A = [102], Reference B = [103] and Reference C = [104]

A summary of the most common types of energy storage technologies are as follows [92, 105]:

- Mechanical storage systems
    - Pumped hydro storage, water is pumped up to a higher point where it is stored, when electricity is required the water flows through turbines to generate electricity. Generally, pumped hydro requires lots of land and specific geography and is suited to large scale storage (>500 MWh), it currently makes up 87% of all grid electricity storage in terms of power [92]. Pumped hydro is unlikely to be suitable for the energy store at the fast charging station because it requires specific geography such as lakes and mountains.
    - Compressed air energy storage, ambient air is passed through compressors and stored in underground caverns, when electricity is required the air is combined with natural gas and passed through combustion turbines to generate electricity. There are two large scale (>500 MWh) installed compressed air plants [92] and

research is being conducted on smaller scale projects. Compressed air is also likely to be unsuitable for use as the energy store at the fast charging station because it also requires specific geography, such as large underground caverns.

  - Flywheel energy storage, a motor is used to spin an object where the energy is stored as kinetic energy, when electricity is required the spinning object turns a generator to generate electricity. Flywheels are typically used for storing small capacities of energy (the largest plants are 5 MWh [92]) but can operate at high powers. Flywheels may be suitable for use as the energy store at the fast charging station depending on the energy and power requirements, such as if the energy store needs to operate at high power, as seen in Ragone plot in Figure 2.12.

- Electrochemical storage systems
  - Secondary batteries, connecting a power supply across battery terminals charges the battery storing the energy in the active masses of the electrodes, when electricity is required a load is connected across the battery terminals. There are many different types of secondary batteries used for a variety of applications, from low energy and high power, similar to flywheels, through to medium energy applications. The largest secondary battery is currently 129 MWh [92]. Secondary batteries are likely to be suitable for use as the energy store at the fast charging station because they are suitable for a wide range of energy and power requirements.
  - Flow batteries, the charge and discharge principles are similar to that of a secondary battery however the energy is stored in liquid electrolytes, which are stored in tanks. Flow batteries are suitable for larger scale projects, with an 800 MWh project currently under construction in China [92]. The energy capacity, which is determined by the size of the tanks, can be designed separately to the power capacity, determined by the size of the cell. Flow batteries may be suitable for use as the energy store at the fast charging station depending on the energy and power requirements.
- Chemical energy storage
  - Hydrogen, electricity is used to electrolyse water to produce hydrogen, the hydrogen is stored in tanks, caverns or combined with other materials, when electricity is required the hydrogen is either passed through a fuel cell or combusted in a gas turbine to generate electricity [105]. Hydrogen is suitable for very large scale long duration storage and it has been suggested that hydrogen could be used instead of natural gas, however there are issues with cost, efficiency and storing the hydrogen. Hydrogen is currently unlikely to be suitable

for use as the energy store at the fast charging station because of low efficiencies and lack of maturity at the scales required.

- Synthetic natural gas, similar to hydrogen except instead of storing the hydrogen directly, the hydrogen is combined with CO_2 to form synthetic natural gas [105].

- Electrical storage systems
  - Double-layer capacitors, also known as supercapacitors, are charged and discharged in a similar way to secondary batteries. Supercapacitors are appropriate for high power, low energy applications and are used for similar applications as flywheels [105]. Supercapacitors, similarly to flywheels, may be suitable for use as the energy store at the fast charging station depending on the energy and power requirements, especially if the energy store needs to operate at high power as seen in the Ragone plot in Figure 2.12.
  - Superconducting magnetic energy storage, current is passed through a superconductor coil, which has zero resistance when kept below a certain temperature, and energy is stored in the magnetic field created by current flow in the superconducting coil, when electricity is required the circuit is completed and the device discharged [105]. Superconducting magnetic energy storage is not a mature technology, hence is currently unlikely to be suitable for use as the energy store at the fast charging station because of lack of maturity at the scales required.

The fast charging station is likely to require a small to medium energy store, i.e. not a pumped hydro or compressed air energy storage scale device. Only relatively mature technologies were considered in this thesis as the focus is not on developing a new type of energy storage technology. For this thesis, the three main energy storage types considered are, lithium-ion batteries, lead-acid batteries and supercapacitors. These technologies are chosen as they cover a wide range of requirements and these technologies are described in detail in the following section. In general, lead-acid batteries are cheaper per unit energy stored but operate at much lower power rates with lower cycle lives, supercapacitors are much more expensive per energy stored but operate at very high power rates and have very high cycle lives, while lithium-ion batteries are in between the two as shown in Table 2.6.

Table 2.6 Comparison three types of energy stores

Lithium-ion batteries, lead-acid batteries and supercapacitors [21, 34]

	Lithium-ion	Lead-acid	Supercapacitors
Capital cost per unit energy	Medium	Low	High
Maximum discharge	80 C	10 C	1000 C
Efficiency	95 %	80 %	98 %
Cycle life	2000	400	1000000
Self-Discharge	3 % $month^{-1}$	4 % $month^{-1}$	80 % $month^{-1}$
Specific energy	300 Wh kg^{-1}	40 Wh kg^{-1}	15 Wh kg^{-1}

The values shown in Table 2.6 are typical values however the value can vary for each battery depending on design. For example lead-acid batteries can be designed to have cycle lives over 5000 [106], however they then become more expensive.

2.3.2.1 Lithium-ion Batteries

The principles of lithium-ion battery operation have been described in Section 2.1. There are many different types of lithium-ion battery and a comparison of the different types are shown in Table 2.7. Lithium-ion batteries were discovered and developed in research laboratories in the 1970's and 1980's before being commercialised in 1991 by Sony [107]. In recent years the cost has decreased rapidly from over 1,000 \$ $(kWh)^{-1}$ for the battery pack in 2006 to less than 400 \$ $(kWh)^{-1}$ in 2014 [22]. The specific energy has also increased significantly, from under 100 Wh kg^{-1} in 1990 to over 250 Wh kg^{-1} in 2014 [7], which has led to their use in EVs.

The cycle life of lithium-ion batteries can be many thousands of cycles however for many of the potential applications a cycle life of 1,000 is all that is required. For example, consumer electronics generally become outdated before the battery reaches its cycle limit. Take for example an EV that can travel 200 miles, a cycle life of 1,000 would enable the EV to complete 200,000 miles. For grid scale applications, higher cycle lives may be required.

Table 2.7 Comparison of different types of lithium-ion batteries [30, 34]

	Capital cost	Typical power	Cycle life	Thermal runaway	Specific energy	Energy density
LCO	Low	1 C	700	150 °C	240 Wh kg^{-1}	640 Wh l^{-1}
LFP	Med	5 C	2000	270 °C	150 Wh kg^{-1}	300 Wh l^{-1}
NMC	Low	3 C	4000	210 °C	200 Wh kg^{-1}	400 Wh l^{-1}
NCA	Low	3 C	1000	150 °C	240 Wh kg^{-1}	670 Wh l^{-1}
LMO	Low	10 C	500	250 °C	240 Wh kg^{-1}	360 Wh l^{-1}
LTO	High	10 C	4000	N/A	130 Wh kg^{-1}	230 Wh l^{-1}

The two most significant disadvantages of lithium-ion batteries are the lack of recycling and safety concerns. Recycling is difficult as there may be many different materials inside a lithium-ion battery, as illustrated in Table 2.7. Safety concerns are related to the thermal runaway temperatures shown in Table 2.7, as above this temperature the battery will get hotter and hotter causing catastrophic failure, such as fire.

2.3.2.2 Lead-acid Batteries

The lead-acid battery has been around significantly longer than lithium-ion batteries, having been invented in 1859. Similarly to Lithium-ion batteries, there are many different types of lead-acid batteries, the most common differentiation being between flooded and valve regulated lead-acid batteries [108]. If charging at too high rate occurs, electrolysis of the water in the electrolyte may occur to produce hydrogen and oxygen. The difference between flooded and VRLA batteries is in the way they deal with this produced gas. Flooded batteries use a vent to allow the gas to escape, this means they periodically need to be topped up with water. VRLA batteries do not allow the gas to escape, unless a certain pressure is exceeded, meaning that the gases can be recombined to produce water and no topping up is therefore required.

Lead-acid batteries are operated in a similar way to lithium-ion in that the common charging technique is to use a CC – CV process and discharging is conducted using constant current. One of the main operational differences is that, while lithium-ion batteries generally have coulombic efficiencies around 99%, the coulombic efficiency of lead acid cells is lower, typically between 80 and 90% [109].

In terms of the other comparators, compared to lithium-ion cells, lead-acid batteries have lower cycle lives and lower specific energy and energy density than lithium-ion batteries, as shown in Table 2.6. The primary advantages of lead-acid batteries include the low capital costs and the ability to recycle the batteries, with over 95% of lead-acid batteries being recycled [30].

2.3.2.3 Supercapacitors

Supercapacitors were discovered in 1957 [110] and they are now commercialised but are not sold on the same scale as lithium-ion cells. Conventional capacitors have been around for much longer, since the 1700's. The supercapacitor is similar to a capacitor however has an energy density many order of magnitudes higher [105]. Although the energy density is higher than conventional capacitors, it is still significantly less than lead-acid and lithium-ion energy density, as shown in Table 2.6.

The main advantages of supercapacitors, are their good rate ability and their long cycle lives. Their main disadvantages are their low energy density compared to batteries and their high cost per unit energy stored.

2.3.3 Literature Review into Stationary Energy Storage at Fast Electric Vehicle Charging Stations

With an understanding of the important aspects associated with using a stationary energy storage at a fast charging station, i.e. the grid connection and types of stationary energy storage, this section investigates what research already exists into fast charging stations with stationary energy storage. The section is divided into academic research and commercial projects.

2.3.3.1 Academic Projects

There are many research papers written on the topic of stationary energy storage at fast charging stations and much of the current research focuses on management of the power flow. In [111] it was proposed that the stationary energy storage could be provided by a battery and superconducting magnetic energy storage hybrid system, the focus of the work was on the control strategy for the hybrid system. Similarly, in [112] flywheel energy storage was proposed for the stationary energy storage and the control strategy of the system investigated.

Other research papers look at the management of power flow but also add renewable electricity generation to the fast charging station with stationary energy storage. In [113] photovoltaic electricity generation was added to the fast charging station and a power flow management technique proposed. In [114] photovoltaic electricity generation was also paired with the fast

charging station and the whole system modelled. These systems provide the benefit of a fast charging station but also enable photovoltaic generation to be installed on the grid in locations where it may not have otherwise been possible to install the photovoltaic generation due to grid constraints, i.e. too much photovoltaic generation on the distribution network.

Another popular topic regarding stationary energy at fast charging stations is the design of the power electronic converters. In [115] a converter was designed for DC-DC power transfer between the charging station with stationary energy storage and the EV, the efficiency was quoted as over 99.5% for a wide operating range. In [116] DC-DC bidirectional converters were investigated to charge and discharge the stationary energy storage at a fast charging station and a specific type to converter chosen.

One difference between the research papers on stationary energy storage at fast charging stations is the number of EVs that are to be charged in a given time period and therefore the capacity and C-Rate of the stationary energy storage. In [103] the stationary energy storage is used to smooth out power fluctuations as different numbers of EVs arrive to charge. This results in a small capacity stationary energy storage that can operate at high C-Rates. At the other end of the spectrum, in [102] the stationary energy storage is used to store energy from the night, when few EVs are charging through to the day when many EVs are charging, resulting in a large capacity but low C-Rate stationary energy storage. In between these two examples are cases such as [104] where the stationary energy storage is used to store energy for one EV and then charges up once the EV leaves the fast charging station.

Some research has also looked at optimising the size of the stationary energy storage. In [117] an optimisation method was proposed for the capacity of the stationary energy storage based on costs and it was found that using stationary energy storage is not always the optimal solution but in some cases it can reduce costs and peak network load. This method was however proposed for PHEVs while in reality it is unlikely PHEVs would require fast charging stations as they could simply switch to running on gasoline if they run out of energy.

In [118] the effect of varying the number of EVs using the fast charging station each day on the size of the stationary energy storage was demonstrated. This research paper was part of a larger project whereby a demonstrator of the fast charging station was constructed [119]. In [120] a fast charging station system with supercapacitors was also constructed and experiments conducted to demonstrate the benefit for the electricity grid. In [121] a 64.2 kWh lithium-ion battery was used as the stationary energy storage for two fast charging points in Japan.

2.3.3.2 Commercial Projects

There are some examples of fast charging stations with stationary energy storage being constructed and installed. As expected, details of these systems are commercially sensitive and not readily available, however a select few of the projects are detailed below.

In Redwood City, California [122] energy storage has been installed with 16 DC fast chargers and is expected to save $7,000 per annum in demand charges. In Belgium and Germany, two fast charging stations using second life batteries have been installed at highway rest areas [123]. Stationary energy storage can also be used to charge electric buses, which generally require higher powers than EVs however the buses operate to a schedule so the charge and discharge regime of the stationary energy store is known [124]. For fast charging of buses in Geneva [125] supercapacitors are being used as the stationary energy storage to charge the buses at up to 400 kW.

Several projects have also been announced but not yet constructed where stationary energy storage is proposed at a fast charging station. It has been announced that 34 fast charging stations with lithium-ion batteries as the stationary energy storage will be installed along the Trans-Canada highway [126]. Two pilot locations for fast charging stations with lithium-ion batteries as the stationary energy storage have also been announced in Europe [127].

2.3.4 Conclusions from Stationary Energy Storage at Fast Charging Stations

The electricity grid is currently in a period of great change with changing demand from EVs and changing generation from uncontrollable renewable generation. Benefits of using stationary energy storage at a fast charging station include being able to use cheaper electricity at different times of the day to charge the stationary energy storage. When the stationary energy storage is not being used by the fast charging station there is also the potential for the energy storage to be used for other grid balancing services. A stationary energy store at the fast charging station combined with distributed electricity generation could also potentially enable the installation of distributed electricity generation at locations where this was not previously possible.

Although these ideas have potential for future benefits, in terms of fast charging stations being installed now, the primary benefit of energy storage is to reduce the maximum power demand from the grid. Lowering the maximum power demand reduces standing charges based on maximum capacity and can also negate the need for electricity grid infrastructure upgrade. The exact cost savings associated with a lower grid connection are likely to be highly dependent on

the exact location of the fast charging station as demonstrated by the large variations in connection costs found.

There are a variety of energy storage comparators and for each application it must be decided, which comparators are most important. No one energy storage technology will be suitable for all applications. For the fast EV charging station the energy storage will likely be small to medium size, therefore the large scale technologies such as pumped hydro and compressed air are not considered. Three technologies, lithium-ion, lead-acid and supercapacitors have been chosen that cover a wide range of the spectrum in the small to medium scale energy storage categories and these will be considered later in the thesis.

In terms of research already conducted into stationary energy storage at fast charging stations, there is clearly a consensus that stationary energy storage can be used at fast charging stations to lower the impact on the electricity grid. Many academic research papers exist and many commercial projects have been constructed or are currently in preparation.

There is however little research focus on optimising the capacity of the stationary energy storage. Optimising the capacity of the stationary energy storage is key as it must be large enough to ensure EV drivers arriving at the fast charging station do not have to wait because there is not enough energy in the stationary energy storage to charge their EV but small enough to make economic sense. Only one academic paper was found on optimising the stationary energy storage capacity and it focused on PHEV's, which are not considered in this thesis as it is thought they would refill with gasoline rather than use a fast charging station. The author's research into stationary energy store optimisation is detailed in Chapter 4.

2.4 Background to Thermal Modelling

This section looks at the fast charging limit of the EV cooling system and cell temperature limits in more detail. These limitations will likely be overcome through the design of innovative battery cooling systems, which can be designed through the use of thermal modelling. This section therefore starts by looking at current cooling systems used to cool lithium-ion batteries and then details of how thermal modelling is conducted. The section ends with a review of published research conducted into the thermal modelling of batteries.

2.4.1 Battery Cooling Systems

EV battery cooling systems are required to cool the cells in the battery pack to ensure that the cells do not exceed their temperature limits, which can result in the reduction of cell lifetime or

catastrophic failure as a result of thermal runaway if the cells become too hot. A second requirement for EV battery cooling systems is to keep all the cells in the battery pack a similar temperature to ensure cells do not degrade at different rates [128]. There are several ways to classify EV cooling systems [128], including:

- Does the cooling system provide heating and cooling or only cooling?
- Is the cooling fluid air or liquid?
- Does the cooling system pre-condition (active cooling) the cooling fluid or is ambient or cabin air used (passive cooling)?
- How is the heat transferred between the battery cells and the cooling fluid?

Cooling systems for batteries are not standardised with each manufacturer using its own preferred cooling design, the design of which is determined by aspects such as cost, weight and required cooling power. In terms of the method of heat transfer away from the battery cells, two examples are shown in Figure 2.13, one for cylindrical cells and one for pouch cells. The cylindrical cell cooling design shown on the left of Figure 2.13 is similar to that used by Tesla [129], where the coolant flows in a heat pipe next to the cells. The pouch cell cooling design seen on the right is similar to that used by LG [130], where cooling fins in between the pouch cells conduct heat to the cooling fluid underneath the cells, the fins may be solid metal or have coolant flowing within the fin.

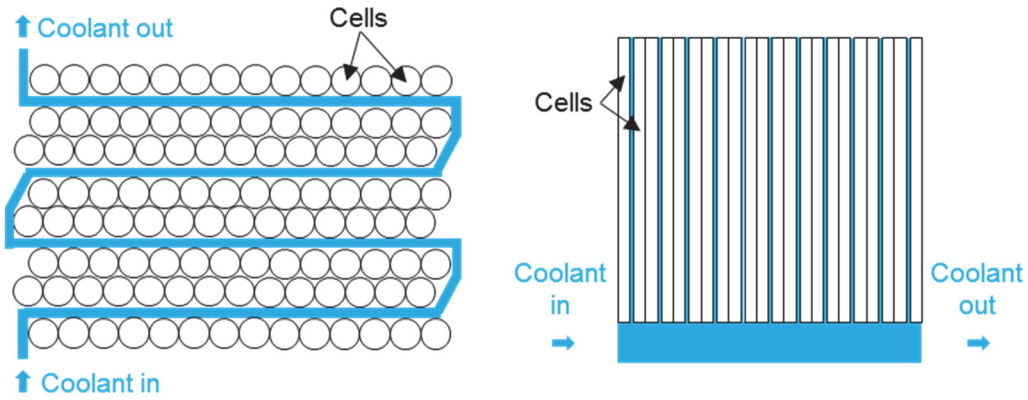

Figure 2.13 Example cell cooling techniques

Figures created by adapting data from [129, 130]

Research has been conducted into improved cooling system design for EVs to deal with the heat generated during fast charging [131]. Better cooling system design can create efficiency improvements however to achieve larger gains the cooling system will have to be made larger and heavier, which is not good for an EV. A more radical idea is to use stationary cooling at the fast

charging station [132], this means an EV does not have to drive around with an oversized cooling system to deal with the occasional fast charge. When an EV is charging at the fast charging station, in addition to the electricity delivered to the EV battery, coolant also flows from the charging station through the EV battery. This system is not currently commercially available but could be the subject of future research.

It is unclear exactly what the design of future cooling systems to deal with the excess heat generated during fast charging will look like, however, whatever the design it is likely thermal modelling will be required to assist with the design of the cooling system. The following sections therefore provide a background to thermal modelling of lithium-ion cells at high rates.

2.4.2 Overview of Thermal Modelling

The physical phenomena of a battery occur over a wide range of time and length scales. When modelling batteries it must therefore be decided on what length scale the model should be created. Modelling at smaller length scales adds more complexity and computational power but can increase the accuracy of the model [133]. Length scales vary from atomic variations to heat transfer over the entire battery pack, as noted below:

Atomic Scale < Particle Scale < Electrode Scale < Cell Scale < Module Scale < System Scale

The details of the chemistry inside the cells is not a focus of this thesis, hence the author has focused on thermal modelling at cell scale and above. Operating lithium-ion batteries within a limited temperature range, usually between 15°C to 35°C, is important for extending the lifetime of the battery [26]. Operating outside the specified temperature range will reduce the lifetime of the battery and, in addition, if the battery becomes too hot and the temperature exceeds the thermal runaway onset temperature, thermal runaway can occur leading to catastrophic failure [25]. Thermal modelling of lithium-ion batteries is therefore required during the battery design process to ensure the battery is designed to operate safely within the specified limits.

Generally, thermal models of batteries start with the first law of thermodynamics, relating the internal energy of the system (*U (J)*), the work done by the system (*W (J)*) (positive when energy transfer is out of the system) and the heat transferred into the system (*Q (J)*) (positive when energy transfer is into the system), as defined in Equation 2.2.

$$\Delta U = Q - W$$

Equation 2.2

Equation 2.2 is expressed in energy terms however each term can be divided by time to express the equation in terms of power. For battery models, the rate of change of internal energy of the system and the rate of heat transfer into the system are standard conditions for all thermal models. The rate of change of internal energy is related to the heat capacity (C_p *(J* K^{-1}*)*), the system temperature (T_1 *(K)*) and time (*t (s)*), as expressed in Equation 2.3. The rate of heat transfer into the system can either by conduction, convection or radiation modes, and is related to the thermal conductivity of the material (*k (W* m^{-1} K^{-1}*)*), the area (*A* (m^2)), length (*x (m)*), the temperature outside the system (T_2 *(K)*), the convective heat transfer coefficient (*h (W* m^{-2} K^{-1}*)*), and the Stefan-Boltzmann constant (*σ (5.67×*10^{-8} *W* m^{-2} K^{-4}*)*) as expressed in Equation 2.4.

$$\frac{d\Delta U}{dt} = C_p\left(\frac{dT_1}{dt}\right)$$

Equation 2.3

$$\dot{Q} = \frac{kA_1}{x}(T_2 - T_1) + hA_2(T_2 - T_1) + A_3\sigma(T_2^4 - T_1^4)$$

Equation 2.4

The rate work is done by the system is specific to batteries and is equal to the rate heat is generated or consumed in the battery ($\dot{Q}_{gen}$ *(W)*) and this is described in more detail in Section 2.4.2.1 below. Equation 2.2 for a battery can therefore be re-written in the form shown in Equation 2.5.

$$C_p\left(\frac{dT_1}{dt}\right) = \dot{Q} - \dot{Q}_{gen}$$

Equation 2.5

The length scale and model complexity determines how Equation 2.5 is used. For a systems level model this equation could be used once to model an entire battery pack. For a cell scale model this equation may be used thousands of times at thousands of points inside the cell. Two models can be seen in Figure 2.14 for the same cell. The model on the left treats the whole cell as the system and averages the internal energy, heat transfer and heat generated and consumed across the cell. On the model on the right each node is a system where there is internal energy and heat generation and consumption while the lines connecting the nodes indicate the heat transfer. On the model on the right the material properties, heat generation and consumption and heat transfer vary across the cell depending on the location.

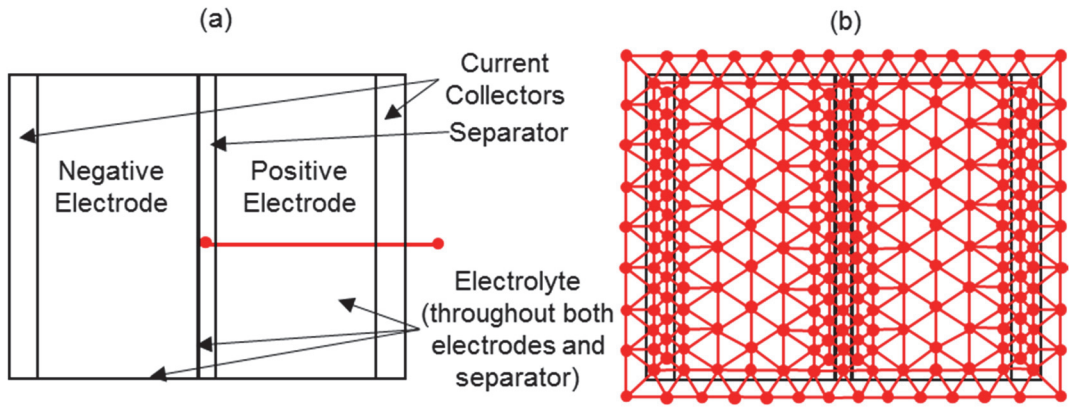

Figure 2.14 Thermal models of the same cell

Cell simplified to a single point (left) and detailed 2D model of cell (right)

Even though the model on the right of Figure 2.14 is clearly more complicated, the underlying equation is the same, using Equation 2.5. The difference is the model on the left uses the equation once while the model on the right uses the equation hundreds or thousands of times. The thermal models are time step models solving for temperature. For each time step the model calculates the temperature at each node before stepping forward in time and again calculating the temperature at each node. For models with more than a handful of nodes numerical solving techniques are used to calculate the temperature.

2.4.2.1 Heat Generation and Consumption

The final unknown of Equation 2.5 is the heat generation ($\dot{Q}_{gen}$ *(W)*), where this term quantifies the amount of heat generation and heat consumption at each point. In the majority of thermal models two heat generation terms are considered [134-136]: ohmic heating and reversible entropic heat. Depending on the required model complexity additional terms can be considered, including the heat produced or consumed by any chemical reaction, which includes side reactions which cause cell ageing and the heat of mixing, which is as a result of concentration gradients in a cell, however these terms are often negligible [137]. The chemical reaction in the cell is endothermic (absorbs heat) during charge and exothermic (generates heat) during discharge however in almost all cases the cell temperature increases during charge as the chemical reaction is weak in comparison to other heat sources [138].

The ohmic heating term is the heat generated as current passes through the cell and is always generating heat when a current exists. It is related to the current through the cell (*I (A)*) and the cell resistance (*R (Ω)*), as per the middle term of Equation 2.6. The entropic heat term is the entropy change of the cell reaction and it can either generate or consume heat. The entropic heat term is equal to the current multiplied by the temperature (*T (K)*) multiplied by the rate of change

in OCV of the cell (V_{OCV} *(V)*) with temperature, which varies depending on the cell SoC, as per the right term of Equation 2.6.

$$\dot{Q}_{gen} = I^2R + IT\frac{dV_{OCV}}{dT}$$

Equation 2.6

The entropic heat term therefore requires significant cell characterisation of the OCV versus temperature across the range of SoC which is a time consuming task [139]. Depending on the current rate of charge or discharge of the cell, either the ohmic heating term or the reversible entropic heat term may dominate. The ohmic heating term is proportional to the current squared while the entropic heat term is only directly proportional to current.

The resistance of the cell varies with time based on the cell SoC, current and temperature. Depending on the model complexity the resistance may also vary at different locations within the cell. If a single value for the cell resistance is used and the voltage of the cell (*V (V)*) and the cell OCV (V_{OCV}) are known the cell resistance (*R (Ω)*)) can be found using Equation 2.7 and the cell current (*I (A)*).

$$R = \frac{|V - V_{OCV}|}{I}$$

Equation 2.7

2.4.2.2 Equivalent Circuit Modelling

To make a thermal model predictive therefore requires the battery electrical response to be known and this can be accomplished using equivalent circuit modelling [140]. Equivalent circuit modelling is used to predict the voltage and current of a cell for a given load or power source profile. To understand an equivalent circuit model the relative complexity of models and their responses are shown in Figure 2.15. In its simplest sense, Figure 2.15a, a battery can be modelled simply as a voltage load or source but this does not give an accurate response to dynamic load changes [141]. In Figure 2.15b, the voltage varies with SoC. In Figure 2.15c an internal resistance is included, which accounts for the voltage drop or increase during discharge or charge. Figure 2.15d includes a resistor capacitor pair, where the capacitor adds a time dependent element to the model. The model can involve multiple resistor capacitor pairs in various configurations and it is up to the user to decide on the model complexity, where a common model often found in literature involves 2 resistor capacitor pairs and a resistor in series [142].

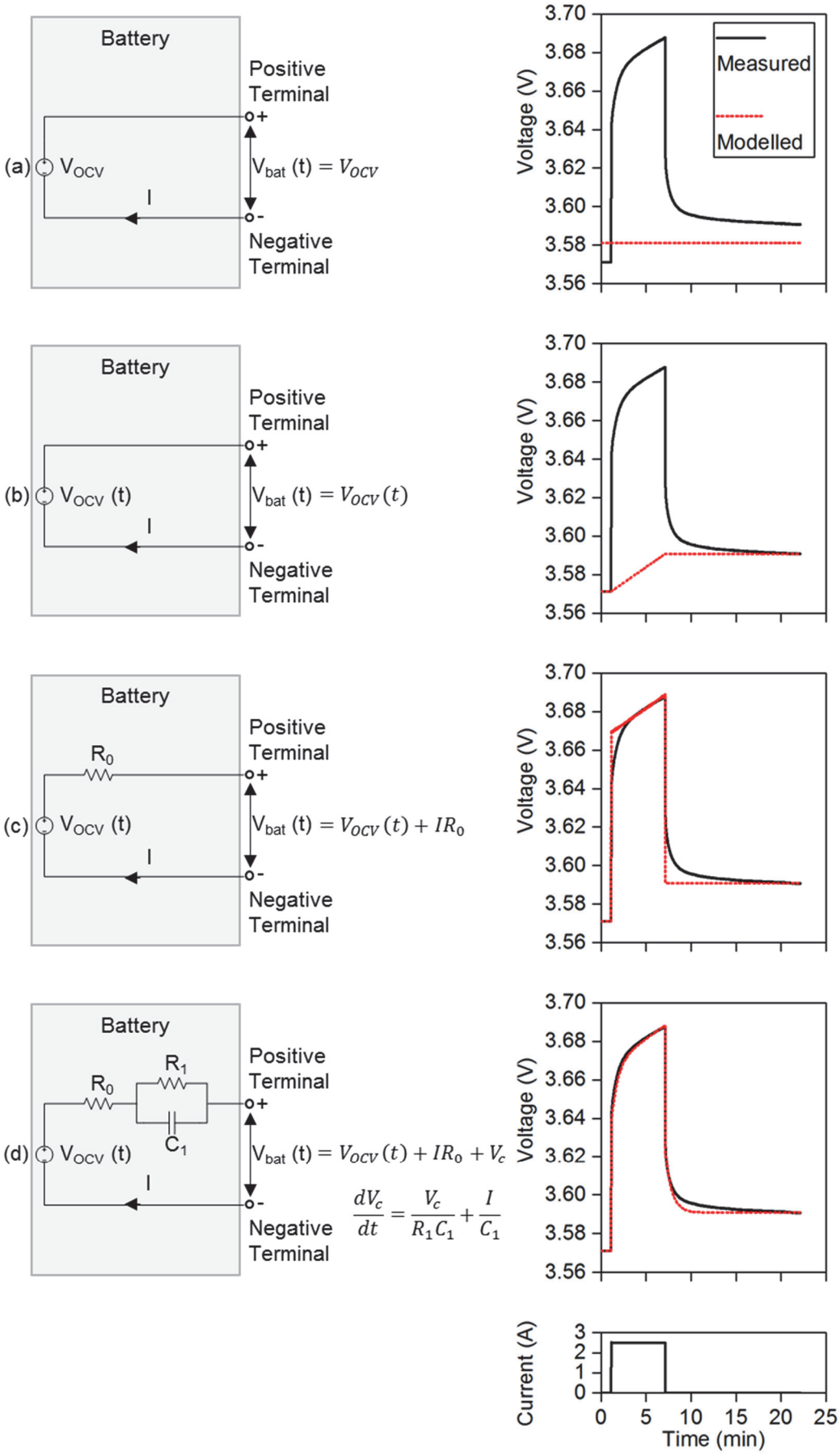

Figure 2.15 Equivalent circuit models of batteries and their voltage results

The charging current applied to the battery can be seen at the bottom of the figure

One issue with the equivalent circuit modelling method is that the resistance and capacitor values are not constant, as they vary with SoC, temperature and current [143]. An equivalent circuit model therefore consists of many large tables of data of values for the resistances and capacitances at different SoCs, temperatures and currents. As the model steps through time, it looks up the values of capacitance and resistance based on the SoC, temperature and current at the time.

This data is time consuming to obtain, at multiple SoCs, temperatures and currents a pulse test must be conducted on the battery. The results of the pulse test can be used to find the resistance and capacitance values. Researchers have also obtained good results matching modelled voltages to measured voltages using equivalent circuit modelling models [144].

2.4.3 Thermal Models of Batteries in Literature

In literature, there is a large range of thermal models. In this section some example thermal models are discussed for cylindrical, pouch and prismatic cells before looking at module and pack thermal modelling. In each case, the goal of the thermal model is to predict the battery temperature during charging and discharging. A common theme for the papers in the literature review is that complex battery characterization is required to obtain the inputs for the models. Many of the models below estimate the cell parameters, such as the heat capacity and thermal conductivity, using knowledge of the material make up of the cell, however often this is difficult to obtain.

In [145] a model of a cylindrical cell is created to estimate the internal temperature of the cell. The model volume averages the density, heat capacity and thermal conductivity meaning the temperature can be calculated by programming the finite difference calculations. The model achieves a good correlation between the measured and simulated temperatures, with a maximum error of less than 3°C. This model is contrasted by a different model of cylindrical cell [146], where the density, heat capacity and thermal conductivity are different for the casing, current collectors and the cell active materials. This model uses finite element modelling software to determine the temperature across the cell and the temperature trends follow correctly however the maximum error between the simulated and measured temperature is 5.2°C after a 3C discharge. In [147] a model of a cylindrical cell was created using 3D computer software. This model found an average error of 2°C over a range of discharge rates, including 0.5C, 1C and 1.5C. In [148] a thermal model of a cylindrical cell was created, using different properties for the cell core and surface. In this model the parameters were estimated during initial cycling and then these results were used to estimate the temperature in future cycling.

In [149] a thermal model of a pouch cell was created and validated using experimentation. This thermal model included an equivalent circuit model of the cell and had maximum errors of less than 1.1°C during discharges up to 5C. In [150] a 2D thermal model of a pouch cell was created, again equivalent circuit modelling was used to perform electrical modelling. This model was validated for three lithium-ion chemistries, NMC, LTO and LFP and the model matched experimental data within 2°C. In [151] a mathematical model was created of a pouch cell during charging, the model was coupled with an electrical model and the temperature distribution across the pouch cell estimated. The model was validated experimentally with errors up to around 5°C between the simulated and modelled temperatures.

In [152] a thermal model of a prismatic cell was proposed, the cell was tested using cooling and insulation to simulate the cell being in the middle of a battery pack. The measured surface temperature matched the modelled surface temperature within 1°C for the majority of the time during a 2C discharge and a 0.5C charge. In [153] a prismatic cell was thermally modelled and it was shown how including radiative heat transfer improved the model accuracy, however including the radiative heat transfer increases the model complexity. The model was validated experimentally at rates up to 3C and the accuracy was usually within 1°C. In [154] a prismatic cell was modelled to determine the core temperature during operation, this model also included an electrical model of the cell. The model was validated experimentally with temperature sensors placed in the core of the cell, the maximum core temperature error was found to be 2°C.

In [150] a thermal model of a pouch cell was created and validated experimentally, the model of the cell was subsequently used in a model of a module. The model was not validated experimentally however predicted temperature variations between the cells in the middle of a module and the cells on the outer edge of the module were found to be up to 3°C. In [155] a model of a battery module consisting of multiple cylindrical cells was created. The model was again only validated for a single cell and experiments on a module were not conducted.

2.4.4 Conclusions from Thermal Modelling

Thermal modelling is important to design battery pack cooling systems to keep cells within required temperature limits. It has been demonstrated that at the cell level and above, thermal models generally use the same principles, regardless of whether the cell parameters are lumped together or detailed models of the materials inside the cell are used. The heat generation during fast charging is likely to be a critical factor with ohmic heating being proportional to the charging current squared likely to prove the most significant factor.

As the principles of thermal modelling are well understood, many researchers have created models of cells that accurately predict the temperature of cells. There is less literature regarding the thermal modelling of battery modules and packs. One reason for this is the level of complexity of the individual cell models and the amount of effort to obtain the cell parameters required for the thermal models. As the thermal response of the battery may become a barrier to fast charging it is important to have models that are simple to characterise but accurate so they can be used in battery pack design to design cooling systems. The author's research into thermal modelling is detailed in Chapter 5.

2.5 Conclusions from Background

An overview of the topics covered in this thesis have been presented in this chapter. The main conclusions from this chapter include:

- EVs are required to reduce air pollution and combat climate change, Section 2.2
- One barrier to the uptake of EVs is the lack of fast charging, Section 2.2.1
- To achieve faster charging, advances in battery chemistry are required, Section 2.2.2.1
- If these chemistry advances are achieved, obtaining the required power from the electricity grid and the heat generated during charging are likely to remain barriers to fast charging, Section 2.2.2.1
- Stationary energy storage can be used at a fast charging stations, Section 2.3
    - At present, the main benefit to using stationary energy storage at fast charging stations is to reduce the maximum electricity grid connection power and thereby avoid infrastructure upgrade costs, Section 2.3.1
    - These grid connection costs vary significantly depending on location, Section 2.3.1
    - In the future, there may be other benefits such as charging the energy storage at times of lower electricity cost and smoothing power fluctuations, Section 2.3.1
    - Depending on the requirements, lithium-ion, lead-acid or supercapacitors may be appropriate for use as the stationary energy storage, Section 2.3.2
    - The requirements, i.e. capacity and charge and discharge rate, of the stationary energy storage are not currently well understood, Section 2.3.3
- Thermal modelling can be used to design the battery cooling system to keep the cells within acceptable temperature ranges during fast charging, Section 2.4
    - Thermal models with different levels of complexity use similar underlying principles, Section 2.4.2
    - The ohmic heat generation is proportional to the current squared and is likely to dominate the thermal limit to fast charging, Section 2.4.2.1

- Existing thermal models of batteries produce good results for cell temperature when compared to experimental results, Section 2.4.3
- These existing models do however require significant, time consuming tasks to obtain the required thermal parameters, which are not normally included on the cell datasheets, Section 2.4.3

What is clear from the literature review is that although other researchers have studied using stationary energy storage at fast charging stations, none have focused specifically on how large, in terms of capacity, the stationary energy storage needs to be. Researchers state sizes for the stationary energy storage however very few attempt to justify the size of the stationary energy storage and most simply assume a size and look at the results.

A key parameter to determine the optimal stationary energy storage size is the time of day that future EVs will use fast charging stations, which dictates when and how fast the stationary energy store will charge and discharge. It was found that the estimates other authors used for predicting the time of day usage of fast charging stations were not adequate, a literature review regarding this is conducted in Chapter 3. The first research objective for this thesis is therefore to propose a novel method to predict the time of day that future EVs will use fast charging stations. The second research objective for this thesis is then to use this output to propose a novel method to determine the size of the stationary energy storage at the fast charging station.

From the literature review it was shown that there are many thermal models that can predict the surface temperature of cells. Few of these models however extend to battery modules and packs, one reason for this is the difficulty in obtaining the thermal parameters of the cells. The third research objective of the thesis is therefore to create a method to easily obtain the cell parameters required for thermal modelling of battery modules and packs. It is also thought from the literature review that the thermal response of the EV battery is a potential limit to the future fast charging ability due to the additional heat generation when the battery is charging at high rates, defined here as a rate over 1C. Therefore the fourth research objective of the thesis is to demonstrate a thermal model that works well at high rates.

The thesis research question is: how can the electricity grid capacity and cell thermal limitations of electric vehicle fast charging be overcome? To answer the research question the thesis therefore has the following research objectives along with their placement in the thesis:

1. Create a method to predict at what time of day people will use fast charging stations, Chapter 3
2. Create a method to determine the required size of stationary energy storage to be used at fast charging stations, Chapter 4
3. Create a simple method to obtain the parameters required for thermal modelling of lithium-ion cells, Chapter 5
4. Demonstrate a lithium-ion cell thermal model that can be used for high rate applications, Chapter 5

One further idea that was considered during the PhD was to use a hybrid solution for the stationary energy storage, for example an energy store consisting of lead-acid cells and supercapacitors. While conducting preliminary research into this topic it was noticed that there are currently no thermal models that are applicable for multiple types of energy storage devices (lithium-ion, lead-acid and supercapacitors). This type of model has the potential to work, as the literature review in Section 2.3.2 showed that all three types of energy stores have some similarities, such as all being electrochemical devices and all having an internal resistance. A model covering all three types of energy store would be useful and so this gives rise to the fifth and final research objective of the thesis:

5. Extend the lithium-ion cell thermal model to lead-acid and supercapacitor cells, Chapter 5

Chapter 3 Fast Charging Station Usage

The aim of this chapter is to model and predict the number of EVs using a fast charging station as a function of the time of day, using a forecasting modelling technique. The analysis is conducted using a dataset from the northwest USA [156] however the methods proposed could be applied to any similar dataset and as such the methods described in this chapter are one of the novel outputs of this thesis. There is one published journal paper associated with this section: Thomas S. Bryden, George Hilton, Andrew Cruden, Tim Holton, Electric vehicle fast charging station usage and power requirements, Energy, Volume 152, June 2018, Pages 322-332, 10.1016/j.energy.2018.03.149 [28]. After being published in June 2018, at the time of thesis submission in February 2019, this paper has six citations.

This chapter concerns fast charging powers and so it is important to know the charging capability of current EVs and fast chargers. The fast chargers have been described in Section 2.2.2 and a table of a selection of EV charging capabilities can be seen in Table 3.1.

Table 3.1 Commercially available EVs and their maximum charging power

EV	Maximum Charging Power (kW)	Battery Capacity (kWh)	WLTP Combined Range (miles)	Efficiency[1] (miles / kWh)	Maximum Charge rate[2] (miles / min)	References
Audi e-tron	150	95	248.5	2.6	6.5	[157, 158]
Hyundai KONA	77	64	289	4.5	5.8	[157, 159]
Jaguar I-PACE	85	90	292	3.2	4.6	[46, 157]
Nissan Leaf	50	40	177	4.4	3.7	[41, 157]
Tesla Model S	120	100	424*	4.2	8.5	[39, 157]

1 Calculated as (WLTP Combined Range) / (Battery Capacity)
2 Calculated as (Maximum Charging Power) * (Efficiency) / 60
* Taken from Tesla website, not WLTP Combined Range

3.1 Motivation for Predicting Usage

When investigating stationary energy storage at fast EV charging stations one critical parameter is estimating the time of day when EV drivers will want to use the fast charging station. This usage dictates when and how fast the stationary energy storage will need to charge and discharge within the constraint of a fixed grid connection capacity. When many drivers are using the fast charging station the energy store will discharge and when few drivers are using the fast charging station the energy storage will charge. The aim of the chapter is therefore to estimate this usage pattern and estimate the number of vehicles using a fast charging station throughout the day. The details of how this usage is converted into a charge and discharge regime for the stationary energy store, along with the method to determine the capacity, are detailed in Chapter 4.

A time length of one day is chosen for estimating the usage because, as discussed in Section 2.2, this is often the maximum duration for the potential stationary energy storage technologies considered for this project, for storage durations longer than one day the use of batteries is considered uneconomical [21]. There will be variations in fast charging station demand throughout the weeks and months, for example more people wanting to use fast charging stations for their long distance journeys around holidays and variations over the weekend, which are analysed in Section 3.6.

The motivation for this chapter came about as it was believed that the inputs for fast charging station usage by time of day that other authors had used were unrealistic and often the fast charging station usage was not the focus of the research. In [118] the fast charging station usage was assumed to be directly proportional to the number of cars on the road. In [160] the usage was directly proportional to the current usage of gas stations. Both of these studies crucially did not take into account that most EVs will utilise overnight slow charging and hence predicted usage peaks in the morning and evening when there are most vehicles on the road, in the method described in this chapter a fully charged battery at the start of the day is assumed. In [161] a questionnaire was used to ask people to estimate when they might use a fast charging station in the future and the usage of fast charging stations predicted from the results. In [162] the usage predicted was based on commuters using the fast charging station, while in [163] the usage was based on people forgetting to charge their EV overnight and hence using fast charging stations in the morning.

Importantly, all the studies mentioned do not take into account long distance journeys and all the studies also assume low EV battery capacities, between 10 and 54 kWh, despite the fact that some low cost EVs will soon have battery capacities over 60 kWh. The method adopted in this chapter is novel as the fast charging station usage is predicted based on current driving habits,

regular slow charging is taken into account, larger EV battery capacities are assumed and the study looks solely at long distance journeys.

3.2 Forecast Modelling

This chapter studies and develops forecast modelling to predict the future and is hence an inexact science however the aim is to study future scenarios, to quote Henri Poincaré: “It is far better to foresee even without certainty than not to foresee at all” [164]. The forecasting is made less reliable as the automotive industry is currently in the process of four major changes driven by disruptive technology [165]. One of these changes is electrification, i.e. more EVs, the other three are connectivity, autonomous driving and diverse mobility. These changes and their potential impacts on fast charging station usage are described below.

Connectivity refers to vehicles being connected to the internet by a mobile network and also connected to users smart devices [166]. Connectivity can enable services such as checking the vehicle’s location, battery level, tyre pressure readings and sending information about the vehicle’s technical status to car services. The impact of connectivity on EV charging includes the connection of the vehicle to the vehicle owner’s calendar [167], which could enable the smarter charging of EVs. The EV would know from the calendar which journeys were to be conducted in the future and therefore how much energy was needed from charging for these journeys. In addition, communication between infrastructure, such as fast charging stations, and vehicles could enable drivers to book a time slot to charge their EV to spread out the demand at fast charging stations.

Autonomous driving refers to vehicles driving themselves without human control. There are different levels of autonomous driving, ranging from the common adaptive cruise control and lane centre technologies through to fully autonomous vehicles that can drive without a human in the vehicle [168]. An impact of autonomous vehicles on EV charging is that fully autonomous EVs could potentially drive themselves to charging stations when the vehicle is not in use, which could lower the number of fast charges required as each vehicle receives more slow charges.

Diverse mobility or vehicle sharing refers to sharing the usage of a vehicle fleet between members of a scheme [169]. Individuals do not personally own a vehicle, instead they pay based on a per journey basis. When an individual wants to make a journey one simply summons the vehicle. Diverse mobility therefore goes hand in hand with connectivity and autonomous driving, meaning the vehicle drives itself to where it is required. One impact of diverse mobility on fast charging of EVs is that it could enable people to simply swap vehicles on long distance journeys meaning they do not have to stop to fast charge their vehicle. On the other hand, diverse mobility may mean

that vehicles are utilised much more, i.e. they are driving for near 100% of the time because as soon as they have dropped someone off they are picking someone else up, meaning regular fast charges are required.

Clearly these three major changes will affect the automotive industry, and also the usage of fast charging stations, significantly in the future. The analysis conducted in this chapter uses current journeys conducted in gasoline vehicles to estimate when fast charging stations will be required in the future. The assumption is that people will need to conduct the same journeys in the future that they conduct now, where this assumption does also recognise some of the changes described above. Even with connected vehicles, autonomous driving and diverse mobility, the journeys people make will still be largely dictated by the same requirements as now, for example needing to see relatives or driving to a meeting for work. There is therefore no direct adjustment for these three major automotive industry changes, they are discussed here to ensure the reader is aware of the limitations of the forecast modelling conducted in this chapter.

3.3 Method for Predicting Usage

The method proposed to predict fast charging station usage relies on the use of GPS data from current gasoline car journeys, assumes all the journeys are instead conducted using EVs and then estimates when fast charging stations will be used. The method of using gasoline car data to predict EV usage has been used in the past. In [170] gasoline vehicle data was used to determine that, based on average driving distances, an EV with a range of 100 miles would cover 95% of journeys. The issue with using average distances when designing EVs is that people will not buy the car if it meets only their average needs and not nearly all of their requirements.

In [11] the gasoline GPS data was used to create a plot of daily distance driven versus the percentage of drivers for whom the distance satisfied 100% of their daily driving requirements. It was found that although 44.7 miles was the mean daily distance driven an EV, if an EV with a range of 44.7 miles was introduced this would only satisfy 100% of the journeys conducted by around 2% of the population. In other words, 2% of the population never drove their car more than 44.7 miles in a single day over the course of the survey. The method proposed in this section uses a similar methodology, in that historical gasoline vehicle GPS data is used to predict EV requirements, however the method proposed focuses on fast charging, a topic which is not researched in the other studies.

The GPS data required for the method includes start and end date and time of the trips, the distance travelled for each trip and whether the trip begins or ends at home or at work. Some sample data from one car for three days can be seen in Table 3.2.

Table 3.2 Required data format for fast charging station usage model

This table shows 13 trips while the whole study consists of over 750,000 trips

Vehicle identifier	Trip start	Trip end	Distance travelled (miles)	Does the trip end at home or work?
311	21/08/2005 06:51	21/08/2005 07:03	3.078273	no
311	21/08/2005 08:43	21/08/2005 09:38	25.67754	no
311	21/08/2005 11:58	21/08/2005 12:05	1.951106	no
311	21/08/2005 13:43	21/08/2005 14:12	24.44847	no
311	21/08/2005 14:16	21/08/2005 17:02	178.1173	no
311	21/08/2005 17:06	21/08/2005 18:21	80.26314	no
311	21/08/2005 19:00	21/08/2005 22:34	233.3845	yes
311	22/08/2005 06:44	22/08/2005 07:05	9.64803	yes
311	22/08/2005 10:41	22/08/2005 10:50	4.312316	no
311	22/08/2005 10:56	22/08/2005 11:09	4.230295	no
311	22/08/2005 12:31	22/08/2005 12:40	4.232781	yes
311	22/08/2005 15:55	22/08/2005 16:18	9.681585	yes
311	23/08/2005 04:27	23/08/2005 04:59	29.26161217	no

One aspect missing from the data is the exact location, for example was the journey conducted on city roads or motorways. The use of location data could improve the accuracy by determining exactly what type of journey the driver was making, this data however is not commonly available due to privacy constraints.

The main assumptions are that all gasoline cars are replaced with EVs and that people will continue to make the same journeys in EVs as they currently do in gasoline cars. The method subsequently uses this historical gasoline driving data to predict fast charging station usage and charger power ratings assuming all the trips are conducted in such EVs. Two further assumptions are:

1. A slow charge to a fully charged state will occur whenever the vehicle is at home or work or whenever the vehicle is parked for more than 8 hours
2. After a vehicle has been driven greater than an assumed distance, defined below, after a slow charge a fast charge is required, this assumed distance is varied throughout the analysis

The first assumption is made as the analysis is regarding the future when there are significantly more EVs on the road and as such it assumed that slow chargers will be common to charge EVs when stopping for long periods or at home or work. Being able to charge an EV at home or work

or wherever there is a slow charging station is an advantage of EVs over gasoline vehicles, EVs do not require specific trips to be made to gas stations. It is therefore assumed that, if all vehicles on the road are EVs, slow chargers will be common.

The second assumption is made to estimate when a fast charge is required. One issue with this assumption is that with use of detailed journey planners, EV drivers will know how many fast charges are required for a journey and so may not always drive their maximum distance before using a fast charging station. For example, assuming a 200 mile driving range and a 300 mile journey, the driver would know one fast charge is required and so may use a fast charging station 150 miles into the 300 mile journey, while for this case the model would assume the fast charge occurs after 200 miles. However, as more fast charging stations are installed the EV driver will have more options of charge locations and so it is likely that the driver would want to go as far as possible before recharging. If the EV driver uses the fast charging station earlier in their trip it may move the fast charge station usage peak slightly earlier in the day.

The assumed distance, hereafter referred to as driving range, is not the automaker's advertised EV range but the distance that the EV driver will drive before requiring a fast charge. This distance is equal to the range of the EV minus the buffer energy in the EV battery that the driver leaves to feel comfortable that their EV will not run out of energy. The driving range is varied throughout the section, for analyses later in this section 200 miles is taken as a base case for the driving range. Many affordable EVs being released now have ranges of over 200 miles, for example the Chevrolet Bolt [40], 238 miles $37,495, and the Tesla Model 3 [39], 215 miles $35,000. Although it is unlikely drivers of these EVs would be comfortable driving 200 miles between charges, the trend for larger battery capacities and greater ranges is clear so 200 miles is a reasonable assumption for the future driving distance between charges.

To use these assumptions to estimate the fast charging station usage variation throughout the day Equation 3.1 is used. It is assumed that the fast charge occurs once the EV has driven the assumed driving range after a slow charge, when it is assumed the EV will be fully charged. The average speed during the trip is used to determine the time of day that the fast charge occurs (FC_{time} *(s)*), this is calculated using the trip start (t_s *(s)*) and end time (t_e *(s)*), the assumed driving range (d_r *(m)*), the length of the trip (d_t *(m)*) and the cumulative distance travelled since the previous slow charge (d_c *(m)*). An example is shown in Figure 3.1, where the driving range has been assumed to be 200 miles, where two fast charges are required in the day shown, one at around 4:30pm and one at around 8pm.

$$if\ d_c > d_r: FC_{time} = t_s + (t_e - t_s)\frac{d_c - d_r}{d_t}$$

Equation 3.1

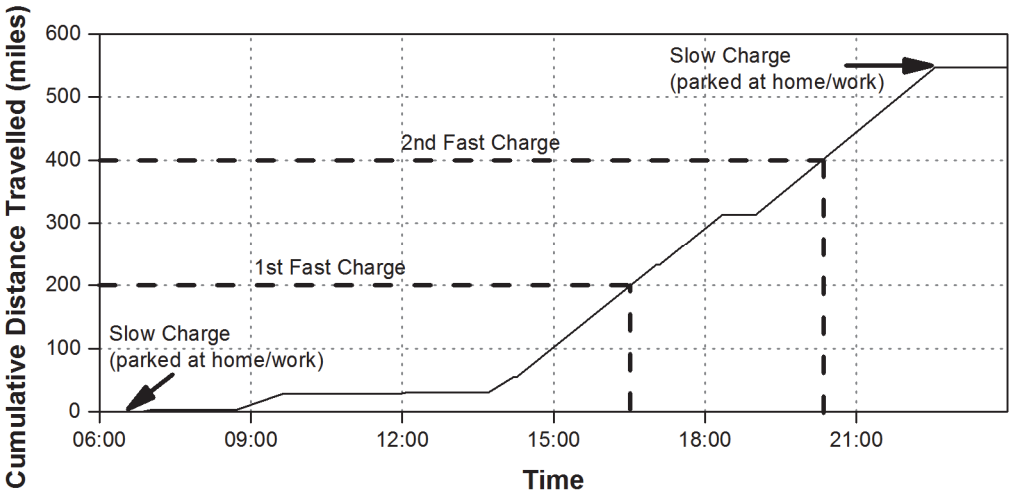

Figure 3.1 Example of assumed fast charge usage during daily driving

The figure is created using the data from Table 3.2

3.4 Description of Data used for Analysis

The method described is demonstrated using data from the Puget Sound Regional Council 2004-2006 Traffic Choices Study [156]. The data is freely available from the NREL Transportation Secure Data Center website [171]. Although the dataset is from 2004-2006 the data is for gasoline powered vehicles and so remains relevant as driving habits have not changed drastically since 2004-2006 and it is assumed that people would conduct the same number of long distance journeys by car today as they would have done in 2004-2006.

The Puget Sound region is in Washington State, USA and includes the city of Seattle. The data was collected by placing GPS data loggers in gasoline cars and recording all trips. The data involves over 750,000 individual trips made by about 275 different households using a range of vehicles. This data was chosen over other GPS surveys as each car in the Puget Sound study was recorded for a long duration, an average of approximately 18 months.

The exact location of the start and end of each trip was not made available due to privacy constraints, however notable data available for each trip includes the start and end date and duration of the trip, the distance travelled for each trip, the vehicle identifier and whether the trip begins or ends at home or at work. An example of the distance travelled each day for one vehicle in the study for one year is shown in Figure 3.2.

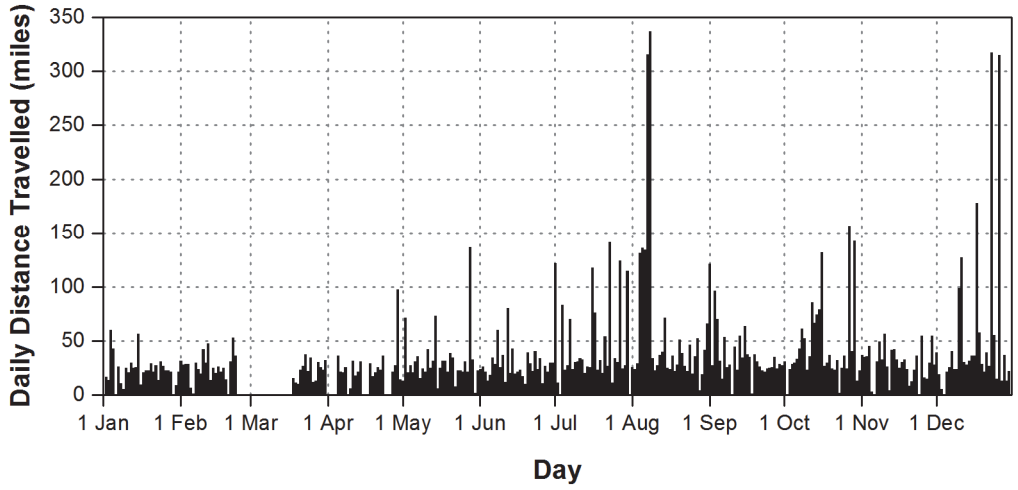

Figure 3.2 Daily distance travelled for a single car from the Puget Sound study

The data includes 4.5 million miles driven and included 185,000 vehicle driving days, meaning that each vehicle drove on average 24.3 miles per day. The mean, standard deviation and maximum values for the trips in the data can be seen in Table 3.3. In Figure 3.3 the number of trips greater than various distances are shown, it can be seen that the majority of the 750,000 trips are less than 40 miles with around 8000 being greater than 40 miles.

Table 3.3 Overview of the data

Parameter	Mean	Standard Deviation	Maximum
Individual trips distance (miles)	6.2	10.1	344
Individual trips duration (minutes)	13.5	14.3	329

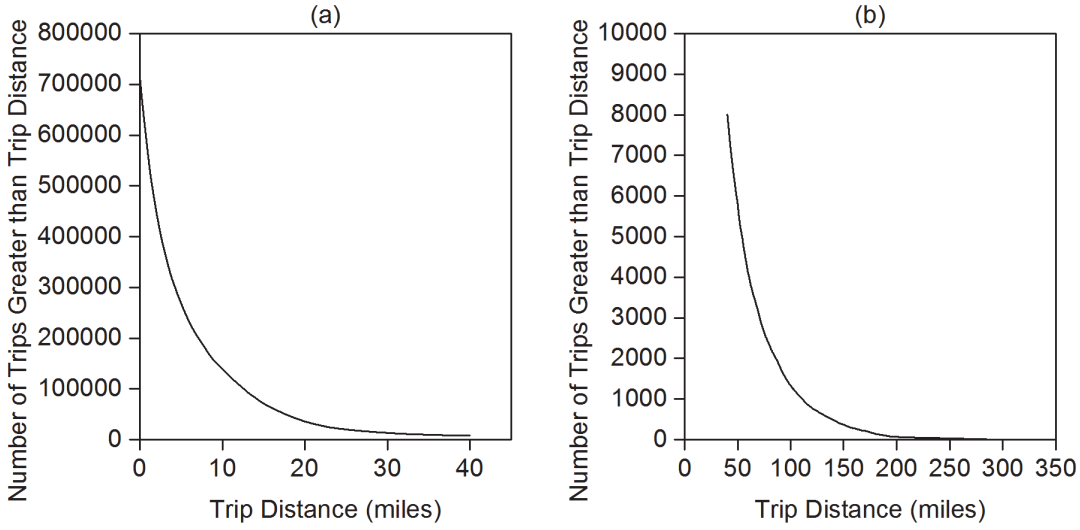

Figure 3.3 Number of trips in the dataset greater than various distances

Both figures are the same graph but on different axes, trips less than 40 miles (left) and trips over 40 miles (right)

The variation in trips throughout the year can be seen in Figure 3.4. Figure 3.4a shows how there is some variation in the number of trips and distance travelled through the months, with the summer months (May-Aug) having more trips and more distance travelled. This seasonal variability is magnified when looking at Figure 3.4b and it can be seen that significantly more long distance trips are made the summer months. Specifically, July and August have almost twice as many journeys over 50 and 100 miles than the other months, potentially indicating people driving long distances for their summer holidays.

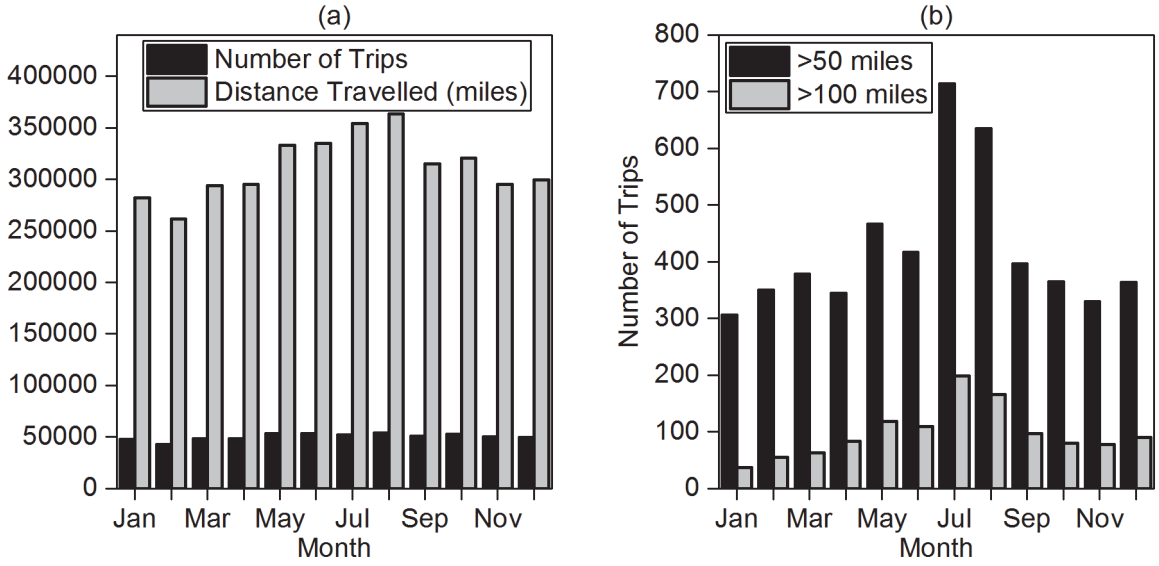

Figure 3.4 Variation in trips throughout the year

Number of trips and distance travelled (left) and number of trips over 50 miles and 100 miles (right)

3.5 Results and Discussion for Predicting Usage

By assuming a driving range (d_r) of 200 miles, using Equation 3.1 and going through all 750,000 individual trips the average predicted time of use of fast charging stations throughout a day is shown in Figure 3.5.

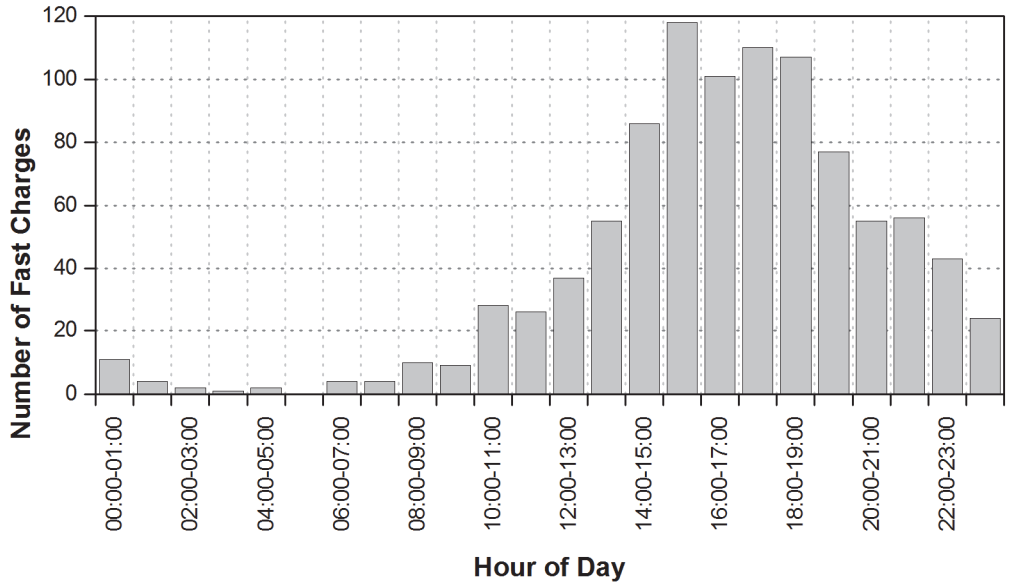

Figure 3.5 Fast charging station usage throughout one day

The results are interesting as contrary to other studies, which predict fast charging usage peaks in the morning and evening, the results shown here predict fast charging station usage will peak between 3 pm to 7 pm in the evening, with 45% of all daily fast charges occurring in these 4 hours. This evening peak is apparent from the method described here as EV drivers charging their EVs overnight are considered while other studies do not consider this, meaning that fast charging station usage during the morning is less likely in the results shown here. Overnight home charging is a significant advantage of EVs over gasoline vehicles and so it is assumed that in the future all EVs will utilise overnight charging, either from a home or street charging point.

The driving range affects the number and time of day that fast charges occur. The effect of varying the driving range between 150 and 250 miles was therefore investigated and the results are shown in Figure 3.6. The absolute values are shown in Figure 3.6a, while Figure 3.6b has been normalised by converting the number of fast charges per hour into a probability that the fast charge will occur within that hour. The results from Figure 3.6b show the shape of the distribution is similar for all three cases, giving confidence that even though the number of fast charges may vary, the shape of the distribution will be the same. It can be seen that the results predict that fast charging stations will be used less in the night and morning and more in the afternoon and evening. The result from Figure 3.6b is the main output from this chapter and is used in future chapters to determine the requirements of the stationary energy storage.

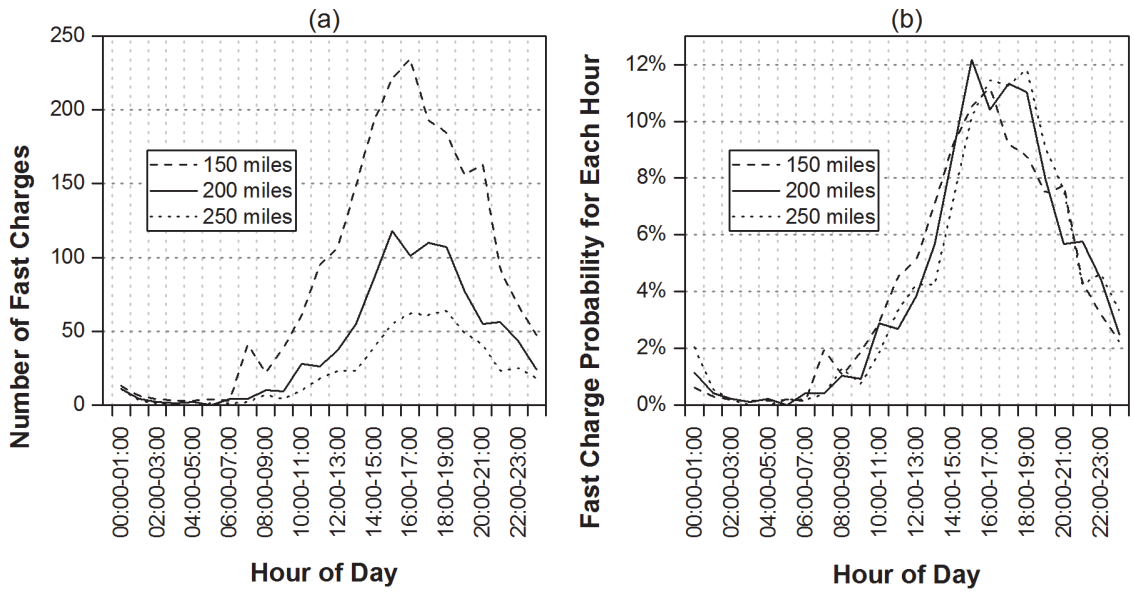

Figure 3.6 Sensitivity study varying the driving range between 150 and 300 miles

Absolute values (left) and normalised values (right)

A peak between 3 pm and 7 pm in the evening means the peak power demand from the fast charging stations will coincide with the peak power demand of the electricity grid, which occurs around 5 pm in the UK [172]. This highlights the benefit of using stationary energy storage at the fast charging station as if the stationary energy store is not used, additional peak electricity generation capacity will be required to cope with the electricity demand from fast charging stations.

The fast charging usage peak also occurs around the same time of day as the slow charging peak [173], which is predicted to occur in the evening when people come home and plug in their EV. For this reason, smart charging solutions, where slow charging events are shifted to other parts of the day or night to reduce peak demand [174], may be required.

From Figure 3.6b it can clearly be seen that the fast charging station demand, and therefore the electricity demand at the fast charging station, is predicted to vary throughout the day. The use of stationary energy storage at the fast charging station could therefore reduce the peak electricity demand and therefore the grid connection costs.

As described in Section 3.2, the automotive industry is currently going through multiple large changes and it is impossible to forecast exactly what the automotive industry will look like in the future. The method adopted in this section has the advantage of using few assumptions and so users of the method will be able to understand the limitations of the method and therefore the limitations of the results. This will enable users to make decisions based on the results because they understand limitations. Other key considerations include:

- The method only considers fast charging station usage for long distance journeys. There may be other people who use fast charging stations, such as people who do not have access to slow charging at home or work or people who forget to charge their EV overnight.
- The exact location of the fast charging station is not considered and may affect the daily usage, for example a fast charging station a few hours from London may have significantly higher usage on a Friday evening with people leaving London for the weekend.
- It has been assumed that the EV will be fully charged when stopping for 8 hours or stopping at home or work. This may not be the case, especially if the EV driver is staying away from home overnight, less slow charging would increase the usage of fast charging stations.
- As seen in Figure 3.6a, the actual number of fast charges is very sensitive to the distance the EV travels between fast charges. The actual number is therefore highly variable depending on the future range capability of EVs and the buffer energy that EV drivers will leave in the battery to give them confidence that they will not run out of energy during their trip. The method is based purely on EV energy analysis, while in reality psychological factors must also be taken into account, for example range anxiety.
- The results displayed here are specific to the participants of the Puget Sound survey and the results will likely vary depending on the user population. People from the USA are known for driving long distances in larger cars compared to consumers in Europe or Japan, meaning people from the USA may require more fast charges.

An interesting topic for further work includes looking more at the psychological factors, such as variations in the way EV drivers will use their battery [175]. Some drivers will recharge when the battery is 60% full while others will wait until 10% full before recharging and it would be interesting to try and take this into account in the method and see the impact on the results. It would also be interesting to conduct similar analysis with a dataset from a different country to see how the results varied.

3.6 Additional Fast Charging Station Usage Results

The actual number of fast charges per million vehicles is a useful metric for organisations planning the rollout of fast charging stations to ensure there are sufficient numbers of fast charging stations available for the number of EVs on the road. The actual number of fast charges can be found by dividing the values seen in Figure 3.5 by the number of days in the survey multiplied by the number of cars. By summing all the values in Figure 3.5, the total number of fast charges required over the survey period is 970, which can be converted to 5,200 fast charges per day per

million vehicles. In the UK, there are currently around 30 million cars, so, for example, if half of these cars were replaced with EVs the fast charging infrastructure would have to cope with 80,000 (5,200 fast charges per day per million vehicles x 15 million vehicles) fast charges per day.

This actual value is highly dependent on the driving range of EVs in this case assumed as 200 miles. The graph in Figure 3.7 demonstrates how the number of fast charges per day is predicted to vary depending on the driving range. As the driving range increases more of the journeys could be completed without fast charging the EV battery and this is why the number of fast charges is predicted to decrease with increasing driving range. As driving range increases there will be less fast charges per million EVs however increased driving range will increase EV uptake meaning more EVs on the road. Even with driving range improvements and hence less fast charges there is always likely to be a market for fast charging stations as potential EV owners often ask for public charging facilities before buying the EV [176].

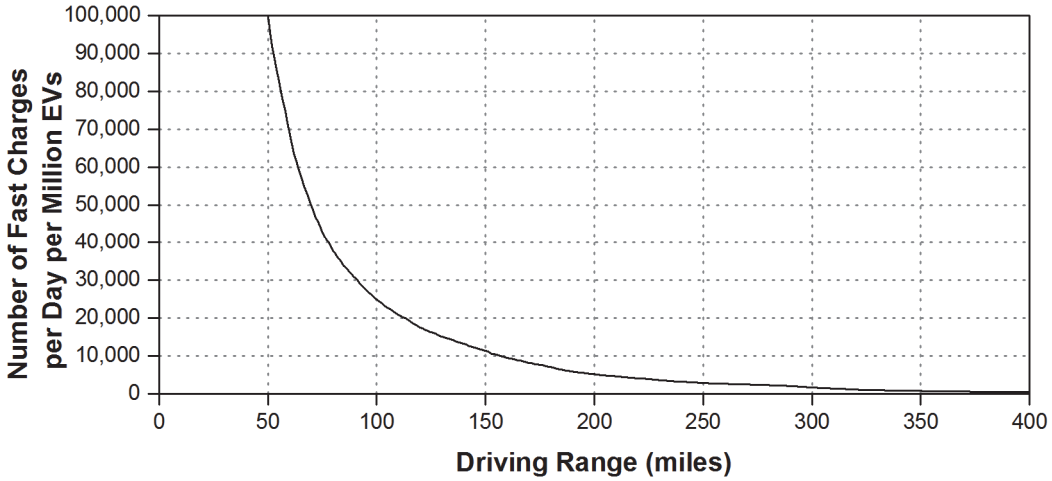

Figure 3.7 Number of fast charges required per day for various assumed EV driving ranges

Figure 3.6 demonstrated how the usage of the fast charging stations is predicted to vary throughout one day. The results displayed however were the average results for all days, there will however also be variation in usage based on the day of the week. Figure 3.8a shows the variation in number of fast charges by day of week. The average for all days is the value previously mentioned of 5,200 fast charges per day per million vehicles, as before the driving range is assumed to be 200 miles. It can be seen that fast charging station usage is predicted to peak over the weekend. This is likely because during weekdays people are making shorter regular journeys, namely commuting to work, while over the weekend people travel longer distances to get away for the weekend. Figure 3.8b shows the same plot as Figure 3.5, converted to a per million vehicles value, for a Sunday, the day when most fast charges are required.

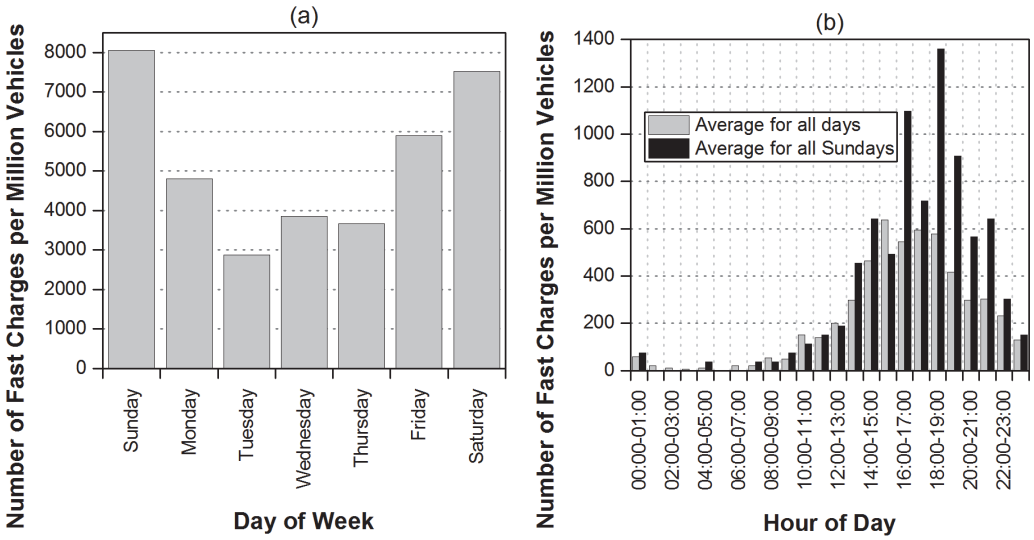

Figure 3.8 Variations in number of fast charges by day of week

Day of week variation in number of fast charges (left) and fast charges by time of day on Sundays (right), the driving range is assumed to be 200 miles

As well as variation by day of week there will also be variation in fast charging station usage by time of year. The data used was from the United States where it is thought people are most likely to take long distance journeys around the holiday periods of Christmas or Thanksgiving. The predicted fast charging station usage around Christmas and Thanksgiving is shown in Figure 3.9. From the data available there are not enough instances of fast charges being required around holidays to draw definitive conclusions, with only 29 and 53 fast charges required over the one Thanksgiving week and two Christmas weeks respectively. It does however make sense that more long distance journeys would be made around holidays and so when designing fast charging stations, holiday periods should be considered.

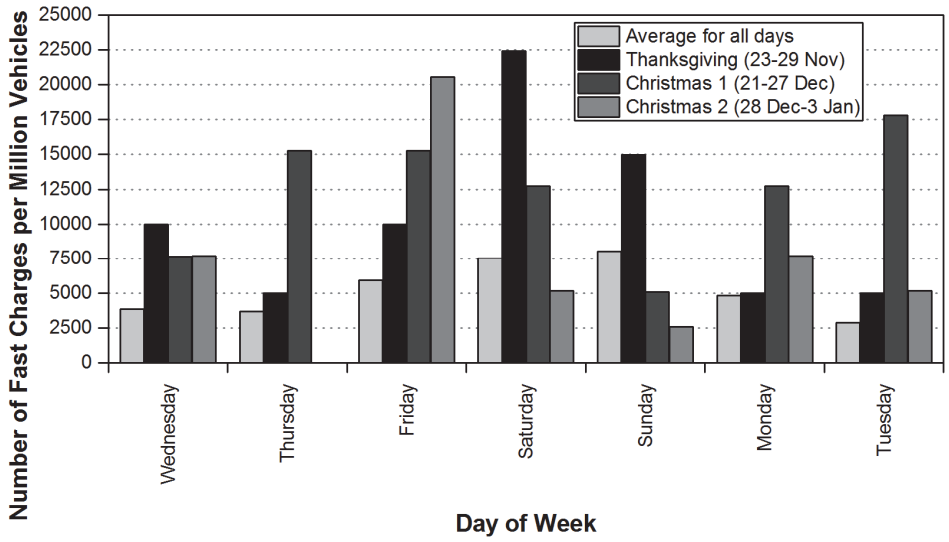

Figure 3.9 Fast charge by day of week around holiday periods

3.7 Required Fast Charging Power

This section describes a novel method to estimate the fast charging power required to satisfy consumer requirements, by consideration of the length of time drivers stop during long distance journeys. This information is critical to organisations developing or installing fast charging stations to ensure the fast charging stations are future proof, meaning they do not have to be regularly replaced as charging powers increase, and also critical for automakers, informing them of the charging powers that EVs should be able to achieve to satisfy consumer requirements. Currently the fast charging powers may be dictated by charging standards, the two most important fast charging standards outside China are the CCS and CHAdeMO standards [177]. The majority of fast chargers installed currently are rated at 50 kW peak, however both the aforementioned standards have stated their intention to support 350 kW charging in the future. 350 kW charging is chosen based on the technical specifications, such as voltage and current equipment limits, rather than what potential EV owners require. The method suggested here, instead of looking at how fast the charging can technically be, looks at the problem from a different angle, how fast might people want the charging to be.

For example the electrical power required for an EV charging rate to be equivalent to that of a gasoline vehicle refilling at a petrol station has been determined as around 5 MW [11], this value includes the fact that EVs are more efficient at converting stored energy into movement. EV drivers may accept slower refill times as they may have to visit fast charging stations less than they currently visit gas stations since the majority of their charging will be conducted at home or work. This is because on the majority of days the daily distance travelled in a car does not exceed the range of the EV, Swedish and German data showed the average daily distance travelled to be less than 35 miles [178] and the USA study [11] mentioned in Section 3.3 found an average daily driving distance of 45 miles. When charging an EV, EV drivers are also free to do other activities whereas at a gas station they must operate the gas pump. As stated previously, despite these advantages, recharging time is still seen as a major hurdle to overcome before the widespread consumer adoption of EVs.

The USABC [179] creates battery targets required for a commercially successful, mass market full battery EV. The USABC target for fast charging is 80% SoC to be delivered in 15 minutes [180]. For a 100 kWh EV this is equal to a charging rate of 320 kW. This is a similar rate to a recent target set by the White House to achieve 350 kW charging [181]. In both examples the reasons for choosing the charging targets are not clear however the method suggested in this section can be used as an alternative means of setting charging targets. Since this method is based on real world driver

behaviour it may be applied to markets with very different traveller needs to those of the USA, for example in Asian mega cities or in European conurbations.

The method suggested in this section looks at current driving habits to determine the charging rate required to enable EV drivers to complete their long distance journeys in the same time that they currently do in gasoline vehicles. From the GPS journey data, long distance journeys are identified, the duration of inter journey stops and the distance travelled after the stop are examined to determine the required charging power to satisfy a journey.

In [11] the range an EV needs to satisfy current driving habits was examined. This study states the number of daily adaptations drivers would have to accept to meet their driving habits depending on the assumed range of the EV. An adaptation day is a day on which the driver would have to do something different to what they normally do, such as rent a vehicle capable of driving long distances or take longer over their journey, charging their EV along the way. These adaptations could potentially be avoided if fast charging were available, meaning the driver could complete the journey in an EV in the same time as in a gasoline vehicle. This section examines current driving habits to define a fast charging rate that avoids driver adaptations.

3.7.1 Method for Determining Fast Charger Power

The same dataset from the Puget Sound region is used. As the GPS locations of the journeys are not known, long distance journeys are found in the data by finding instances where the car travels a long time (t_1), stops for a short time (t_b) not at home or work and then drives again for a further long time (t_2), in consecutive trips, as seen in Table 3.4.

Table 3.4 Constraints for long distance trip data
All three conditions must be met in consecutive journeys

Description	**Constraint**
Trip 1	$>t_1$
Stationary period between trips 1 and 2	$<t_b$ not at home or work
Trip 2	$>t_2$

These constraints are designed to capture long distance journeys made by the gasoline vehicles. The stationary period in between the two trips signifies a break the driver may take during a long distance journey. This break may be at a service station where, if the driver was driving an EV, they could recharge their vehicle. The stopping time is therefore the length of time that a fast charger could be connected to the EV. The distance travelled after the stop in trip 2 dictates how much energy needs to be transferred to the EV during the stop.

The distance travelled in trip 2 (d_2 *(mile)*) can then be divided by the stopping time (t_b *(min)*) to determine the charging rate (FC_{rate} *(mile min^{-1})*) in miles per minute that needs to be applied to the EV during the stop to satisfy the trip, seen in Equation 3.2.

$$FC_{rate} = \frac{d_2}{t_b}$$

Equation 3.2

The duration of the trips before and after the stop can be varied. If shorter journeys are included there are more instances of long distance stops in the data but there is less confidence that the driver is on a long distance journey, while for longer trip durations the opposite is true. In the results section values of 1.5 hours, 1 hour and 1.5 hours are chosen for t_1, t_b and t_2 respectively.

3.7.2 Fast Charging Power Results and Discussion

Using the methodology described above, the power requirements to charge the EVs on long distance journeys are displayed in this section. The stopping time (t_b) is chosen to be less than 1 hour, this time length is chosen because longer stops may mean the driver has reached a destination and hence are not considered. The base case for trip durations is chosen as an initial 1.5 hour trip (t_1) followed by a 1.5 hour trip (t_2). It should be noted that these 1.5 hour trip times do not relate directly to the long distance definition given previously, a journey where the EV range is exceeded, with a base case of 200 miles, as in a 1.5 hour trip it would not be possible to drive 200 miles. 1.5 hour trips have been chosen because two consecutive 1.5 hour trips are long enough to give confidence that the driver is on a long distance journey but short enough to give enough data points for the analysis.

With these criteria, and going through all 750,000 individual journeys in the data, Figure 3.10 shows how long people stopped during long distance journeys and how far they travelled after this stop in the subsequent journey, there are 204 journeys where the criteria are met. It is clear from Figure 3.10a that people often stop for short periods of time during long distance journeys, with 60% of stops being for less than 12 minutes.

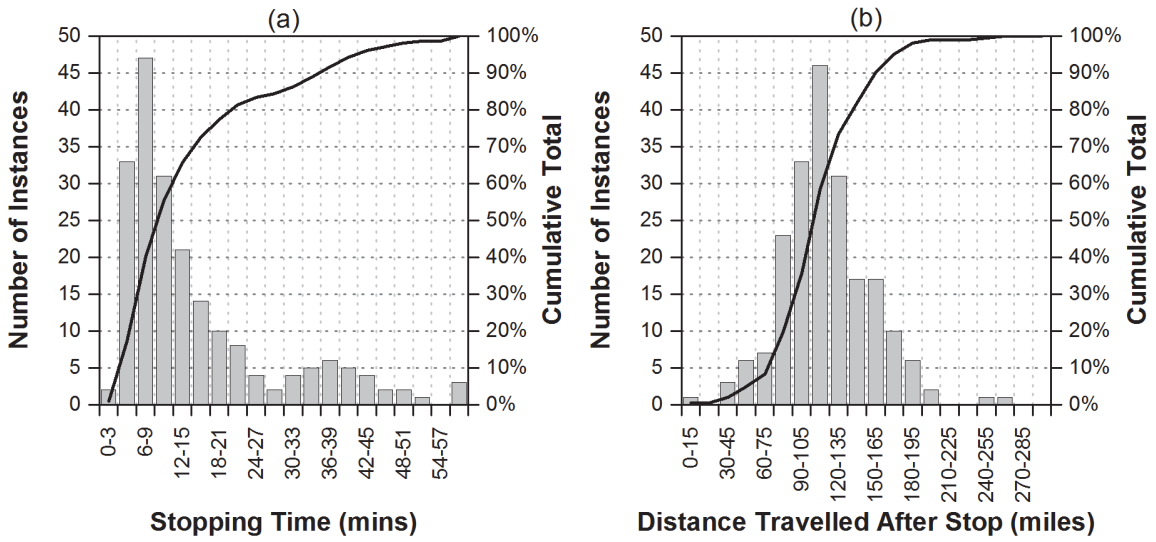

Figure 3.10 Long distance journeys involving a stop

How long people stop during long distance journeys (left) and how far they travel after the stop (right)

Using Equation 3.2 the charging rate required to satisfy the journey is found and the results of this are shown in Figure 3.11. The charging rate is given in miles per minute, so if the vehicle travelled for 100 miles in the trip 2 and stopped for 10 minutes during the break, the charging rate to satisfy the journey would be equal to 10 miles per minute. To convert the charging rate into a charging power the charging rate can be divided by the efficiency of the EV, in miles per kWh, i.e. for each kWh of energy in the battery the EV can travel for a certain distance. This value depends on the EV, for example for the large Tesla Model X SUV [39] the figure is 3.5 miles $(kWh)^{-1}$ (351 miles range from a 100 kWh battery), while for the smaller BMW i3 [182] the value is 4.4 miles $(kWh)^{-1}$ (124 miles range from a 28 kWh battery). If a conservative estimate of 3 miles $(kWh)^{-1}$ is used then 10 miles min^{-1} is the equivalent of 200 kW. From Figure 3.11a, to satisfy 80% of journeys the charging rate must be 20 miles min^{-1} or 400 kW.

The trip durations used in this analysis can be varied, for example Figure 3.11b shows the extreme curves when the trip before the stop (t_1) and the trip after the stop (t_2) were varied between 1 hour and 2 hours. From this graph it is clear that to satisfy 80% of journeys the charging rate must be between 18 and 23 miles min^{-1}, i.e. between 360 to 460 kW.

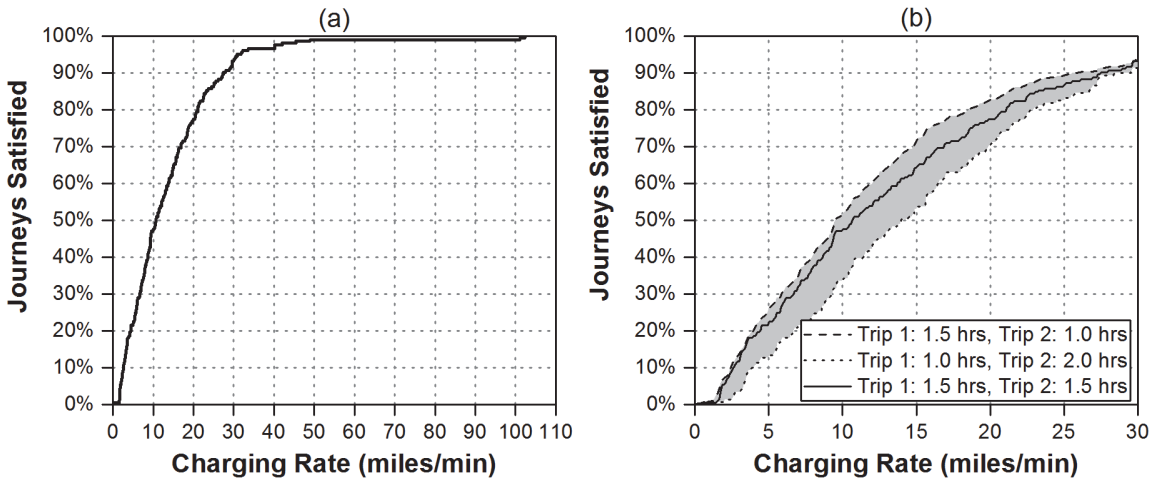

Figure 3.11 Journeys satisfied for various charging rates

Created using the constraints discussed in this section (left) and a sensitivity study varying the constraints (right)

It has been shown that the majority of stops while on long distance journeys are for a short period, with 60% of stops being less than 12 minutes duration. This presents a problem for fast charging as people are accustomed to short duration stops during long distance journeys. This means the fast charger can only be connected to the EV for a short time period, meaning the required energy must be delivered at high power.

For current fast charging levels of 50 kW, i.e. around 2.5 miles/min, Figure 3.11b shows this satisfies only about 10% of long distance journeys. As stated previously, several projects have recently been announced looking at installing charging stations capable of up to 400 kW charging power and so these new charging stations are likely to satisfy 80% of driver's requirements. One issue is that the charging rates in Figure 3.11 are the average charging rates. To achieve an average charging power of 400 kW the charging rate must start off higher than 400 kW as current batteries charge at a slower rate the longer they are plugged into a charging station.

3.8 Conclusions from the Usage of Fast Charging Stations

Two novel methods, one to estimate usage patterns of fast charging stations and one to estimate user defined fast charging powers, have been described in this Chapter in Sections 3.3 and 3.7.1. Both methods are regarding forecasting and as such the major changes currently occurring in the automotive industry, including connectivity, autonomous driving and diverse mobility, are likely to impact the results. The methods have the advantage of requiring few inputs and assumptions so that users of the methods can understand the limitations of the methods when making decisions based on the methods.

The method to predict fast charging station usage is classified as novel as the usage is predicted based on current driving habits, with regular slow charging also taken into account, larger EV battery capacities are assumed and the method looks solely at long distance journeys. The method to estimate the fast charging power required to satisfy EV driver requirements is novel as it addresses charging power requirements based on driver requirements rather than the current method of using the technical limitations of charging equipment.

The primary results from this chapter are the graphs in Figure 3.6b and Figure 3.11, a graph showing the predicted usage of fast charging stations throughout the day and a graph of typical power rating required. These are used in subsequent chapters to estimate when and how fast the stationary energy storage will need to charge and discharge.

Chapter 4 Requirements of the Stationary Electrical Energy Storage

To overcome the challenge of not being able to obtain a high enough power connection from the electricity grid at the required fast charging station location it is proposed that stationary energy storage is used. Stationary energy storage allows the energy required to charge EVs to be drawn from the grid over a longer time period thereby lowering the grid connection power required and grid connection capacity. Other researchers have studied the use of stationary energy storage at fast charging stations and there are multiple commercial examples of these systems being installed by companies, as described in Section 2.3.3. As described in this earlier literature review these projects generally focus on the power flow management or the power electronics and little research has been conducted on the optimisation of the stationary energy store capacity.

Optimising the capacity of the stationary energy storage is key as it must be large enough to ensure EV drivers arriving at the fast charging station do not have to wait because there is insufficient energy or capacity available at the charging station to charge their EV but simultaneously small enough to make economic sense. The aim of this chapter is therefore to develop a novel method to optimise the size of the stationary energy store based on an acceptable waiting time. There is one journal paper associated with this chapter, which is currently submitted, Thomas S. Bryden, George Hilton, Borislav Dimitrov, Carlos Ponce de León, Andrew Cruden, Rating a Stationary Energy Storage System within a Fast Electric Vehicle Charging Station Considering User Waiting Times.

From the literature review it was determined that the exact costs of connecting to the grid vary considerably depending on the exact location, depending on whether spare capacity is available or if a large infrastructure upgrade is required. The focus of this chapter is therefore less on the actual results and more on the development of a novel method to determine the optimum size, which could be used at any potential fast charging station location. In the initial method section the model is introduced using basic assumptions to aid with understanding of the model. Later in Section 4.2, it is demonstrated how the model could be used for a specific location.

The method proposed is programmed using MATLAB, the code is available in Appendix B and the model is described in detail in Section 4.1. The model uses the results from the previous chapter regarding the anticipated arrival time distribution of EVs at fast charging stations, as shown in Figure 3.6. Random number generation is used to model when EVs will arrive at the fast charging station, with the random arrival times weighted to this arrival time distribution. For an assumed

number of station fast charging points and an assumed capacity of stationary energy store the waiting times of the EVs using the fast charging station can then be calculated. The Monte Carlo method is used to account for the variations in the random number generation. The assumed number of fast charging points and an assumed capacity of stationary energy store can then be varied until the required average EV waiting time is achieved.

The acceptable average waiting time is therefore a critical parameter used throughout this chapter. There is however little research into how long people are willing to wait to recharge their EV. When an EV owner requires a fast charge they may have no choice but to wait for a fast charger as they may not have sufficient range to complete their journey. Longer waiting times will however mean people are less likely to purchase an EV in the first place. A report into queueing in general [183] found that the maximum time people are willing to wait in line is 5 minutes 54 seconds and so this is considered as the maximum waiting time later in the chapter.

4.1 Description of Model for Determining Energy Storage Requirements

The author's model consists of two parts, where in the first part the number of fast charging connection points at the fast charging station is determined and in the second part the capacity of the stationary energy store is determined. This model structure is shown in the flow chart in Figure 4.1, and these two model parts are now described in more detail.

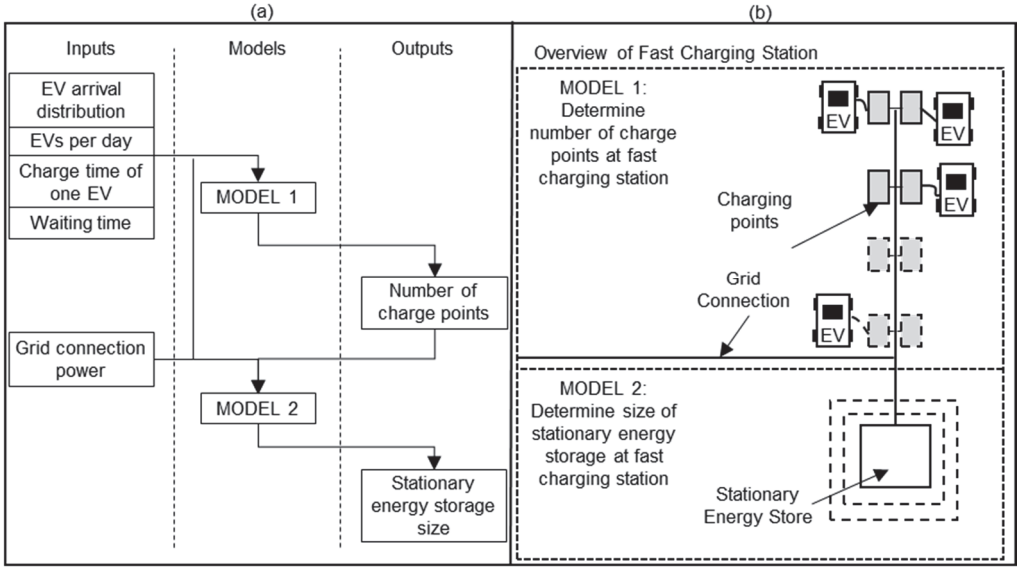

Figure 4.1 Overview of model to determine stationary energy store size

Flow chart, detailing inputs, outputs and stages (left) and illustration of different parts of model (right)

To understand how the model works, the model is initially demonstrated in this section with very basic assumptions before a more realistic scenario is demonstrated in Section 4.2. These basic assumptions include:

- Exactly 100 EVs use the fast charging station each day, being the assumed average fast charging station usage in the UK based on the following calculation. The average number of fast chargers per million EVs per day is 25,000, taken from Figure 3.7 and assuming a conservative EV driving range of 100 miles. The number of UK gas stations per million vehicles is 236 (8,407 gas stations [184] / 35.6 million vehicles [185]). If it is assumed the ratio of gas stations to fast charging stations in the future is the same, the average number of fast charges per day per fast charging station is around 100 (25,000 / 236). This value relies on many assumptions and will also vary considerably from location to location depending on the number of nearby fast charging stations and the number of vehicles passing the fast charging station.
- The probability of an EV arriving at a fast charging station during each hour of the day is as shown in Figure 4.2, where this result is taken from Chapter 3.
- The average acceptable waiting time is 15 seconds, this being chosen because, from the results shown later in this section, in Section 4.1.1.1, it means less than 1% of fast charging station users must wait more than 6 minutes. As described above, 6 minutes is a critical waiting time that other research has suggested should not be exceeded.
- The size of all EV batteries is 60 kWh and each EV charges at 360 kW from 0% to 100% SoC, thereby taking exactly 10 minutes to charge. These assumption are made to make the demonstration of the model clearer. In Section 4.2 these assumptions are modified to better reflect real conditions.
- The available peak grid connection power at the fast charging station location is 720 kW. This is highly dependent on the fast charging station location and is assumed here for the demonstration of the model.

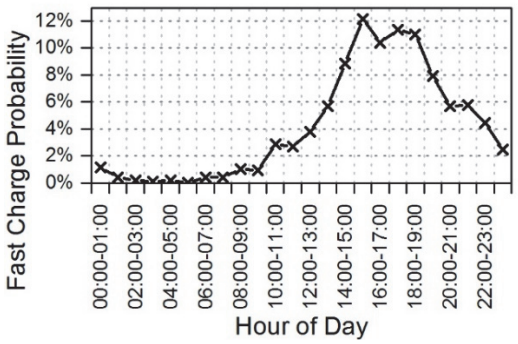

Figure 4.2 Probability of an EV arriving at the fast charging station in each hour of the day

Taken from Figure 3.6b

4.1.1 Determining the Number of Charging Points (Model 1)

Similar to a conventional petrol station having multiple petrol pumps, a fast EV charging station will have multiple charging points. In this section the method to determine the number of charging points that should be installed at a fast charging station is described. The number of fast charging points required is determined based on the acceptable time that EV drivers arriving at the fast charging station may be required to wait. The waiting time is the total time spent at the fast charging station minus the time it would take to charge if a charge point is free on arrival and there is sufficient power and energy to charge the EV at the maximum allowed power. A waiting time simulation is conducted and the output of the simulation is the expected waiting time versus the number of charging points. For example, if there is only one charging point, queues will develop and the average waiting time will be high however if there are tens of charging points nobody will have to wait and the average waiting time will be low.

4.1.1.1 Overview of Method

The model for this section was created in MATLAB and has an overall simulation time length of one day and a time resolution of one second. The flow chart detailing the model in this section is shown in Figure 4.3. The model in Figure 4.3 is run multiple times and varies the number of fast charging points at the fast charging station, starting at one fast charging point and increasing the number of fast charging points until the waiting time is deemed acceptable, for example the average waiting time of 15 seconds mentioned above.

The first step is to create a vector for the arrival times of each EV that uses the fast charging station in the day. The vector is the length of the number of EVs simulated that use the fast charging station each day, in this case 100, with one cell for each EV. The arrival time for each EV is randomly generated but weighted according to the specified probability of an EV arriving at each hour of the day as detailed in Figure 4.2.

The model then steps through each second of the day and looks up in the arrival times vector to see if an EV arrives in this second. If an EV does arrive, the EV starts charging if there is a free fast charging point. The EV then leaves the fast charging point after the defined charging time for one EV, in this case 10 minutes, has passed. If however, the EV arrives and there are already EVs charging and there are no free charging points the arriving EV must join a queue and wait. The average waiting time can then be found by summing the waiting times for each EV in the day and dividing by the number of EVs using the fast charging station in the day.

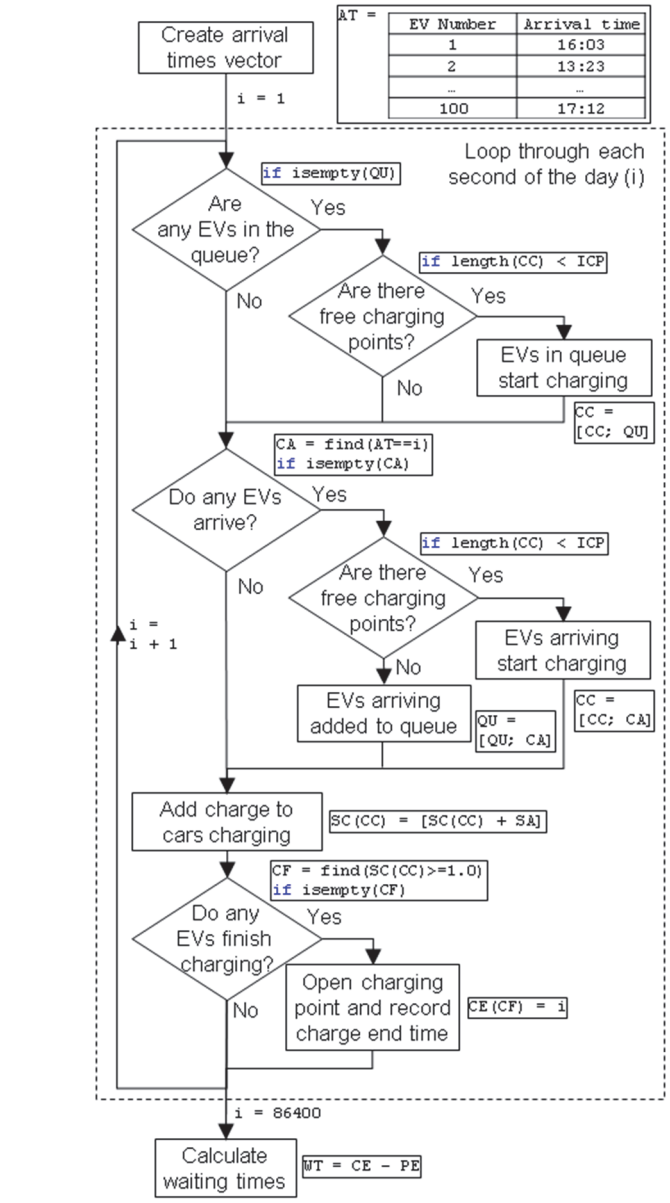

Figure 4.3 Flow chart detailing steps for Model 1

The * indicates where model 2 varies from model 1

The results of the analysis are highly dependent on the randomly generated arrival times, weighted according to Figure 4.2, therefore a simulation using the Monte Carlo method is conducted and described below [118]. This simulation involves running the analysis described

above for many thousands of days and working out an overall average waiting time. For each run, the model creates a new arrival times vector and steps through each second in the day. To check that sufficient number of days are included in the Monte Carlo simulation, the model can be run multiple times with the same number of days and if the results are the same for each run, i.e. it converges, the simulation has been conducted with a sufficient number of days. For example, if the simulation was run three times, each for 500 days, and the average waiting time was determined in the first, second and third runs as 20.21 seconds, 45.03 seconds and 5.54 seconds respectively, it would mean that the simulation did not include enough days and the number of days would need to be increased. If however the same analysis was run three times but using 100,000 days and the average waiting time for each run was determined as 34.95 seconds, 34.93 seconds and 34.96 seconds it would mean the simulation included enough days. For the models in this chapter each simulation is run three times and if the difference between the highest and lowest results is less than 10% the simulation is complete, 10% was chosen as a trade off between accuracy and computational time.

The results for model 1 include the number of charging points required versus waiting time and an example is shown in Table 4.1, created using the input assumptions detailed previously. An appropriate number of charging points can then be chosen based on the average acceptable waiting time, for this case 15 seconds. It is clear that if this fast charging station only had one charging point installed, the average waiting time is over 2 hours and 87% of drivers arriving at the fast charging station will have to wait more than 6 minutes. With four charging points this drops to an average waiting time of 7.5 seconds and only 0.3%, or around 1 in 300 drivers, have to wait more than 6 minutes. The assumption for the average waiting time was that the average waiting time should be less than 15 seconds and so four charging points are chosen. The probability range that an EV arriving at the fast charging station with four charging points will have to wait a certain number of minutes is shown in Figure 4.4.

Table 4.1 Number of charging points versus waiting time

Number of Charging Points	Average Waiting Time (s)	Probability of Waiting More than 6 minutes (%)
1	7500	87
2	290	28
3	39	3.4
4	7.5	0.3

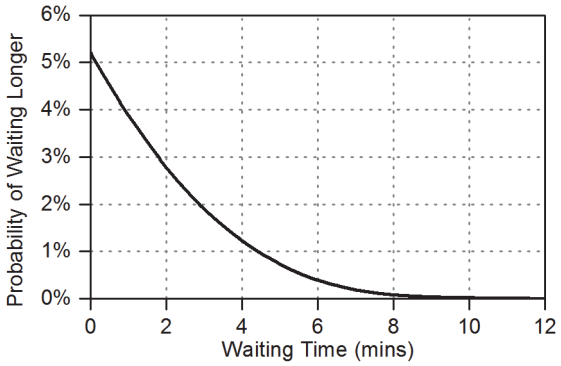

Figure 4.4 Probability of EV arriving at the fast charging station waiting longer than various times

4.1.1.2 Detailed Step Through of Model

In this section a more detailed description of the model is given to aid with understanding. The same assumptions as the previous section are used, however for this demonstration only five EVs use the fast charging station during the day, this is so the step through of the model can clearly be seen on one page. The first step is to create the arrival time vector for each EV and this is shown in Table 4.2, and the vector is created using random number generation weighted according to Figure 4.2, the projected finish time is 10 minutes after the arrival time.

Table 4.2 Randomly generated EV arrival times

Weighted according to Figure 4.2

EV	Arrival Time	Projected Finish Time
#1	15:07:26	15:17:26
#2	15:01:48	15:11:48
#3	18:10:30	18:20:30
#4	15:10:06	15:20:06
#5	12:05:27	12:15:27

Next, the model steps through each second of the day. As illustrated in the arrival times vector in Table 4.2, the first EV arrives at 12:05:27 and before this time nothing happens as there are no EVs charging or arriving. When this EV arrives there is a free charging point and so the EV starts charging. The model steps through each second of the day, as shown in Table 4.3.

Table 4.3 Example of model stepping through each second in the day

Time	
00:00:00 to 12:05:26	No events
12:05:27	EV #5 arrives and starts charging at the free charging point
12:05:28 to 12:15:26	No events
12:15:27	EV #5 finishes charging, set charge end time of EV #5 to 12:15:27
12:05:28 to 15:01:47	No events
15:01:48	EV #2 arrives and starts charging at the free charging point
15:01:49 to 15:07:25	No events
15:07:26	EV #1 arrives but there are no free charging points, put EV#1 in queue
15:07:27 to 15:10:05	No events
15:10:06	EV #4 arrives but there are no free charging points, put EV#4 in queue
15:10:07 to 15:11:47	No events
15:11:48	EV #2 finishes charging, set charge end time of EV #2 to 15:11:48
15:11:49	EV #1 leaves the queue and starts charging
15:11:50 to 15:21:48	No events
15:21:49	EV #1 finishes charging, set charge end time of EV #1 to 15:21:49
15:21:50	EV #4 leaves the queue and starts charging
15:21:51 to 15:31:49	No events
15:31:50	EV #4 finishes charging, set charge end time of EV #4 to 15:31:50
15:31:51 to 18:10:29	No events
18:10:30	EV #3 arrives and starts charging at the free charging point
18:10:31 to 18:20:29	No events
18:20:30	EV #3 finishes charging, set charge end time of EV #3 to 18:20:30
18:20:31 to 23:59:59	No events

The waiting time can then be calculated for each EV by subtracting the projected charge finish time, from Table 4.2, from the actual charge finish time, from Table 4.3 and the calculation is shown in Table 4.4. By summing the waiting times of each EV and dividing by the number of EVs the average waiting time can be calculated, which, for this case, the average waiting time is 3 minutes 13 seconds (00:16:07 / 5). This exact process is then run for many days, for each day a new arrival time vector is created, the model steps through each second of the day and the waiting times are calculated.

Table 4.4 Finish times and waiting times for each of the five EVs

EV	Projected Finish Time	Actual Finish Time	Waiting Time
#1	15:17:26	15:21:49	00:04:23
#2	15:11:48	15:11:48	00:00:00
#3	18:20:30	18:20:30	00:00:00
#4	15:20:06	15:31:50	00:11:44
#5	12:15:27	12:15:27	00:00:00
Total			00:16:07

4.1.2 Determining the Energy Capacity of the Stationary Energy Store (Model 2)

The method in Section 4.1.1 was conducted without using the grid connection power and a similar method is now used to size the stationary energy store. The output from model 1, the number of charging points, is used along with the user defined value for the maximum power available from the grid at the fast charging station location, in this case 720 kW. In the previous model it was assumed that there was always enough power from the grid to charge the EVs, irrespective of the number of charging points. In the model for this section an EV arriving at the fast charging station may have to wait either because there are not enough charging points or because there is not sufficient power or energy available to charge the EV. For the case described in this method there are four charging points, requiring 1,440 kW (360 kW × 4), however at the fast charger location only 720 kW can be taken from the electricity grid.

A stationary energy store can be used to charge EV's at the fast charging station if there is not sufficient power capacity available from the grid. For example, if there are four EVs charging and the grid connection can only support two EVs charging, two of the EVs could be charged using the stationary energy storage. The stationary energy store is incorporated into the model using a variable for the SoC of the stationary energy storage. As the model steps through each second the

SoC of the stationary energy store is calculated by adding or removing the energy taken from the stationary energy store in the current second to the energy in stationary energy store in the previous second.

The EV waiting time due to insufficient power capacity therefore only occurs if the stationary energy store runs out of energy or cannot deliver the necessary charging power. The priority of the model is that EVs are charged first using the grid connection and then using the stationary energy store if the grid connection is not sufficient. Any spare grid capacity is ultimately used to recharge the stationary energy store. A Monte Carlo simulation is then run, similar to model 1, but using the specified number of charging points from the previous model and varying the capacity of the stationary energy store.

The results then include the capacity of stationary energy storage versus the EV waiting time and an example results table is given in Table 4.5. These results are created using the inputs and assumptions detailed previously.

Table 4.5 Size of stationary energy store versus waiting time

For a four charging point charging station where the grid connection is capable of providing 720 kW

Size of Stationary Energy Storage (kWh)	Average Waiting Time (s)	Probability of Waiting More than 6 minutes (%)
0	290	28
50	160	16
100	110	11
150	73	7.2
200	43	4.3
250	29	2.7
300	20	1.7
350	15	1.1
10,000	7.5	0.3

An appropriate capacity of stationary energy store can then be chosen based on the acceptable waiting time. As shown in Table 4.5 to achieve an average waiting time of less than 15 seconds a

stationary energy store with the capacity of 350 kWh is required. Further, for this location, using a stationary energy store with a capacity of 350 kWh reduces the average waiting time from almost 5 minutes (290 s), with no energy store, to less than 15 seconds. It is clear from the results that having no stationary energy store produces the same average waiting time (290 s) as having two charging points in Table 4.1. The last value in Table 4.5 shows the values for a very large stationary energy store. This average waiting time value (7.5 s) is the same as for the four charging points case from Table 4.1, this is because for the case of a very large stationary energy store all of the waiting is as a result of insufficient charging points, as in this scenario there is always sufficient power to charge the EVs.

4.1.2.1 Queueing Priority

One key aspect to be considered for this model is the queuing priority and how the available EV charging power is shared. Simply sharing all available power between all EVs using the fast charging station is the simplest method, however for the case of the fast charging station it will not be the most efficient method, as described below. For example, consider the case where there are two charging points but the grid connection is only capable of providing power to charge one EV at full power at any instant. If two EVs, which can charge in 10 minutes, arrive at the same time and they are each given half the power they will each take 20 minutes to charge, giving an average waiting time of 10 minutes. If however one EV is allowed to charge at full power and the other EV has to wait until the other EV finishes before charging, the first EV does not have to wait and the second EV waits 10 minutes, giving an average waiting time of 5 minutes.

The algorithm used for this model therefore charges EVs that arrive at the fast charging on a first come first served basis. As the model steps through each second the energy capacity remaining in the stationary energy store is examined. If there is not sufficient power capacity available from the grid or in the stationary energy store to charge all the EVs at the fast charging station, the last EV to arrive is stopped from charging and the energy in the stationary energy store and power from the grid are given to the first to arrive EVs.

4.1.2.2 Grid Connection Power

The analysis in this section undertakes a sensitivity study for the same fast charging station case as Section 4.1.2 but at separate locations where the available grid connection powers are different. The inputs of 100 EVs per day, a charging time for one EV of 10 minutes and an acceptable average waiting time of 15 seconds are used and the grid connection power capacity is varied, between a power capable of charging 1 EV (360 kW) and 4 EVs (1,080 kW). This sensitivity study is conducted to represent different locations on the electricity grid.

The results are shown in Table 4.6. For each grid connection power seen in Table 4.6, a table similar to that seen in Table 4.5 was created. The result shown in Table 4.6 is then the smallest stationary energy store that gives a waiting time less than 15 seconds.

Also included in these results is the required C-Rate of the stationary energy store. The C-Rate has previously been described in Section 2.1 and is a measure of how quickly the energy store charges and discharges, with higher C-Rates indicating faster charging and discharging capability. The C-Rate can be used to help determine the best type of stationary energy store because different types of energy store are suitable for different C-Rates, as described in Section 2.3.2. The C-Rate has been calculated using Equation 4.1 and the maximum required power to charge all four EVs (P_{max} *= 1,080 kW*), the grid connection (P_{grid} *(kW)*) and the energy in the stationary energy store (E_{store} *(kWh)*).

$$C_{rate} = \frac{P_{max} - P_{grid}}{E_{store}}$$

Equation 4.1

Table 4.6 Required size of energy store for various grid connection powers

To achieve an average waiting time of less than 15 seconds where each charging station has four charging points

Grid connection capacity (kW)	Size of stationary energy store (kWh)	Maximum C-Rate energy store
360	1,900	0.6
720	350	2.1
1,080	50	7.2
1,440	0	-

It is clear from the results in Table 4.6 that the lower the grid connection capacity, the larger the required stationary energy storage capacity. In other words, in a location where the electricity grid has very little spare capacity a large stationary energy store is required and in areas where there is plenty of spare grid capacity smaller or no stationary energy storage is required. It should also be noted that the larger stationary energy stores are required to operate at lower C-Rates than the locations where there is a higher grid connection power and therefore smaller energy store.

4.2 Design of Fast Charging Station with Stationary Energy Store at Actual Location

In its current state, the author's method has been described under ideal conditions. For example, the EV charging power profile for all EVs using the fast charging station is simply constant 360 kW power for 10 minutes, which takes the battery from 0 to 100% SoC. This will not be the case in reality because, as stated in the background section and Figure 2.9, EV charging powers decrease as the SoC of the EV battery increases. The SoC that the EV will arrive at the fast charging station will also vary based on the preference of the driver of how much buffer energy they want in their battery, the journey being conducted will also vary and the EVs will also have varying battery capacities.

4.2.1 Example Location

To demonstrate the method with more realistic inputs an example location is chosen, in this case the Tesla Supercharger at Elveden Inn in Suffolk, UK, shown in Figure 4.5. The site currently has eight superchargers, providing up to 120 kW each. The site has a 500 kVA transformer stepping the voltage down from 11 kV to 480 V [186] and from this transformer size it is assumed that the maximum grid connection power is 500 kW. The analysis in this section is for a period in the future when EV charging speeds are higher and more EVs are on the roads, the exact future fast charging profiles and station usage assumptions are described in Section 4.2.2. The analysis determines the size of stationary energy storage required at the Elveden Inn charging location to enable this future higher power and more frequent charging without upgrading the current grid connection infrastructure, i.e. the grid connection input remains constant at 500 kW.

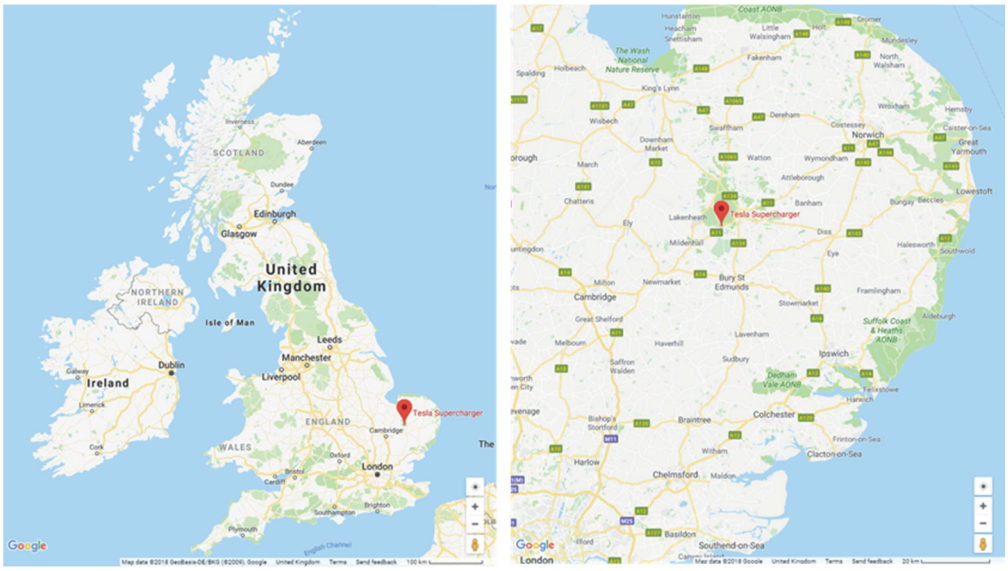

Figure 4.5 Location of Elveden Inn Tesla Supercharger in the UK

4.2.2 Assumptions for Chosen Location

The Tesla charging power profile has previously been illustrated in Figure 2.9, where the charging power is initially constant until around 25% SoC. After the constant power section the power follows an exponential decay according to Equation 4.2, relating the charging power (*P (W)*) to the SoC (*s (%)*). This equation was determined by fitting a line to the Tesla Supercharger data seen in Figure 2.9, the fit can be seen in Figure 4.6. Other variables include the constant charging power (P_{const} *(W)*), the SoC that this constant power can be applied until (s_{const} *(%)*) and the rate that the power decays after the constant power section (*k*).

$$P = \frac{P_{const}}{e^{-ks_{const}}} e^{-ks}$$

Equation 4.2

The SoC with time (*t (s)*) is defined by Equation 4.3, including the arrival SoC of the EV (s_{init} *(%)*) and the energy capacity of the EV battery (*E (J)*). The charging then finishes once the SoC is greater than the EV departure SoC (s_{fin} *(%)*).

$$s = s_{init} + \frac{\sum Pt}{E}$$

Equation 4.3

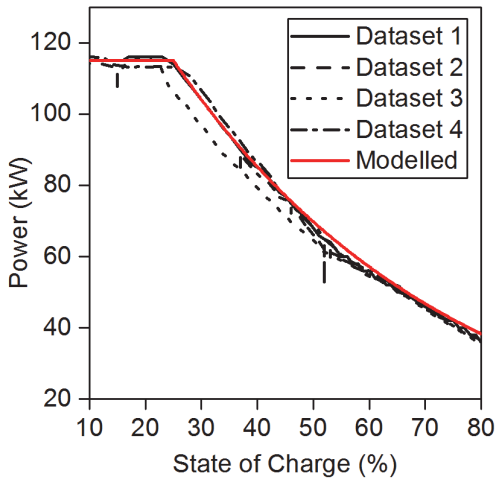

Figure 4.6 Fitting Equation 4.2 to Tesla Supercharger data

The values used for this fit include P_{const} *= 115 kW*, *k = 2.0*, and s_{const} *= 25%*

The output required for input to the model is a charging profile for one EV, in terms of power versus time. This charging profile is obtained using Equation 4.2 and Equation 4.3 and six inputs listed in bullet points below, each EV using the fast charging station will have its own value for each of the six inputs, the assumptions of which are described below.

- Initial constant power value (P_{const} *(W)*)
- The SoC that this constant power can be applied until (s_{const})
- The exponential decay factor (*k*)
- The capacity of the EV battery (*E (J)*)
- The SoC that the EV arrives at the fast charging station (s_{init})
- The SoC that the EV leaves the fast charging station (s_{fin})

Once these inputs have been defined for each EV, they can be used to create a charging profile for each EV, an example of which can be seen in Figure 4.7.

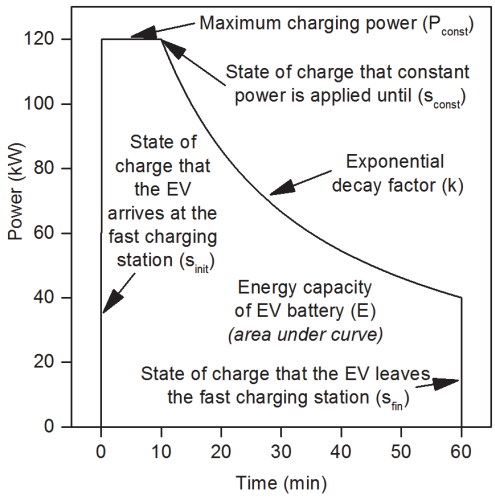

Figure 4.7 Charging profile with variables required to define the charging profile
The values used to create this EV charging profile include P_{const} *= 120 kW*, s_{const} *= 25%*, *k = 2.0*, E *= 100 kWh*, s_{init} *= 5%* and s_{fin} *= 80%*

When defining the inputs, the first four bullet point inputs above are dependent on the future ability of cells to accept fast charge and the size of the battery that EV manufacturers chose to give sufficient capabilities at reasonable cost. The final two bullet point inputs above depend on EV owner behaviour, for example some owners may be comfortable letting their EV battery go to 5% SoC on long distance journeys while others may recharge if the battery starts to go below 30% SoC.

To account for these variations, probability distributions are used for all variables, for example for the initial SoCs, a normal probability distribution with an average value of 15% SoC and 95% of data being between 5% and 25% SoC could be used, seen in Figure 4.8. Random number generation weighted to the normal distribution can then be used to determine the SoC of each EV arriving at the fast charging station. In Section 4.1.1.1 it was described how each EV arriving at the fast charging station was assigned a random arrival time weighted according to Figure 4.2. In the subsequent section, as well as this arrival time, each EV is also randomly assigned a value for each

of the six variables, defining the charging profile of each EV. The probability distributions for each of the six variables are described below and are seen in Table 4.7.

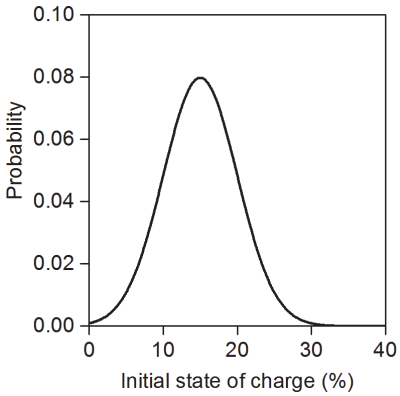

Figure 4.8 Probability distribution for initial SoC example

For each of the six variables, seen in the above bullet points, assumptions are made for what they may be in future EV charging profiles. The assumptions state the assumed mean value and for each variable a normal distribution is created, with the relative standard deviation being taken as 10% for all variables to provide variation from the mean values, the normal distributions for these variables are shown in Table 4.7.

The initial constant power value (P_{const}) is taken as 400 kW as in Section 3.7.2 this was found to be a charging power capable of satisfying 80% of long distance journeys. The SoC that this constant power can be applied until (s_{const}) and the exponential decay factor (k) are dependent on the future battery chemistry, hence the values are taken from the current values for the Tesla EVs seen in Section 2.2.2.2, being 25% and 2 respectively. The future capacity of the EV battery (E) is assumed to be 80 kWh, based on current lower cost EVs, such as the Chevrolet Bolt [40], having battery capacities of 60 kWh and the current trend discussed in Section 2.2.1.1 of EV battery capacities to increase.

The SoC that the EV arrives and leaves at the fast charging station will depend on the EV owner behaviour. For this analysis it is assumed that the normal distribution means for the arrival (s_{init}) and leaving (s_{fin}) SoC will be 20% and 80% respectively with 95% of the data being between 0-40% and 60-100% respectively.

The final variable required for the analysis is the number of cars (n_{cars}) that will use the fast charging station each day. This is also hard to estimate and depends on the future penetration level of EVs and their range capabilities as well as the number of nearby fast charging stations. At the Elveden Inn site, 23,000 cars drove on the 10 miles stretch of road in a day during a 2016 survey [187]. A simple calculation shows that this is about the average for UK roads of 27,000 cars

on a 10 mile stretch of road (244.4 billion miles travelled per year in the UK × 10 miles / 245,800 miles of road in the UK / 365 days per year [185]). Therefore, the average value of 100 cars per day calculated in Section 4.1 is assumed. Again, a normal distribution is used for the number of EVs charging and 95% of the days have between 80 and 120 cars per day.

Assumptions regarding efficiencies include that all power electronic converters shown in Figure 1.1 are 95% efficient, the EV battery is assumed to charge at 95% efficiency and the stationary energy store charges at 95% efficiency and discharges at 95% efficiency [188].

Table 4.7 Assumed values for variables for the location chosen

Variable	Mean	95% of data
P_{max}	400 kW	320 – 480 kW
E	80 kWh	64 – 96 kWh
s_{const}	25%	20 – 30%
k	2	1.6 – 2.4
s_{init}	20%	0 – 40%
s_{fin}	80%	60 – 100%
n_{cars}	100	80 – 120

4.2.3 Results for Chosen Location

The same analysis described in Section 4.1 is conducted using these inputs, including:

- All variables defined in Table 4.7
- The probability of an EV arriving at a fast charging station during each hour of the day as shown in Figure 4.2
- The average acceptable waiting time is 15 seconds
- The available grid connection power at the Elveden Inn fast charging station location is 500 kW

Similar results tables to that shown in Table 4.1 and Table 4.5 were created and it was found that the result to achieve an average waiting time of under 15 seconds requires a charging station with five charging points and a stationary energy storage with a capacity of 1,000 kWh. In the model the stationary energy storage was evaluated in steps of 100 kWh, so the optimum size is between 900 and 1,000 kWh. Using the stationary energy storage at this location reduces the average waiting time from 20 minutes to 13 seconds. To accommodate 400 kW charging at this location

therefore requires a 1,000 kWh energy store and an economic assessment could be conducted and the cost of this energy storage could be compared to the cost of upgrading the electricity grid infrastructure at the charging station location to determine the optimum solution.

For this case the power from the grid and the SoC of the stationary energy store is shown in Figure 4.9. Figure 4.9a shows the case for a day when the stationary energy store is completely depleted while Figure 4.9b shows a day when the stationary energy storage is used less and always has above 70% of energy available. The fully depleted case occurs because for this modelled day many EVs arrive within a short period of time, with 54 EVs arriving between 3 pm and 7 pm. For the day when the energy store is always above 70% SoC the EV arrival times are more spread out throughout the day and only 24 EVs arrive between 3 pm and 7 pm.

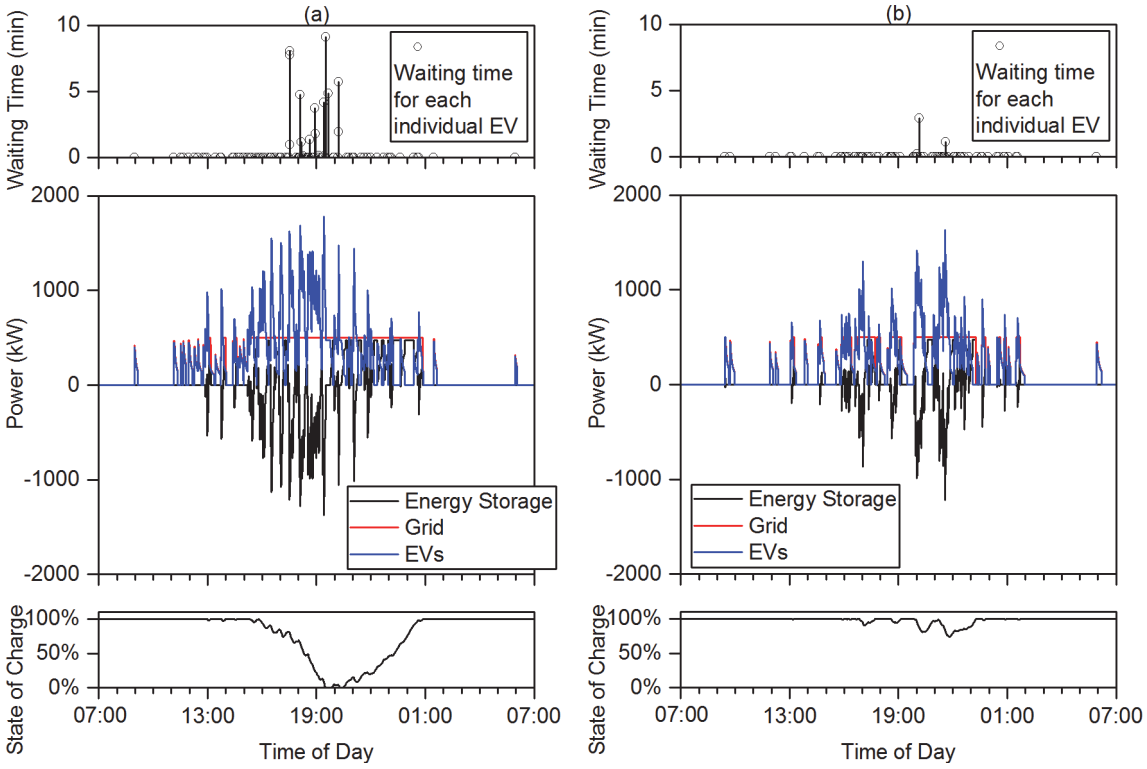

Figure 4.9 Results for two days at the example location

Individual EV waiting times (top), power flows from stationary energy storage (negative is discharge), the grid and to the EVs (middle) and the SoC of the stationary energy storage (bottom) for a day when the stationary energy storage is heavily used (left) and lightly used (right)

As can be seen in Figure 4.9, for these days, the maximum power that the charging EVs need is 1,800 kW, however the use of the stationary energy store means that the grid connection power is never more than 500 kW. It can be seen that when the power required by the EVs is above

500 kW the energy store discharges while when the power required by the EVs is less than 500 kW the grid recharges the energy store.

Also from Figure 4.9 the waiting times for all EVs using the fast charging station are illustrated. For the day when the stationary energy store is completely depleted, 16 cars have to wait with the longest waiting time being 9 minutes, while for the day when the energy store is used little only 3 cars need to wait, with the longest wait being 3 minutes. The average waiting time during the day from Figure 4.9a is 30 s, while for Figure 4.9b the average waiting time is 3.3 s.

4.3 Discussion Regarding the Stationary Energy Store Results

The decision whether to use stationary energy storage at a fast EV charging station will likely be driven by whole system economics, capital and operating costs. This will vary from location to location and will be a function of how many EVs require to be charged each day, the power capacity of the electricity grid connection used and the cost to upgrade the electricity grid connection. The example location demonstrated in Section 4.2 illustrates how the method proposed can be used in an actual location to size the stationary energy store. The method requires assumptions that have been justified in Section 4.2.2, however future work could look in more detail at any of these assumptions.

For example, the acceptable waiting time could be made longer resulting in the use of a smaller, cheaper stationary energy store, however to encourage EV uptake short waiting times are critical. The length of time people are willing to wait is a psychological question and could be investigated in future work. Another assumption, namely the EV charging power profiles, are likely to change in the future as the batteries change and EVs are able to charge at higher powers. All the model parameters described in this chapter can be easily modified to produce relevant results for any EV charging power profiles, waiting times or location.

One of the most interesting results from this work is the queuing priority. It has been discussed how, when the constraint is the amount of power available to charge the EVs, it is better to charge the EVs using a first come first served algorithm rather than sharing all the power equally. This may be counterintuitive to think that curtailing power to some users can reduce average waiting times, however the first come first served algorithm results in a lower average waiting time. This is a key consideration that people installing fast charging stations with limited power must understand, that it is not always optimal to simply share the power equally.

The results from Table 4.6 show how the capacity and C-Rate of the stationary energy store can vary significantly depending on the available grid connection power. This means that there is not

simply one energy storage technology that can be used for all fast charging stations. For example, from the results of Table 4.6, when the grid connection is capable of charging one EV a very large stationary energy store that operates at low C-Rates is required. This may mean lead acid or flow batteries are used for the stationary energy storage device, while for the case when the grid connection is capable of charging three EVs a small stationary energy storage device that operates at high C-Rates is required and so supercapacitors or flywheels may be chosen due to their good rate ability [188].

4.4 Conclusions from the Requirements of the Stationary Energy Store

If a fast charging station is required at a certain location where there is insufficient grid connection power available there are two options, either upgrade the power rating of the electricity grid connection or use a stationary energy store to buffer the energy between the electricity grid and the EV. In this chapter a novel method to size the stationary energy store at fast EV charging stations has been proposed based on the acceptable waiting time of EVs arriving at the fast EV charging station. The results can be used in an economic assessment comparing the cost of the stationary energy storage to the costs of upgrading the electricity grid infrastructure at the fast EV charging station location to determine the ultimate most cost effective solution.

The method proposed has been demonstrated for an actual charging station location where the grid connection infrastructure is rated at 500 kVA and the charging points rated at 120 kW. It has been shown how this site could be upgraded to support future 400 kW charging without upgrading the current grid connection infrastructure. The results are that a 1,000 kWh stationary energy store is required, and this reduces the average waiting time from 20 minutes to 13 seconds. In future work, the cost of a 1,000 kWh energy store can be compared to the cost of upgrading the electricity grid infrastructure at the charging station location to determine the optimum solution.

In the Section 2.2.2.1 it was identified that one of the future limitations to the fast charging of EVs is the ability to draw the required power from the electricity grid. The method proposed in this chapter can be used to size a stationary energy store at a fast charging station to overcome this limitation and allow fast charging stations to be installed at locations where previously the grid could not accommodate them. Future work could look at improving the initial modelling assumptions, namely regarding future fast charging power profiles, acceptable waiting times and finding ways to accurately estimate the number of EVs that will use a fast charging station at a given location. Even if these assumptions are improved the method presented in this Chapter can be used in its current form.

Chapter 5 Energy Storage Thermal Modelling

To overcome the challenge of dealing with the additional heat generated in the EV battery during fast charging, thermal modelling can be used to design the EV battery cooling system. As described in this chapter, obtaining the parameters required for battery thermal modelling is not straightforward and the parameters are not usually available on cell datasheets or from cell manufacturers. One of the novel outputs of this thesis is a method to obtain the thermal parameters of cells using equipment commonly found in battery laboratories, as detailed in this chapter. It is envisaged that simplifying the cell thermal parameterisation will enable more researchers to undertake modelling of EV batteries, which in turn will lead to novel cooling systems being designed to deal with the excess heat generated during fast charging. There is a published journal paper by the author associated with this chapter: Thomas S. Bryden, Borislav Dimitrov, George Hilton, Carlos Ponce de León, Peter Bugryniec, Solomon Brown, Denis Cumming, Andrew Cruden, Methodology to determine the heat capacity of lithium-ion cells, Journal of Power Sources, Volume 395, August 2018, Pages 369-378, 10.1016/j.jpowsour.2018.05.084 [27].

Once the thermal parameters are obtained, it is demonstrated that the temperature of the cells can be modelled at high rates, defined as being over 1C, and the modelled results are then verified experimentally. The model predicts the cell surface temperature well, generally within 2°C, and the temperature is also predicted well when the cell is placed in a different environment by wrapping the cell in insulation. These results indicate that the cell thermal parameters obtained by the method could be used in 3D models of battery packs to design cooling systems.

As seen in the previous chapter, the stationary energy storage may have to operate at high rates and the thermal model demonstrated may therefore also be useful for design of the stationary energy store cooling system. The chapter therefore ends by demonstrating how it is possible to extend the author's thermal model for use with other energy storage types, including lead-acid batteries and supercapacitors.

The first part of the chapter, Section 5.1, discusses why the particular thermal model is chosen and details the theory behind the thermal model. Section 5.2 then discusses the two most important thermal parameters for the thermal modelling of cells and battery packs, the heat capacity and thermal conductivity, and details why they are hard to obtain for cells. To obtain these parameters and verify the model, experiments are conducted in the laboratory and Section 5.3 details the experimental setup. The main novel output from this chapter is the robust, simple method to obtain the thermal parameters, which is detailed in Section 5.4. The heat capacity of the cells is then verified by performing comparative experiments in a calorimeter and

these experiments are detailed in Section 5.5. The heat capacity results, comparing the novel method proposed in this PhD to the standard method of calorimetry, are shown in Section 5.6. It is then demonstrated how the model can be used to model the surface temperature of the cells in Section 5.7. The results are discussed in Section 5.8 before the model is extended to address lead-acid cells and supercapacitor cells in Section 5.9.

5.1 Description of the Thermal Model

The first step is to choose the thermal model to use. To keep the thermal model as general as possible, initially the simplest thermal model was considered, being a cell model similar to that shown in Figure 2.14a, where the entire cell is treated as single point with uniform temperature and heat is transferred to and from the cell. To determine whether this type of thermal model, where the cell has a uniform temperature, is appropriate the Biot number can be used [189]. The Biot number (*B*) is the ratio of the internal thermal resistance (R_{in} *(K* W^{-1}*)*) divided by the external thermal resistance (R_{out} *(K* W^{-1}*)*), as defined in Equation 5.1. If the Biot number is less than 0.1 the simple model with uniform cell temperature may be appropriate.

$$B = \frac{R_{in}}{R_{out}}$$

Equation 5.1

Values for the internal and external thermal conductivity found by other researchers [137], were 3.3 K W^{-1} and 8.9 K W^{-1} respectively. The Biot number, calculated using Equation 5.1, is therefore calculated as 0.37, thereby indicating that the uniform cell temperature model is not appropriate.

The next simplest model is therefore used for thermal modelling of the cell. In this model heat is generated at a point inside the cell where this point has a specific heat capacity and a mass. The heat is then transferred from the inside of the cell to the cell surface where it is assumed there is no mass or specific heat capacity. Finally, the heat is transferred from the cell surface to the ambient environment as shown in Figure 5.1. The internal and external heat transfer coefficients include all heat transfer modes, namely conduction, convection and radiation. If heat is consumed within the cell or the ambient temperature is higher than the cell temperature then the heat will flow in the opposite direction to that illustrated in Figure 5.1, the model has previously been reported in [137].

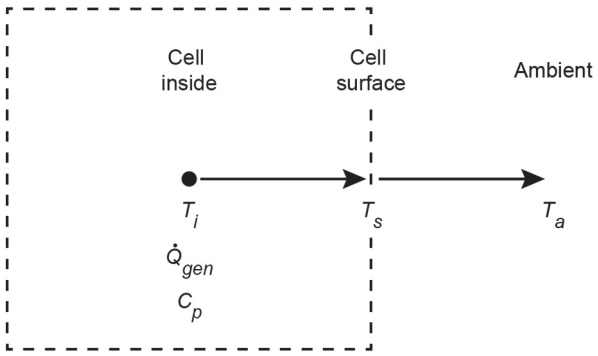

Figure 5.1 Overview of cell thermal model

In the following section the equations describing the thermal model are derived. By applying Equation 2.5 to the point on the cell inside, the result is shown in Equation 5.2. The change in internal energy is related to the heat capacity ($C_{p,i}$ *(J* K^{-1}*)*) and the rate of internal temperature (T_i *(K)*) change with time (*t (s)*), as per the equation on the left hand side of Equation 5.2. $\dot{Q}_i$ (*W*) and $\dot{Q}_{gen,i}$ (*W*) are the heat transferred to and the heat generated at the cell inside point respectively.

$$C_{p,i}\left(\frac{dT_i}{dt}\right) = \dot{Q}_i - \dot{Q}_{gen,i}$$

Equation 5.2

Heat transfer has previously been described in Equation 2.4, and can be a result of any of the three modes, conduction, convection or radiation. For this model, all heat transport modes are lumped together and a single internal heat transfer coefficient (h_i *(W* m^{-2} K^{-1}*)*) is used. The rate heat is transferred from the cell inside to the cell surface is given on the right hand side of Equation 5.3, with the internal cell area (A_i *(*m^2*)*) and the cell surface temperature (T_s *(K)*).

$$\dot{Q}_i = h_i A_i (T_s - T_i)$$

Equation 5.3

The internal heat transfer coefficient and the internal cell area do not change and so to use standard terms these are substituted for the inverse of the internal thermal resistance as shown in Equation 5.4.

$$h_i A_i = \frac{1}{R_{in}}$$

Equation 5.4

Substituting Equation 5.4 into Equation 5.3 and then substituting the combined equation in Equation 5.2 gives Equation 5.5.

$$C_{p,i}\frac{dT_i}{dt} = \frac{1}{R_{in}}(T_s - T_i) - \dot{Q}_{gen,i}$$

Equation 5.5

Measuring the internal temperature of a cell is not possible with basic laboratory equipment as to place a thermocouple inside the cell to determinate internal temperature would require a glove box to provide an inert atmosphere in which the cell can be modified without internal cell components reacting with oxygen and or water. To eliminate the internal cell temperature from Equation 5.5, Equation 2.4 is again applied but this time at the cell surface point, giving Equation 5.6. $C_{p,s}$ ($J\ K^{-1}$) is the surface heat capacity, $\dot{Q}_s$ (W) and $\dot{Q}_{gen,s}$ (W) are the heat transferred to and the heat generated at the cell surface point respectively

$$C_{p,s}\left(\frac{dT_s}{dt}\right) = \dot{Q}_s - \dot{Q}_{gen,s}$$

Equation 5.6

At the cell surface there is assumed no mass so the heat capacity is zero and internal energy does not change, giving Equation 5.7. It is also assumed that there is no heat generation at the cell surface, giving Equation 5.8.

$$C_{p,s}\left(\frac{dT_s}{dt}\right) = 0$$

Equation 5.7

$$\dot{Q}_{gen,s} = 0$$

Equation 5.8

The heat transferred to the cell surface is equal to the heat transfer from the cell inside to the cell surface plus the heat transfer from the ambient to the cell surface, as shown in Equation 5.9. The heat transfer from the cell inside to the cell surface is the negative of Equation 5.3 and is shown in the middle of Equation 5.9. The heat transfer from the ambient to the cell surface is related to the external heat transfer coefficient (h_o ($W\ m^{-2}\ K^{-1}$)), the external area (A_o (m^2)), the surface temperature and the ambient temperature (T_a (K)) and is shown on the right of Equation 5.9.

$$\dot{Q}_s = h_i A_i (T_i - T_s) + h_o A_o (T_a - T_s)$$

Equation 5.9

Similar to above, the singular heat transfer term accounts for all modes of heat transfer and the external area will not change so the product of $h_o A_o$ is exchanged for the inverse of the external

thermal resistance. Making this substitution and substituting Equation 5.7, Equation 5.8, and Equation 5.9 into Equation 5.6 gives Equation 5.10. The physical meaning of Equation 5.10 is that the heat transferred to the surface point is equal to the heat transferred away from the surface point.

$$0 = \frac{1}{R_{in}}(T_i - T_s) + \frac{1}{R_{out}}(T_a - T_s)$$

Equation 5.10

Equation 5.10 can then be solved for the internal cell temperature, as stated in Equation 5.11.

$$T_i = \frac{R_{in}}{R_{out}}(T_s - T_a) + T_s$$

Equation 5.11

The internal cell temperature from Equation 5.11 can then be substituted into Equation 5.5 to give Equation 5.12, which simplifies to that seen in Equation 5.13.

$$C_{p,i}\frac{d\left(\frac{R_{in}}{R_{out}}(T_s - T_a) + T_s\right)}{dt} = \frac{1}{R_{in}}\left(T_s - \left(\frac{R_{in}}{R_{out}}(T_s - T_a) + T_s\right)\right) - \dot{Q}_{gen,i}$$

Equation 5.12

$$C_{p,i}\left(\frac{dT_s}{dt}(R_{in} + R_{out}) - R_{in}\frac{dT_a}{dt}\right) = T_a - T_s - \dot{Q}_{gen,i}R_{out}$$

Equation 5.13

The experiments conducted in this chapter are on individual cells and so the ambient temperature is the air surrounding the cell. The ambient temperature is therefore assumed to be constant, giving Equation 5.14. Equation 5.14 is then substituted into Equation 5.13 to give Equation 5.15.

$$\frac{dT_a}{dt} = 0$$

Equation 5.14

$$C_{p,i}\frac{dT_s}{dt}(R_{in} + R_{out}) = T_a - T_s - \dot{Q}_{gen,i}R_{out}$$

Equation 5.15

The output to the model is the surface temperature of the cell, which is obtained by using a time step (Δt (s)), i.e. using an explicit Euler to discretise the ordinary differential equation. The substitutions seen in Equation 5.16, Equation 5.17 and Equation 5.18 can therefore be used.

$$\frac{dT_s}{dt} = \frac{T_{s(t)} - T_{s(t-1)}}{t_{(t)} - t_{(t-1)}}$$

Equation 5.16

$$T_s = T_{s(t-1)}$$

Equation 5.17

$$\dot{Q}_{gen,i} = \dot{Q}_{gen,i(t)}$$

Equation 5.18

Substituting these equations into Equation 5.15, gives Equation 5.19, which can be rearranged to give Equation 5.20. It is assumed that the heat capacity, internal thermal resistance and external thermal resistance are constant and do not vary during the experiments.

$$C_{p,i}\frac{T_{s(t)} - T_{s(t-1)}}{t_{(t)} - t_{(t-1)}}(R_{in} + R_{out}) = T_a - T_{s(t-1)} - \dot{Q}_{gen,i(t)}R_{out}$$

Equation 5.19

$$T_{s(t)} = \frac{T_a - T_{s(t-1)} - \dot{Q}_{gen,i(t)}R_{out}}{C_{p,i}(R_{in} + R_{out})}\left(t_{(t)} - t_{(t-1)}\right) + T_{s(t-1)}$$

Equation 5.20

As stated in the background section there are two commonly used terms for the heat generation in a lithium-ion battery, ohmic heat generation, proportional to the current squared, and entropic heat generation or consumption, proportional to the current. The method in the following sections involves charging and discharging the cells at the manufacturers quoted maximum charge and discharge rates. The model is also used in fast charging at high rates, over 1C. At these high rates the ohmic heating is dominant as the ohmic heating is proportional to the current squared.

The entropic heat generation term ($Q_{gen,ent}$ *(W)*) can be seen below in Equation 5.21. Other researchers [137] found that including the entropic term produced only a small reduction of the maximum temperature error from 2.3°C to 1.8°C. In this study by other reserachers the cell was cycled at 10 A (4C), the heat generation from ohmic heating was found to be around 3.1 W. The value for dV_{OCV}/dT varies with SoC, the researchers found a value of -0.3 mV K^{-1} at 0% SoC however between 20% and 100% SoC the absolute value was always less than 0.1 mV K^{-1}. Assuming a worst case scenario with the cell at 60°C, the entropic heat generation is found to be 1.0 W at 0% SoC (*10 A × (60°C + 273) × 0.3 × 10^{-3} V K^{-1}*) however over 20% SoC the entropic heat

generation is less than 0.33 W. For this high rate thermal modelling study the entropic heat generation term is therefore ignored.

$$Q_{gen,ent} = IT\frac{dV_{OCV}}{dt}$$

Equation 5.21

Only considering ohmic heat generation means that the heat generation term is as per Equation 5.22 and is related to the cell current (*I (A)*) and the cell resistance (*R (Ω)*), which varies with time throughout the model. The modulus brackets and the negative sign indicate that heat is always generated at the point.

$$\dot{Q}_{gen,i(t)} = -\left|{I_{(t)}}^2 R_{(t)}\right|$$

Equation 5.22

The cell resistance has previously been described in Equation 2.7 and this equation is repeated in Equation 5.23 and is reliant on the cell voltage (*V (V)*), cell OCV (V_{OCV} *(V)*) and cell current.

$$R = \frac{V_{(t)} - V_{OCV(t)}}{I_{(t)}}$$

Equation 5.23

Substituting Equation 5.23 into Equation 5.22 gives Equation 5.24.

$$\dot{Q}_{gen,i(t)} = -\left|\left(V_{(t)} - V_{OCV(t)}\right)I_{(t)}\right|$$

Equation 5.24

For this research, the voltage and current are obtained from experiments. In the future, if the model is to be made truly predictive, the thermal model demonstrated in the following sections would need to be combined with a model to predict the voltage of the cell based on a current profile [190]. These models are widely available such as the equivalent circuit models described in Section 2.4.2.2.

The OCV of the cell is obtained from a look up table for the cell, where the look up table contains data relating the SoC of the cell to the OCV, where an example of this characteristic is shown in Figure 5.2.

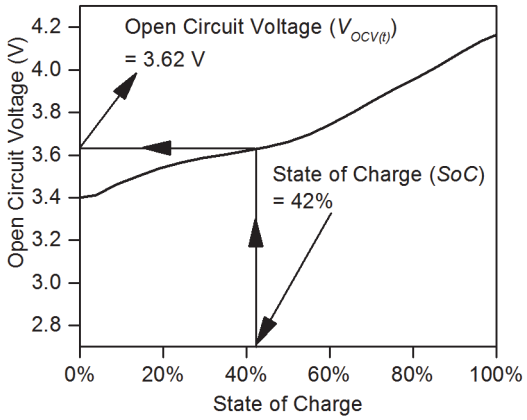

Figure 5.2 Determining the OCV using the SoC

The SoC (*SoC*) of the cell is obtained using the coulomb counting method using Equation 5.25, the cell current and cell nominal capacity (Cap_{nom} *(Ah)*). The initial SoC can be found by leaving the cell to rest and using the lookup table, from Figure 5.2, to relate the voltage to the SoC.

$$SoC_{(t)} = SoC_{(t-1)} + \frac{I_{(t)}\left(t_{(t)} - t_{(t-1)}\right)}{Cap_{nom}}$$

Equation 5.25

For example, if a 10 Ah cell initially at 20% SoC is charged at 3 A for 1.5 hours, the SoC is 65%, as seen in Equation 5.26. Although this demonstration shows a 1.5 hour time, later on in the chapter, 0.1 seconds is used as the time step and so a new SoC is calculated every 0.1 seconds.

$$SoC_{1.5hours} = 0.2 + \frac{3 \times (1.5 - 0)}{10} = 0.65$$

Equation 5.26

The underlying thermal equation for this chapter can therefore be seen in Equation 5.27, which is found by substituting Equation 5.24 into Equation 5.20.

$$T_{s(t)} = \frac{T_a - T_{s(t-1)} + \left|\left(V_{(t)} - V_{OCV(t)}\right)I_{(t)}\right|R_{out}}{C_{p,i}(R_{in} + R_{out})}\left(t_{(t)} - t_{(t-1)}\right) + T_{s(t-1)}$$

Equation 5.27

To use Equation 5.27 to predict surface temperature the model steps through time and at each time calculates a new value for the surface temperature. The initial conditions are therefore the surface temperature ($T_{s(0)}$) and SoC (SoC_0) at the initial time (t_0). The known constant values are the cell nominal capacity (Cap_{nom}), the ambient temperature (T_a), the heat capacity ($C_{p,i}$), the internal thermal resistance (R_{in}) and the external thermal resistance (R_{out}). The method for each time step is as follows:

1. Determine the cell voltage ($V_{(t)}$) and cell current ($I_{(t)}$), this could be done with an equivalent circuit model but in this chapter the cell voltage and current are measured during the experiments
2. Calculate the SoC of the cell using Equation 5.25
3. Lookup the value for the cell OCV ($V_{OCV(t)}$) in the SoC versus OCV table, i.e. Figure 5.2
4. Calculate the surface temperature using Equation 5.27

5.2 Heat Capacity and Internal Thermal Resistance

Of the five known constant values, the cell nominal capacity is easily found on cell datasheets and the ambient temperature is recorded during each experiment. There are three unknown terms, which are related to the thermal parameters: the heat capacity, the internal thermal resistance and the external thermal resistance. The heat capacity and internal thermal resistance are the two most important thermal parameters as they are specific to the cell and, once known, the cell could be placed in a more complex scenario, such as a battery pack, and the heat capacity and internal thermal resistance would remain the same. In this case of placing the cell in a model of a battery pack, the external thermal resistance would change depending on the placement within in the battery pack. The external thermal resistance therefore changes depending on where the cell is placed while the heat capacity and internal thermal resistance remain constant. If the cell is placed in a 3D finite element thermal model, the heat capacity and internal thermal resistance would need to be input by the user while the 3D model would calculate the external thermal resistance.

5.2.1 Heat Capacity

The heat capacity of the cells is a critical thermal parameter that is required for all cell thermal models, irrespective of the thermal model employed. The heat capacity of an object is a measure of how easy it is to change the temperature of the object by transfer of heat. Depending on the required model complexity there may be one value for the heat capacity of the entire cell [137, 151, 191-197] or multiple values at different locations within the cell [148, 198, 199], representing the different materials that the cell is constructed from. From the review of thermal models, the method of using one value for the heat capacity of the cell is currently the most popular method for researchers.

An intermediate example is shown in Figure 5.3 where there are two values used for the heat capacity in the thermal model, one for the cell inside and one for the cell casing. This model could be made more complicated by including the individual geometries and associated heat capacities

of all the components inside the cell, i.e. the current collectors, electrodes, electrolyte and separator. In contrast, the model could be made more simplistic by lumping the heat capacity of the cell inside and cell casing together to obtain one value for the heat capacity of the cell. The choice of complexity, as with all modelling, is a trade-off between accuracy, complexity and time. For the model described in Figure 5.1 there is only one value used for the heat capacity of the cell.

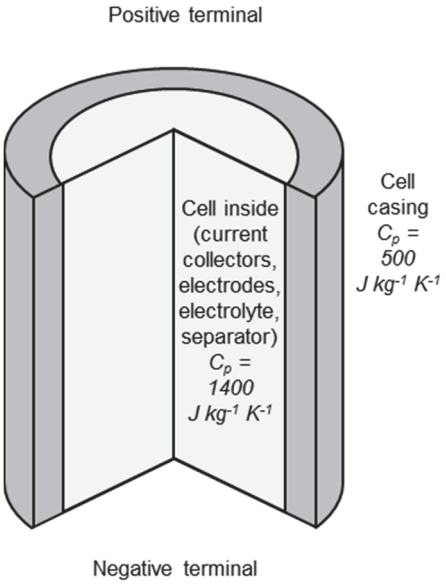

Figure 5.3 Cylindrical cell with different heat capacities for the cell inside and casing

When using a single value for the heat capacity of the cell it is often difficult to determine the heat capacity. The heat capacity of cells is generally not stated on cell datasheets and manufacturers often do not provide data on the specific heat capacity of their cells. Later in this chapter experiments are conducted on four lithium-ion cells, for each cell the manufacturer was contacted but in all cases could not provide data regarding the heat capacity of the cell.

The most popular method to determine the heat capacity of an entire cell ($C_{p,cell}$) involves a weighted sum of the heat capacities of the materials inside the cell [151, 192, 193, 195, 197]. This can be performed using Equation 5.28, where the masses (m_1, m_2, *etc*) and heat capacities ($C_{p,1}$, $C_{p,2}$, *etc*) of each material in the cell are known.

$$C_{p,cell} = \frac{m_1 C_{p,1} + m_2 C_{p,2} + \cdots + m_n C_{p,n}}{m_1 + m_2 + \cdots + m_n}$$

Equation 5.28

This method can be seen in use for the cell seen in Figure 5.3 in Equation 5.29, where the mass of steel casing is 0.01 kg and the mass of the cell inside is 0.06 kg. The problem with this method is that detailed information regarding the materials inside cells is rarely available. The cell can be

deconstructed and the materials inside determined chemically however taking apart a cell requires specialist equipment and is not trivial.

$$C_{p,cell} = \frac{0.01 \times 500 + 0.06 \times 1400}{0.01 + 0.06} = 1270\ J\ kg^{-1}\ K^{-1}$$

Equation 5.29

A second common but less popular method is to use calorimetry [191, 200], this involves placing the cell in a calorimeter, applying heating to the cell and measuring the temperature response. During calorimetry the inside of the calorimeter is kept at the same temperature as the cell surface by measuring the cell surface temperature and heating the calorimeter walls. This means that there is zero heat transferred away from the cell in the calorimeter during the experiment and so all heating energy goes into raising the cell temperature meaning the heat capacity can be calculated, this is described in detail in Section 5.5. The problem with this method is that calorimeters are expensive, often costing more than £100,000 and not commonly available in many laboratories.

This inability to easily and accurately determine the heat capacity of lithium-ion cells is therefore a barrier to research into thermal modelling. A new method to determine the specific heat capacity of cells using common equipment found in most battery laboratories is therefore proposed by the author in the subsequent sections, where this method requires only a battery analyser, temperature sensors and a fan. This method is one of the novel outputs of the PhD and the results from the method are verified by determining the heat capacities of the cells using calorimetry.

5.2.2 Internal Thermal Resistance

As well as the specific heat capacity of a cell, a second parameter required for many thermal models is the internal thermal resistance of the cells [201]. As described in Section 2.4.2 there are three types of heat transfer: conduction, convection and radiation. Convection heat transfer occurs in fluids and so is possible inside the cell in the electrolyte, this may be taken into account in very detailed cell models however generally is ignored due to the limited mobility of the fluid [202]. The internal thermal resistance is therefore as a result of conduction heat transfer and the equation relating the internal thermal resistance to the thermal conductivity (*k (W m^{-1} K^{-1})*) of the cell is shown in Equation 5.30, with a distance (*x (m)*) and an area (*A (m^2)*).

$$R_{in} = \frac{x}{kA}$$

Equation 5.30

The thermal conductivity of the cell is a measure of how easily heat is transferred through the cell by conduction. The thermal conductivity varies within a cell depending on the direction of heat transfer [203]. Take for example a spirally wound cylindrical cell, an example of which is shown in Figure 5.4, the thermal conductivity will be different longitudinally and radially. Longitudinally, the heat is travelling through the same material while radially the heat is travelling through many layers of different materials. The thermal conductivity is much higher longitudinally because the heat may travel through one material with a high thermal conductivity, for example metallic current collectors with thermal conductivities in the range 237-397 W m^{-1} K^{-1} [204], while radially the heat must travel through materials with low thermal conductivity, for example electrodes and separators with thermal conductivities in the range 0.6-3.9 W m^{-1} K^{-1} [204]. Overall for an 18650 cell other researchers found values for the thermal conductivity of 0.25 W m^{-1} K^{-1} and 30 W m^{-1} K^{-1} in the radial and longitudinal directions respectively [205].

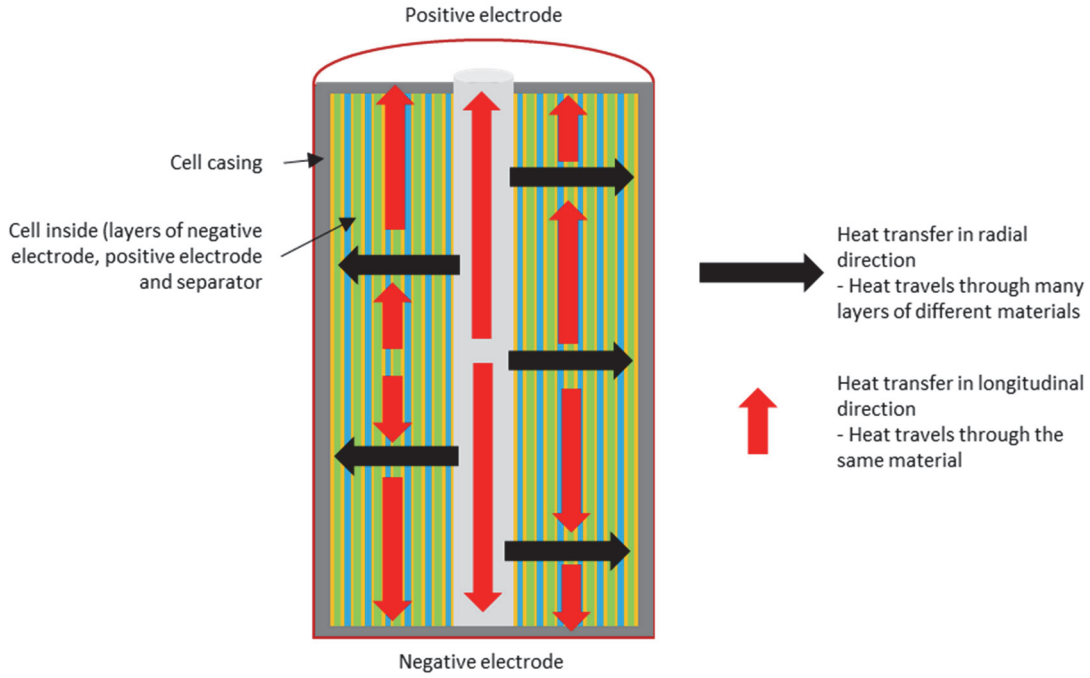

Figure 5.4 Inside of an 18650 cell with conduction heat transfer shown

The thermal conductivity is slightly less important than the heat capacity in large scale models, such as those of whole battery packs [206], which may use the heat capacity of the cells but assume they are a uniform temperature and therefore not include an internal thermal resistance. As an approximation, the model used in this chapter does not differentiate between the thermal conductivity in different directions and uses a single value for the internal thermal resistance. As the model is for high rate applications the temperature changes are large, in the region of 10°C and so an approximation for the thermal conductivity should be appropriate. This approximation

is justified in the results section as the method to determine the heat capacity is shown to work well and the surface temperature is accurately predicted by the model.

5.3 Experimental Setup

The author's aim therefore is to develop a novel method to determine the cell heat capacity and the cell internal thermal resistance that uses laboratory equipment commonly available in battery laboratories. The method is detailed in the subsequent Section 5.4, while in this section the experimental setup to test the method is described.

The experiments conducted in this chapter involve charging and discharging cells at various rates and measuring the surface temperature. A cell being tested is illustrated in Figure 5.5 and the laboratory equipment is described in detail in the following sections and includes:

- Battery analyser and associated wires
- Thermocouples, which connect directly to the battery analyser
- Other equipment:
    - Fans
    - Freezer
    - Safety enclosure

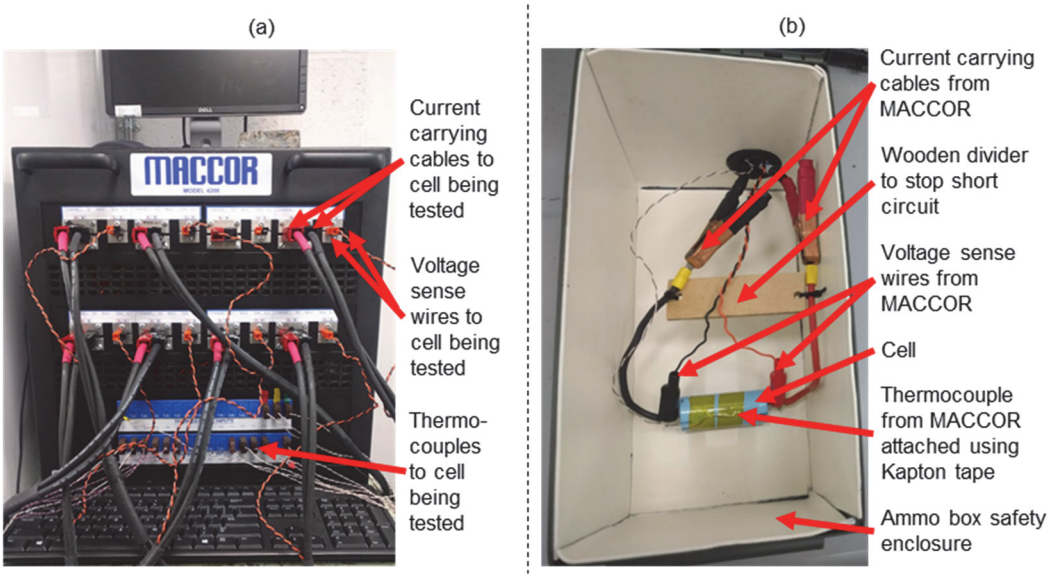

Figure 5.5 Pictures of the experimental equipment

Battery analyser (left) and a cell being connected to the battery analyser (right)

5.3.1 Battery Analyser and Associated Wires

The key piece of equipment is the battery analyser, the battery analyser is manufactured by MACCOR and can be used for experiments where the voltage and current are below 6 V and 240 A respectively, the battery analyser is shown in Figure 5.5a and the technical specifications of the battery analyser are given in Table 5.1.

Table 5.1 Specifications of the battery analyser

	Battery Analyser
Manufacturer	MACCOR
Equipment Number	Model 4200
Channels	8
Thermocouples	32
Maximum Power	2.4 kW
Maximum Voltage	6 V
Voltage Accuracy	0.0012 V
Maximum Channel Current	30 A
Current Accuracy	0.015 A

The battery analyser includes software for setting up charging and discharging experiments, namely MacTest32 software. A schematic of the setup of the cell being tested and the battery analyser are shown in Figure 5.6, where all wires and thermocouples connect directly to the battery analyser. All data, voltage, current and temperature, are also recorded automatically by the computer.

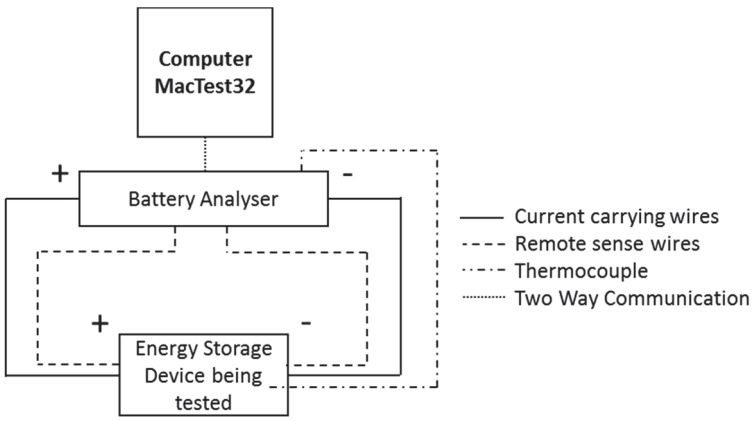

Figure 5.6 Schematic of all connections for battery cycling using the battery analyser

5.3.1.1 Remote Sensing Wires

As shown in Figure 5.5 and Figure 5.6, there are four wires connected to the terminals of the cell being tested, these wires include two current carrying wires and two remote sense wires. The two current carrying wires deliver the current to or from the cell and therefore need to be of an appropriate wire gauge to carry the required current. The two remote sense wires can be thin and only measure the voltage at the cell terminals. This voltage is then fed back to the battery analyser charging and discharging the cell, which can then compensate for any voltage drop that may occur between the charging and discharging equipment and the cell to ensure the voltage at the cell terminals is correct. This unwanted voltage drop could be caused for example by resistance in the current carrying wires, in this case the voltage drop would be equal to the current multiplied by the resistance of the wire.

5.3.1.2 Connection of Wires to Energy Storage Device

A common problem encountered throughout the PhD is how to make a good reliable connection between the wires and the cell under test. This issue was amplified in this PhD work as high rate, meaning high current, charging and discharging is often undertaken. At high currents a poor connection with high resistance (R_{con} *(Ω)*) increases the connection voltage drop (V_{drop} *(V)*), as shown in Equation 5.31, along with the current (*I (A)*). If the remote sensing wires are directly connected to the cell terminal this voltage drop is taken into account in the recorded voltage however for the case of the cylindrical cells the remote sensing wires could not be connected directly to the cell terminal. This means that the connection resistance needs to be minimised.

$$V_{drop} = IR_{con}$$

Equation 5.31

Also, at high currents heat can be generated ($\dot{Q}_{con}$ (*W*)) from the connection resistance, as seen in Equation 5.32. This means the cell may be subject to additional heating and elevated temperatures, reinforcing that a good connection between the wires and the cell is therefore critical.

$$\dot{Q}_{con} = I^2 R_{con}$$

Equation 5.32

There are three types of possible connections for cells: mechanical connection, soldering connection, or welding connection [207]. The advantages and disadvantages of each connection techniques are detailed in Table 5.2. A mechanical connection can consist simply of a spring creating pressure between the cell terminal and the connector or could simply be a nut and bolt.

Table 5.2 Advantages and Disadvantages of different connection techniques

Connection	Advantages	Disadvantages
Mechanical	Simple Easily replace cell being tested	High contact resistance
Soldering	Low contact resistance	Intense heat while soldering may damage cell
Welding	Less heating than soldering	Specialist equipment required Connection not as good as soldering

The choice of connection for the experiments conducted depends on the cell being tested and whether a simple connection slot is available on the device. The connections for each of the three types of cell tested are shown in Figure 5.7. For the prismatic cell the current carrying wire could simply be bolted to the cells, while for the pouch cell copper clamps were constructed and the current carrying wire clamped to the cell terminals. For the cylindrical cells no simple mechanical connection could be created that would give a good connection. Soldering is therefore used as it will give the best connection quality, which, as described above, is crucial for the high currents involved in the experiments. With soldering there is however debate as to whether the connection causes additional degradation to the cell being tested. Degradation is not a focus of this thermal modelling chapter. Whenever a cell is soldered, a charge and discharge of the device at rated conditions is undertaken to ensure the charge and discharge curves look the same before and after soldering.

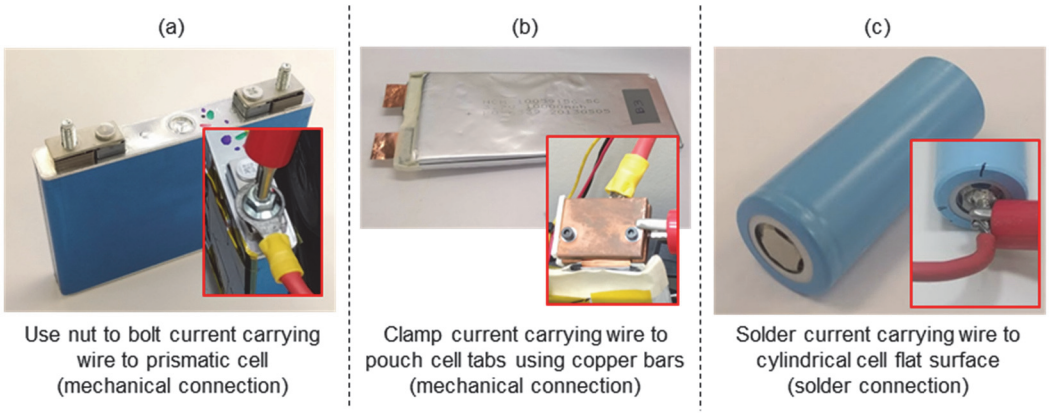

Figure 5.7 Three types of cell tab connections

Screw connection (left), clamped connection (middle) and soldered connection (right)

5.3.2 Thermocouples

Thermocouples are used in the experiments to record the temperature but also for safety reasons as the thermocouples enable automatic shut down of experiments if a certain temperature is exceeded. The thermocouples connect directly to the battery analyser and are type T class 1 thermocouples.

5.3.2.1 Attachment of Thermocouples to Energy Storage Device

The thermocouples are attached to the energy storage devices using kapton tape. It should be noted when setting safety cut off temperatures that the temperature being measured by the thermocouple is the surface temperature of the cell. The temperature inside the cell may be different to that recorded on the surface. For high rate charging and discharging the internal temperature is likely to be higher than that measured on the surface. In a previous study [137] it was found that the internal temperature was 10°C hotter than the surface temperature when a cell was charged and discharged at 8C.

The positioning of the thermocouples on the energy storage device must also be considered. It has been suggested that for safety reasons the thermocouples are placed near the negative electrode as the negative electrode has a higher thermal conductivity and dangerous overcharge reactions at high temperature may occur initially at the negative electrode [208]. The positioning of the thermocouple is important as there can be temperature variations across the surfaces of energy storage devices, as shown in Figure 5.8. From the experiments conducted in this PhD there is not simply one place on the cells that will always be the hottest point as the temperature variations depend on the geometry of cell, the chemistry of the cell and the charging and discharging profile applied. The solution adopted in this thesis is therefore to put as many thermocouples as possible on the energy storage device being tested with an average cell temperature then derived and used, the locations of the thermocouples are detailed for each experiment individually.

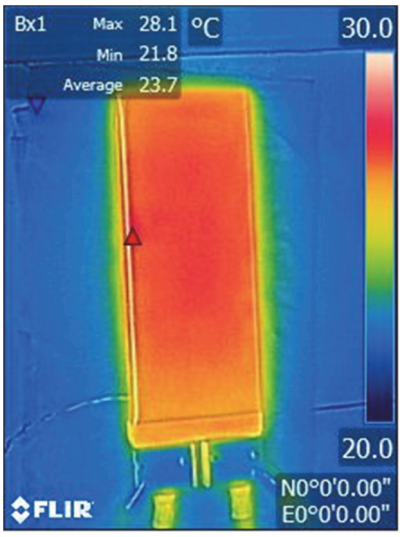

Figure 5.8 Surface temperature variations across a lithium-ion cell during discharge

Showing the hottest temperature in the middle of the cell

To test whether the negative electrode is hotter than the cell surface a NMC 26650 cell was setup for testing with one thermocouple attached to the negative electrode and one thermocouple attached to the cell surface. The cell was charged from 0% SoC to 4.2 V at 5 A (1C), rested for 2 minutes, discharged at 15 A (3C) till 2.75 V then rested for 10 minutes and the results are shown in Figure 5.9. From Figure 5.9 it is clear that the cell surface temperature is always hotter than the cell electrode temperature.

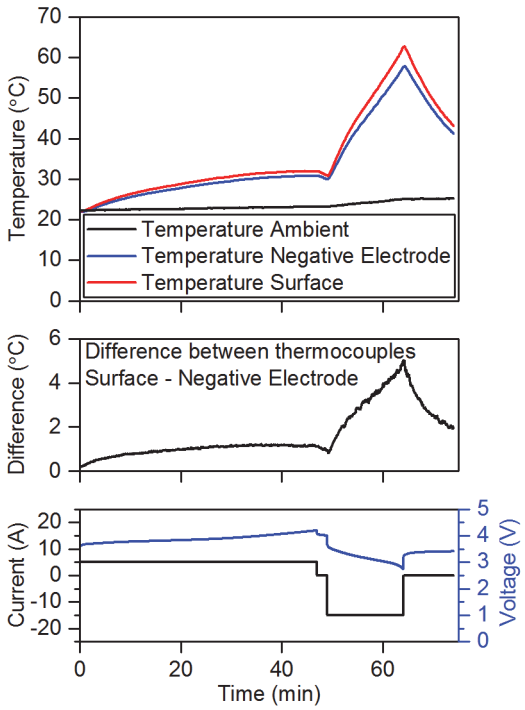

Figure 5.9 Measured surface and electrode temperature of lithium-ion cylindrical cell

5.3.2.2 Calibration of Thermocouples

The accuracy of the thermocouples is ±1.5°C, made up of the accuracy from the MACCOR, ±1°C, and the accuracy of the thermocouple, ±0.5°C. Figure 5.12a shows the problem with the thermocouple accuracy, as when reading the same temperature, the thermocouples read different values.

To account for this inaccuracy the thermocouples are calibrated and the calibration experiment can be seen in Figure 5.10. All thermocouples are taped together and placed in a beaker of water, which is placed on a hot plate with a stirrer. A traditional thermometer is also placed in the beaker of water. The assumption is that all thermocouples and the traditional thermometer are reading the same temperature.

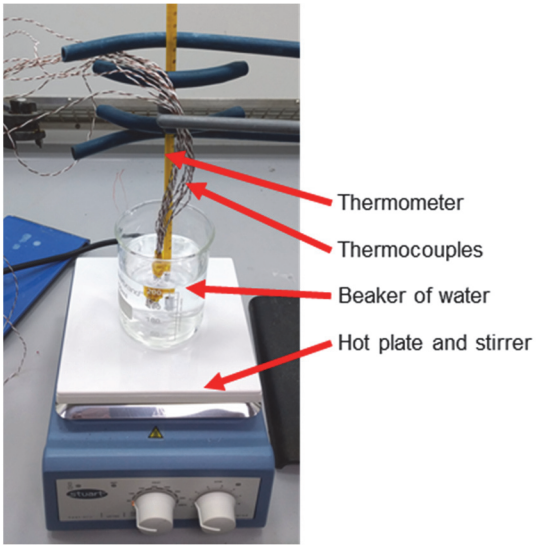

Figure 5.10 Picture of thermocouple calibration experiment

The temperature of the hot plate is then changed periodically thereby changing the water temperature and the temperature results are shown in Figure 5.11a. Temperature measurements using the traditional thermometer are taken at different temperatures, as indicated in Figure 5.11a by the crosses. The temperature recorded by the traditional thermometer can then be plotted versus the temperature recorded by the thermocouples and Figure 5.11b shows the results for one of the thermocouples.

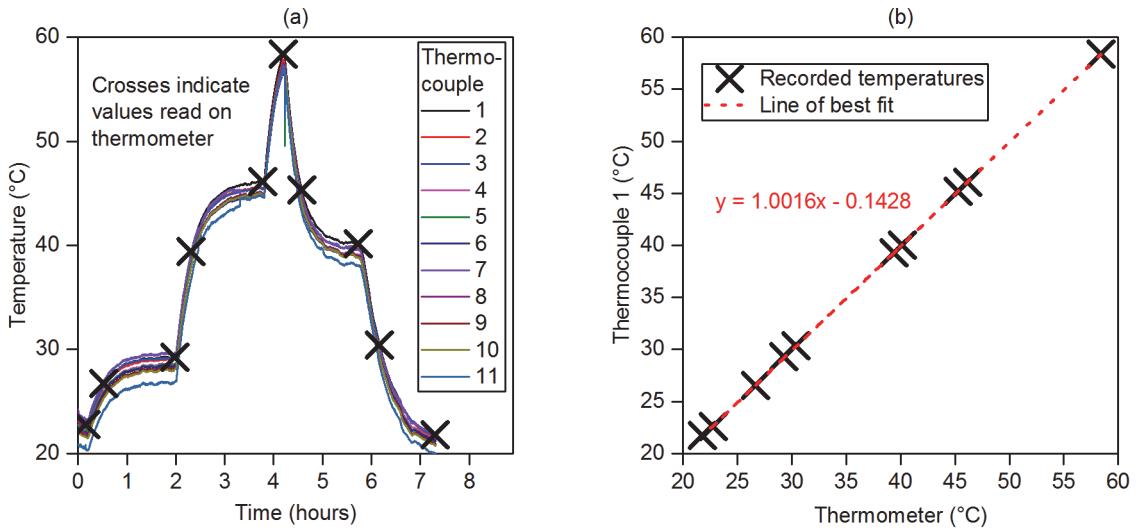

Figure 5.11 Thermocouple calibration experiments results

Temperature of all thermocouples and thermometer (left) and results for thermocouple 1 (right)

Using the line of best fit results from Figure 5.11b, y intercept (c) and gradient (m), the temperature recorded by the thermocouple (T_{therm} *(°C)*) can be converted to the actual temperature (*T (°C)*), using Equation 5.33 for all recorded temperatures. Each thermocouple has its own values of c and m. The temperature results before and after calibration are shown in Figure 5.12.

$$T = \frac{T_{therm} - c}{m}$$

Equation 5.33

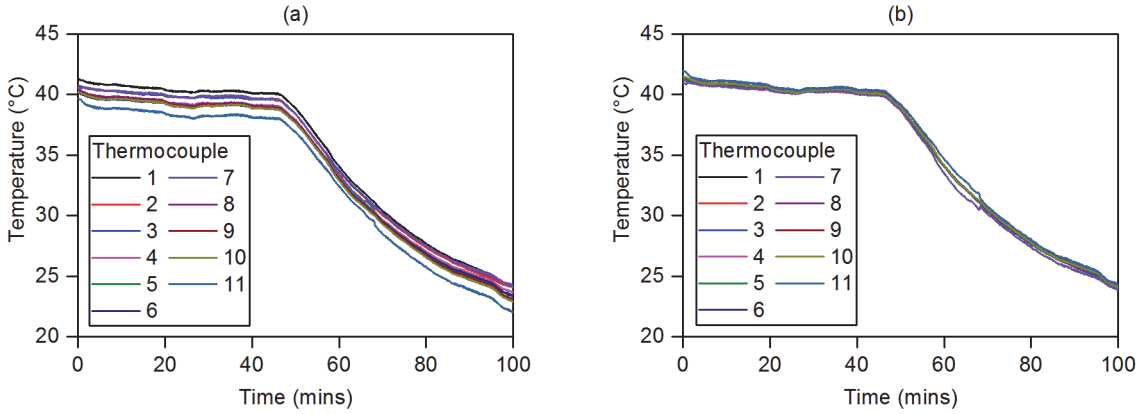

Figure 5.12 Thermocouples reading the temperature of water at the same place

Before applying calibration (left) and after calibration (right)

5.3.3 Other Equipment

In this section additional equipment for the experiments is described, there are three additional equipment devices, the safety enclosure, fans and the freezer.

5.3.3.1 Safety Enclosure

Thermal runaway can result if the lithium-ion cells become too hot, which can result in fire and explosion. Safety precautions are therefore taken while performing experiments on the lithium-ion cells, including having sand buckets and fire extinguishers within easy reach of the cells. Wooden dividers are also used to ensure that the wires connected to the cell terminals could not touch and short circuit the cell, as seen in Figure 5.5b. The experiments are all conducted in safety enclosures. The safety enclosure is shown in Figure 5.13 and consists of an ammunition box that has been coated with insulation material. Holes are drilled in the ammunition box to ensure if a fire does occur pressure does not build up in the box and also to allow the wires and thermocouples to enter the box when the lid is closed.

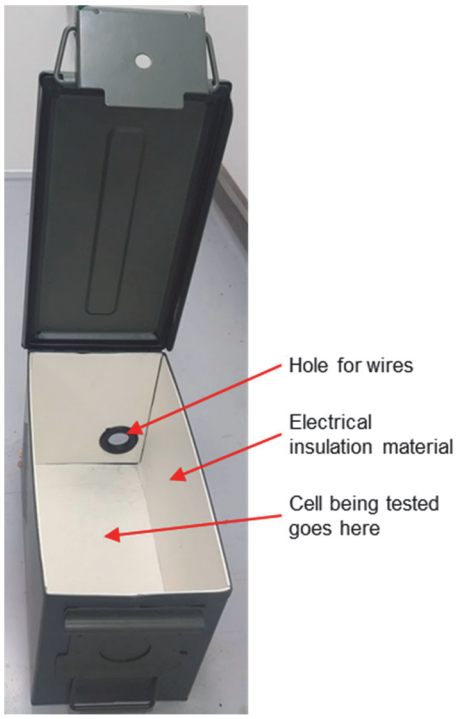

Figure 5.13 Ammunition box safety enclosure with lid open

5.3.3.2 Fans

Fans are used for some experiments to increase the heat transfer from the cell to the ambient. The fans are old computer fans with a fan diameter of 110 mm, the fans operate at 12 V and draw a current of 0.21 A and one of the fans is illustrated in Figure 5.14. The placement of the fans is detailed individually for each experiment.

Figure 5.14 Fan used to increase heat transfer from cell to ambient

5.3.3.3 Freezer

Experiments are conducted in a freezer when lower ambient temperatures are required. The freezer was modified by drilling a hole for the cables required and using insulating foam to seal the drilled hole. The freezer acts as the safety enclosure and so an ammo box is not used in the freezer. A picture of a cell in the freezer before testing is shown in Figure 5.15a. The freezer temperature with nothing inside when set to the minimum and maximum temperatures can be seen in Figure 5.15b. The thermal hysteresis is caused by the freezer compressor control kicking in and out, therefore ambient temperature is not constant.

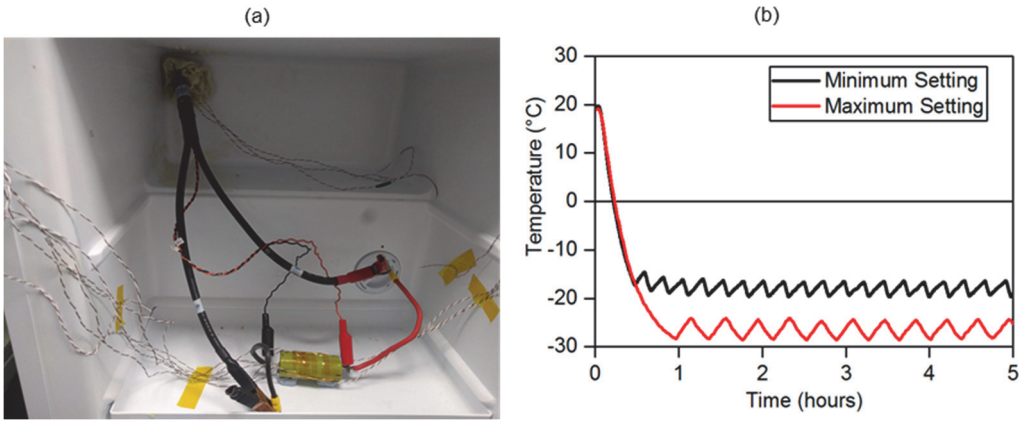

Figure 5.15 Details of freezer experiments

Cell before testing in freezer (left) and ambient freezer temperatures when the freezer is turned on at minute zero (right)

5.3.4 Details of the Cells

Initially the experiments are conducted on four lithium-ion cells, the details of which are shown in Table 5.3. The cells are chosen to test a variety of chemistries and geometries, each of the three cell geometries that may be used in an EV are tested: cylindrical, pouch and prismatic cells. For each of the geometries the cell uses the cathode chemistry NMC, as in the background Section 2.2.1.1 it is described how this is the most common chemistry for use in EVs. The fourth cell is a cylindrical cell of a different chemistry, an LFP cell. The prismatic cell is similar to that used in Honda hybrid EVs.

Table 5.3 Details of the lithium-ion cells tested

	NMC 26650	LFP 26650	NMC Pouch	NMC Prismatic
Manufacturer	AAPortable Power	A123 Systems	AAPortable Power	GS Yuasa
Geometry	Cylindrical 26650	Cylindrical 26650	Pouch	Prismatic
Dimensions	Ø26 mm × 65mm	Ø26 mm × 65mm	11 mm × 60 mm × 162 mm	16 mm × 79 mm × 112 mm
Name	INR-26650-5000	ANR26650M1-B	10059156-5C	LIM5H
Nominal Voltage	3.6 V	3.3 V	3.7 V	3.6 V
Capacity	5 Ah	2.5 Ah	10 Ah	5 Ah
Mass	96 g	76 g	198 g	276 g
Energy density	190 Wh kg^{-1}	110 Wh kg^{-1}	190 Wh kg^{-1}	65 Wh kg^{-1}
Charge cut-off voltage	4.2 V	3.6 V	4.2 V	4.2 V
Discharge cut-off voltage	2.75 V	2.0 V	2.75 V	2.4 V
Maximum continuous charge current	5 A	10 A	10 A	50 A
Maximum continuous discharge current	15 A	70 A	40 A	50 A

One limitation of the experiments conducted in this thesis is that only one cell of each type seen in Table 5.3 was tested, which may be considered poor experimental planning. Better practice is to test multiple cells so that results can be analysed across all samples and ensure that results are as a result of a true physical effect rather than an outlier cell. To make the experiments more reliable, each cell tested was initially charged and discharged to ensure the capacity was the same

as the datasheet. If the cell tested was an outlier and had a different internal resistance to most cells this would be taken into account in the results, as the heat generated in the cell would be different and the method used in the following section to determine the heat capacity of the cell would still be valid. One of the main outputs from this Chapter is the method to determine the heat capacity of cells and later the results are validated using calorimetry, so although only one of each cell type is tested, the method is tested four times. Despite these efforts to make the experiments more reliable, there still may be issues with testing an outlier cell, and in future experiments more cells should be tested, this is included in the further work Chapter 7.

5.4 Method to Determine the Thermal Parameters

In this section the method to determine the heat capacity, the internal thermal resistance and the external thermal resistance, which are required to solve Equation 5.27, are described. This method is one of the novel outputs of the author's PhD. Initially, the experimental setup specific to these experiments is described in Section 5.4.1. The external thermal resistance is determined in Section 5.4.2 and the heat capacity and internal thermal resistance determined in Section 5.4.3, where examples are shown for the NMC 26650 cell.

5.4.1 Specific Details of Experimental Setup

The experimental setup specific to the experiments in the following section includes the addition of fans to provide cooling and the placement of thermocouples on the cells.

5.4.1.1 Positions of Fans

Cooling is required for the method in the following section and so fans are used to blow ambient air across the cells and the use of the fans is illustrated in Figure 5.16. To enhance the air flow around the cells, in all cases the cells are placed on blu tack to elevate the cells from the floor, thereby allowing air to flow underneath the cells. From Figure 5.16, two fans are used in order for the cell to be cooled symmetrically. Although having the fans facing each other may not be the most efficient cooling method, the experiments demonstrated later in this section show how it is an effective method to provide cooling. This setup also ensures symmetry of the cell temperatures because both sides of the cells are subjected to the same cooling. A one fan setup may cool the cell better but would result in one hot side and one cool side.

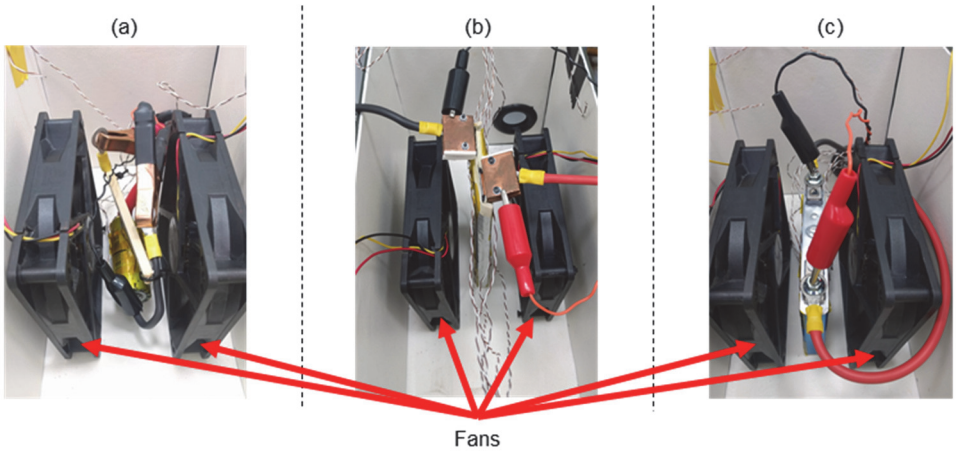

Figure 5.16 Cells under testing with fans

Cylindrical cell (left), pouch cell (middle) and prismatic cell (right)

5.4.1.2 Positions of Thermocouples

The positions of the thermocouples on all cells are illustrated in Figure 5.17. For the cylindrical cells, 9 thermocouples are placed on the cell surface and two ambient thermocouples are used while for the pouch and prismatic cells, 10 thermocouples are placed on the cell surface and one ambient thermocouple used. The ambient temperature is measured in the ammunition box and the ambient thermocouples can be seen in the top left of Figure 5.16. Although the ambient thermocouples are placed inside the ammunition box the experiments are conducted with the ammunition box lid open to allow airflow.

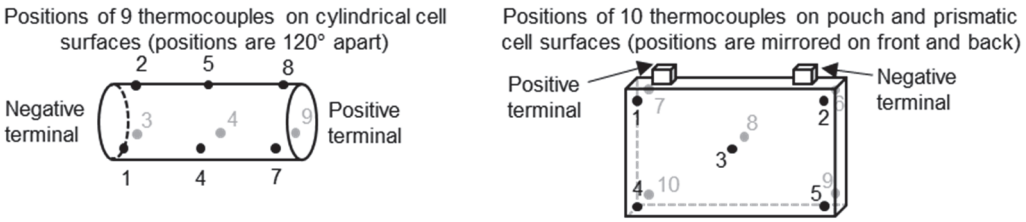

Figure 5.17 Positions of thermocouples on cells

5.4.2 Determining the External Thermal Resistance

Initially the experiments are conducted with the fans turned off. To determine the external thermal resistance a similar method to that described in [137] is used. The cell is taken to 50% SoC by discharging to the cell to the lower cut off voltage and then charging the cell until half the nominal capacity has been added to the cell. The cell is then left overnight and the voltage recorded the following day is taken as the OCV for the test. The cell is then discharged a small amount, less than 5% rated capacity, at the maximum discharge rate allowed by the manufacturer from Table 5.3. The cell is then charged by the same amount of capacity as just removed at the

manufacturers maximum charge rate. This discharge/charge cycle is then repeated until the surface temperature remains constant, dT_s / dt then equals zero and Equation 5.15 then simplifies to Equation 5.34, where $\dot{Q}_{gen}$ is defined by Equation 5.24.

$$0 = T_a - T_s - \dot{Q}_{gen,i} R_{out}$$

Equation 5.34

For the lithium-ion NMC 26650 cell the results are shown in Figure 5.18. The cell is discharged at its maximum discharge current from the datasheet of 15 A until 0.021 Ah are removed, taking 5 s, and then the cell is charged at its maximum charge current of 5 A until 0.021 Ah are added, taking 15 s, as shown in Figure 5.18a. The OCV is recorded before the test as 3.726 V. Figure 5.18b and Figure 5.18c show the heat generated, which is calculated using Equation 5.24, and Figure 5.18d shows the cell surface and ambient temperatures during the experiment. As is clear from Figure 5.18d, after one hour the surface temperature has stabilised and is no longer increasing and the test then continues in a stable fashion for a further hour.

To obtain the variables in Equation 5.34 average values over the final 30 minutes of the test are used (*Section_fin* in Figure 5.18d), the average heat generation is 1.62 W, the average ambient temperature (T_{a_fin}) is 23.7°C and the average surface temperature (T_{s_fin}) is 34.6°C. The external thermal resistance is therefore calculated using Equation 5.34 as 6.7 K W^{-1}.

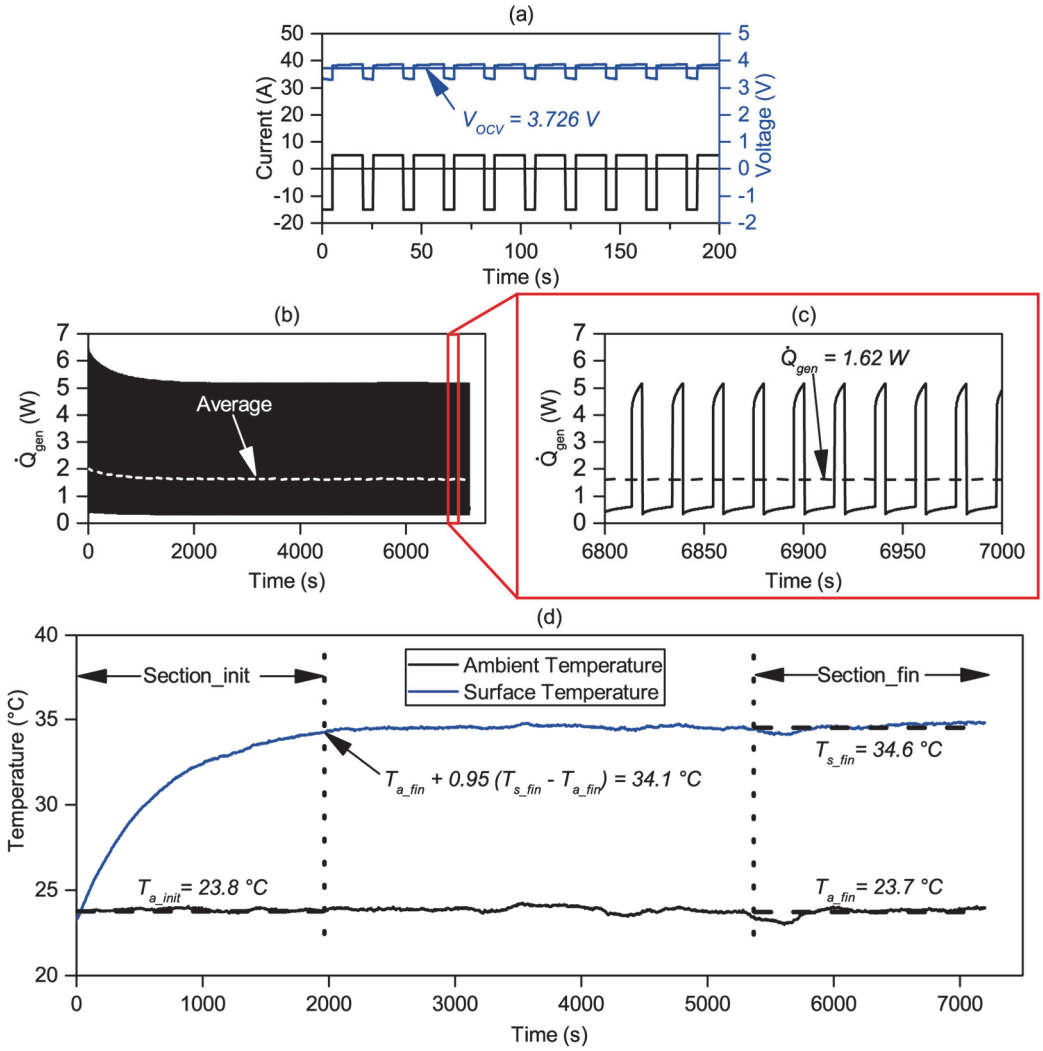

Figure 5.18 Experiment on NMC 26650 cell

Current applied to cell and voltage response for first 200 s (top), heat generation calculated using Equation 5.24 (middle), temperature response of cell (bottom)

5.4.3 Determining the Specific Heat Capacity and Internal Thermal Resistance

To determine the remaining parameters, the same experiment as in Section 5.4.2 is used, however only the period when the surface temperature is increasing is considered. The time period considered runs from 0 minutes until the time when the surface temperature is 95% of the way to the final average surface temperature (*Section_init* in Figure 5.18d). For the case demonstrated in Section 5.4.2, 95% of the way between the final ambient and surface temperatures (23.7°C and 34.6°C respectively) is 34.1°C, which occurs after 1950 s.

Least squares regression of Equation 5.27 is used to fit the surface temperature, with the pre-established value for R_{out}, to find a value for $C_{p,i}\ (R_{in} + R_{out})$, this is the denominator of Equation 5.27. When performing the least squares regression the ambient temperature in the

initial section (T_{a_init}) is used. The least squares regression is programmed manually in a MATLAB model and the script is available in Appendix B. The model steps through values of $C_{p,i}$ $(R_{in} + R_{out})$ between 1 s and 3000 s, increasing each step by 1 s. For each value of $C_{p,i}$ $(R_{in} + R_{out})$ the model calculates the surface temperature with time using Equation 5.27, this modelled temperature (T_{mod} (K)) is then compared to the experimentally measured temperature (T_{exp} (K)) and the least squares error calculated using Equation 5.35. The least squares errors for each value of $C_{p,i}$ $(R_{in} + R_{out})$ are then examined and the minimum error used for the final value of $C_{p,i}$ $(R_{in} + R_{out})$.

$$Error = \sum \left({T_{exp}}^2 - {T_{mod}}^2 \right)$$

Equation 5.35

This is demonstrated for the NMC 26650 cell in Figure 5.19, where the time step used is 0.1 s and the value for $C_{p,i}$ $(R_{in} + R_{out})$ found using the least squares regression model as 750 s. Using the previous value found for R_{out} of 6.7 K W^{-1}, this can be written as in Equation 5.36.

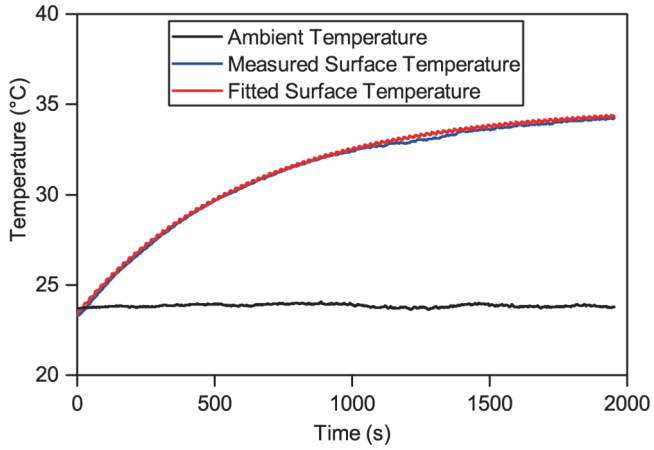

Figure 5.19 Fitting the model to the NMC 26650 cell experiment

Figure shows *Section_init* from Figure 5.18, where the fitted temperature curve has been created using Equation 5.27 and a value of $C_{p,i}$ $(R_{in} + R_{out})$ of 750 s determined using least squares regression

$$C_{p,i}(R_{in} + 6.7) = 750$$

Equation 5.36

The fans are then turned on to blow air over the cell thereby increasing the heat transfer from the cell to ambient and lowering the external thermal resistance. The heat capacity and internal thermal resistance however are assumed to remain the same. The same experiment from Section 5.4.2 is then conducted to find the value of the external thermal resistance with the fans on, although the experiment is only conducted for one hour as the temperature stabilises faster in

this instance. A comparison of the temperature response with and without the fans is illustrated in Figure 5.20.

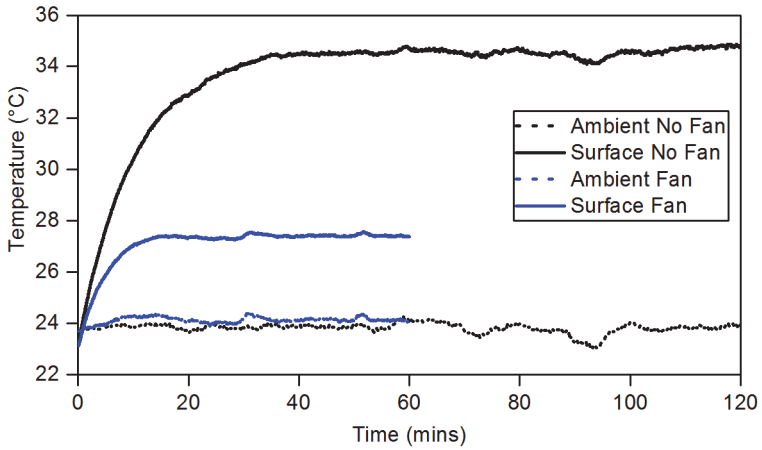

Figure 5.20 Comparison of the NMC 26650 cell temperature response with and without fans

The least squares regression described above is also repeated to find a value for $C_{p,i}\ (R_{in} + R_{out})$ with the fan. For the case with the fan, the values of R_{out} and $C_{p,i}\ (R_{in} + R_{out})$ for the NMC 26650 cell are 1.8 K W^{-1} and 300 s respectively, this gives Equation 5.37.

$$C_{p,i}(R_{in} + 1.8) = 300$$

Equation 5.37

The two simultaneous equations, Equation 5.36 and Equation 5.37, can then be solved to find values for the heat capacity and internal thermal resistance. Solving these equations gives a heat capacity of 93 J K^{-1} and an internal thermal resistance of 1.4 K W^{-1}. The specific heat capacity (c_p *(J kg^{-1} K^{-1})*) is found by dividing the heat capacity by the mass of the cell, listed in Table 5.3. For the NMC 26650 cell the specific heat capacity is found to be 980 J kg^{-1} K^{-1}.

The results for all the cells from the author's new method are given in Section 5.6. The author's novel method is validated initially using the method described in Section 5.2.1 of using a calorimeter and later in Section 5.7 using the surface temperature results.

5.5 Calorimeter Experiments

To verify the specific heat capacity results produced by the new method, experiments were also performed in a calorimeter. The usefulness of the new method is demonstrated as there is not a suitable calorimeter at the University of Southampton and so the experiments are performed at the University of Sheffield. The calorimeter is the Thermal Hazards Technology ARC EV+ calorimeter and the method employed was a method suggested by the manufacturer [209].

The method involves grouping multiple cells together using aluminium tape, with a heater placed in between the cells, as shown in Figure 5.21. The heater is a Kapton heat mat, which is used because the resistance of the heat mat does not change with temperature so the power supplied to the heater is constant throughout the test. This setup means that all the heat generated from the heater is absorbed by the cells. A thermocouple is attached to the outside of the cells with aluminium tape to measure the temperature rise at the surface of the cells.

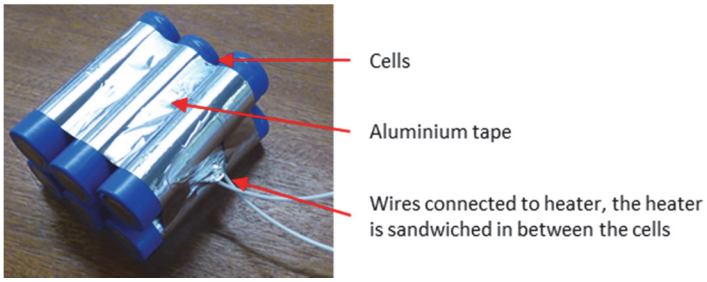

Figure 5.21 Picture of cells being prepared for calorimetry

The example in Figure 5.21 shows six 18650 cells though all the cells actually used for the experiments in this chapter are larger than 18650 cells so less cells were actually used. For the calorimeter experiments, two cells are used for the pouch and prismatic cell calorimetry and three cells for the cylindrical 26650 cell calorimetry. The cells are each weighed individually and then again when combined together with the heater and aluminium tape. The cells with the heater are then hung from string in the calorimeter, such that the cells are suspended away from the calorimeter walls to prevent direct heating and to avoid any possible heat loss by conduction as any heat conduction through the string would be negligible, as shown in Figure 5.22b.

The calorimeter is then sealed and the temperature is set to 25°C and left to rest to allow the cells to equilibrate with the calorimeter, during the 'Temperature equalisation' period between 0 and 100 minutes as shown in Figure 5.22a. The calorimeter is then put in exotherm mode, in which near adiabatic conditions are created within the calorimeter, by setting the temperature to follow the cell surface temperature. This is done by the calorimeter using the cell surface thermocouple to record the temperature. As the surface temperature increases because of heat from the heater, heating is applied to the calorimeter walls to ensure the temperature in the calorimeter is the same as the surface temperature. The inside of the calorimeter being the same temperature as the cell surface means there is no heat transfer from the cell and all the energy from the heater goes into increasing the cell surface temperature.

The power to the heater is applied using a constant voltage power supply. The region of adiabatic temperature rise can be seen during the 'Testing period' between 100 and 250 minutes in Figure 5.22a. Once the temperature of the cells reaches 55°C, the experiment is over and the

calorimeter stops tracking the cell temperature, the heater is switched off to conclude the experiment. A temperature of 55°C is chosen to allow a safety margin before the cell maximum temperature of 60°C, taken from the cell datasheet.

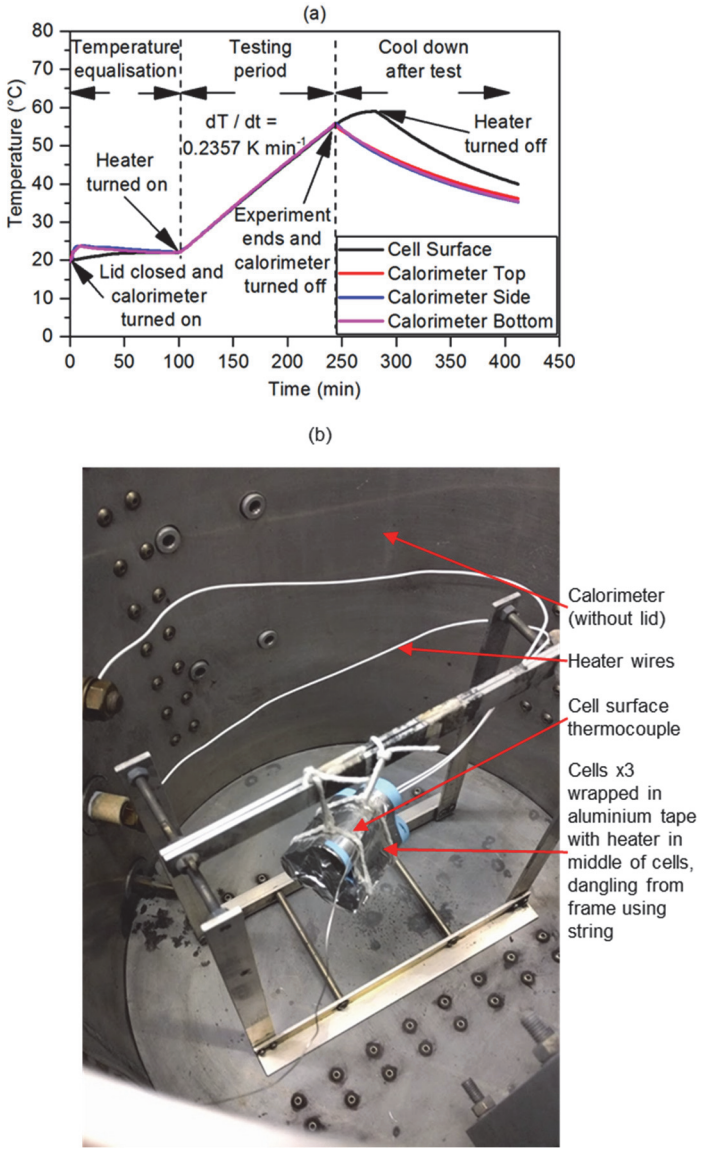

Figure 5.22 Calorimeter experiment for NMC 26650 cell

Results from the experiment (above) and picture of the experiment (below)

The heat capacity of the entire sample placed in the calorimeter (C_{pTOT} *(J* K^{-1}*)*) is found using Equation 5.38. The rate of change of temperature with time (*dT / dt (K* s^{-1}*)*) is taken from Figure 5.22a, namely the slope of the adiabatic temperature rise, and the power (*P (W)*) is calculated as the voltage across the heater multiplied by the current through the heater (for these experiments being 11.97 V and 0.09563 A respectively). The specific heat capacity of the cells is then found by removing the heat capacity of the aluminium tape from the sample by weight using Equation 5.39. The equation uses total sample mass (m_{TOT} *(kg)*) the individual cell mass (m_{cell} *(kg)*), the number of cells (n_{cells}) and the specific heat capacity of aluminium (c_{pAl} *(J* kg^{-1} K^{-1}*)*) and for the

NMC 26650 cells these values are 0.298 kg, 0.096 kg, 3 cells and 913 J kg^{-1} K^{-1} respectively. The specific heat capacity of the NMC 26650 cell is therefore calculated from the calorimetry as 980 J kg^{-1} K^{-1}.

$$P = C_{pTOT}\frac{dT}{dt}$$

Equation 5.38

$$C_{pTOT} = (m_{TOT} - m_{cell}n_{cells})c_{pAl} + m_{cell}n_{cells}c_p$$

Equation 5.39

To determine the accuracy of the calorimeter experiment in determining heat capacity values, a test run is conducted on a sample of three rods of Aluminium, with the same geometry as a 26650 cell. A value for the specific heat capacity of 939 J kg^{-1} K^{-1} is obtained from the experiments, which is within 3% of the value quoted in data books for aluminium of 913 J kg^{-1} K^{-1}.

5.6 Thermal Modelling Results

In this section the results obtained from the author's method are compared to those obtained through calorimetry. The experiments using the author's method are conducted three times without the fans and three times with the fans. The results for the specific heat capacities, internal resistances and external resistances are given in the following sections. As stated previously, the specific heat capacity and internal thermal resistance results of the cells are important, the results obtained using the method proposed could be used in a model of a battery module or pack. The external thermal resistance results are less important because they are specific to the testing conditions described in this section. In a thermal model of a battery module or pack the specific heat capacity and internal thermal resistance would stay the same while the heat transfer away from the cell will depend on the cell location in the module or pack. The external thermal results are presented for reference and are also used in the validation of the model in section 5.7.1.2.

5.6.1 Specific Heat Capacity and Internal Thermal Resistance Results

The results for the specific heat capacity and internal thermal resistance of the cells are given in Table 5.4.

Table 5.4 Results for specific heat capacities and the internal thermal resistances
The values shown for the author's method are the mean values obtained

	NMC 26650	LFP 26650	NMC Pouch	NMC Prismatic
c_p – Author's method	978 J kg^{-1} K^{-1}	1169 J kg^{-1} K^{-1}	1182 J kg^{-1} K^{-1}	1012 J kg^{-1} K^{-1}
c_p – Calorimetry	981 J kg^{-1} K^{-1}	1127 J kg^{-1} K^{-1}	1138 J kg^{-1} K^{-1}	1037 J kg^{-1} K^{-1}
Difference	- 0.3 %	+ 3.8 %	+ 3.9 %	- 2.3 %
R_{in}	1.4 K W^{-1}	1.4 K W^{-1}	0.26 K W^{-1}	0.42 K W^{-1}

5.6.1.1 Specific Heat Capacity Results

A graphical comparison of the specific heat capacities is illustrated in Figure 5.23. For each cell, three experiments are conducted without the fans and three experiments conducted with the fans, giving a total of nine calculated specific heat capacities for each cell. In Figure 5.23 the error bars show the highest and lowest of these nine specific heat capacities calculated using the author's method.

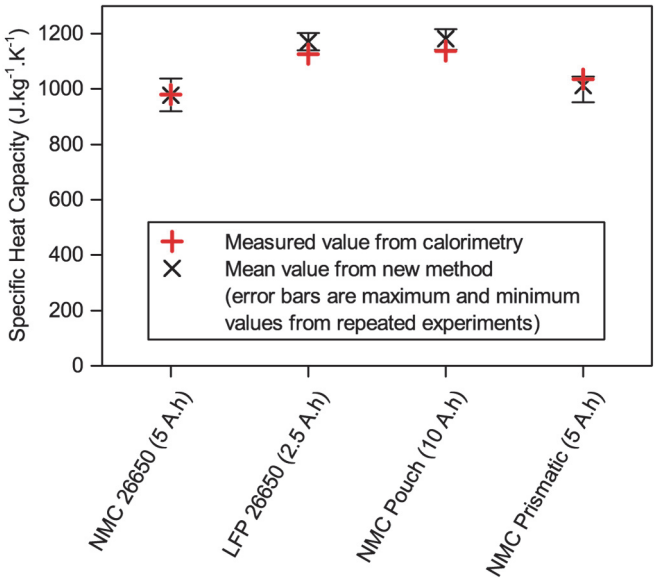

Figure 5.23 Graphical comparison of results obtained using the author's method and results obtained using calorimetry

The reason for variation in results obtained using the author's method is the variation in ambient temperature. All experiments except the NMC prismatic cells had ambient temperature changes of less than 1°C in the *section_init* and *section_fin* stages seen in Figure 5.18d. For the NMC prismatic cell, 50 A is the current continuously applied to the cell and as such the ambient surroundings heated up more. For these experiments the ambient change is kept to under 2.5°C.

The largest percentage difference between the specific heat capacity found for the repeated experiments using the author's method and the calorimeter value is less than 10% in all cases, with the worst case differences for the NMC 26650, LFP 26650, NMC Pouch and NMC prismatic cells being 6.2%, 6.6%, 6.9% and 8.1% respectively.

The results obtained using the author's method evidence good correlation with the results obtained using the calorimeter. The calorimeter results show the LFP 26650 and NMC Pouch cells have higher specific heat capacities than the NMC 26650 and NMC Prismatic cells and the new method correctly predicts this. The order, from the NMC 26650 with the lowest to the NMC Pouch cell with the highest specific heat capacity, is also correctly predicted by the author's method.

5.6.1.2 Internal Thermal Resistance Results

The internal resistance results represent the thermal resistance, mainly due to conduction, from the centre of the cell to the cell surface. It is difficult to validate the internal thermal resistance results because the model used in this thesis is one dimensional and it is assumed that the heat is generated in the cell at a single point. In reality, the heat is generated throughout the cell and the internal thermal resistance is different in all three dimensions. The internal thermal resistance from the experiments are shown in Table 5.5. As can be seen in the results, the two cylindrical cells have similar internal thermal resistance results, which makes sense as they have similar geometry and construction. The pouch and prismatic cells have lower thermal resistances than the cylindrical cells indicating that heat is more easily transferred from the cell centre to the surface in the pouch and prismatic cells than in the cylindrical cells.

Table 5.5 Internal thermal resistance results from experiments

	NMC 26650	LFP 26650	NMC Pouch	NMC Prismatic
R_{in}	1.4 K W^{-1}	1.4 K W^{-1}	0.26 K W^{-1}	0.42 K W^{-1}

5.6.2 External Thermal Resistance Results

The external thermal resistance results represent the thermal resistance, mainly due to convection, from the cell surface to the ambient. The external thermal resistance due to convection is related to the size of the cell but also dependent on the geometry, i.e. cylinder or cuboid. The results for the external resistance are shown in Table 5.6. The results are very similar for both cylindrical 26650 cells, which is logical as they have exactly the same geometry. The results are also very similar for the pouch and prismatic cells, which is also logical as their geometry is similar and they have similar surface areas. The external thermal resistance is lower

for the pouch and prismatic cells than for the cylindrical 26650 cells because of the larger surface area, which makes heat transfer from the cell surface to the ambient easier. In all cases it can also be seen that the thermal resistances decrease with the use of fans as heat transfer is being increased from the cell surface to the ambient.

Table 5.6 External thermal resistance results

	NMC 26650	LFP 26650	NMC Pouch	NMC Prismatic
R_{out} – no fans	6.7 K W^{-1}	6.6 K W^{-1}	3.1 K W^{-1}	3.1 K W^{-1}
R_{out} – fans	1.8 K W^{-1}	1.6 K W^{-1}	0.70 K W^{-1}	0.73 K W^{-1}

5.7 High Rate Thermal Modelling

The results have previously been validated using calorimetry in Section 5.6.1.1 and in this section the results are now validated by measuring the surface temperature of the cells during cycling of the cells. This section also demonstrates the effectiveness of the model for the cell temperatures during high rate (>1C) operation. Modelling the cell temperature during operation is often required to ensure the cell is kept within the required temperature limits and also to calculate the cooling power required.

5.7.1 Validation of Model

The model defined by Equation 5.27 is demonstrated below. Initially the plots of OCV versus SoC for each of the cells are obtained.

5.7.1.1 Open Circuit Voltage

The OCV of each cell is found by charging the cell by 5% of the rated capacity and then allowing the cell to rest for 15 minutes and recording the final voltage, this is repeated for all states of charge 5%, 10%, …, 100% [208]. This test is then repeated during discharge and so a plot of voltage after a 15 minute rest during charge and discharge for a range of SoCs is obtained. The OCV is then assumed to be the average value between the charge and discharge voltage values, as demonstrated in Figure 5.24a for the NMC 26650 cell. Before each charge and discharge test the cell is left overnight, and it is therefore assumed that the values at the start of each charge and discharge test are the OCV at 0% and 100% states of charge. The OCV versus SoC for each cell are shown in Figure 5.24b.

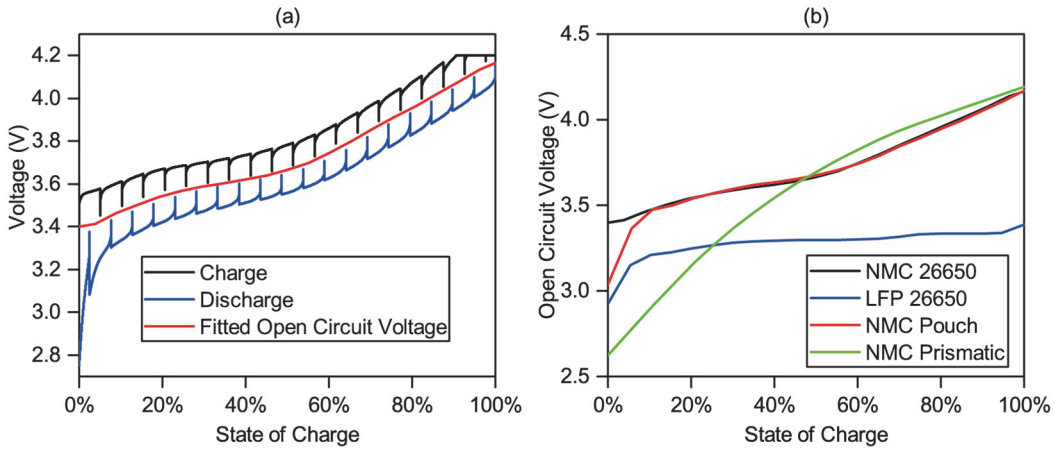

Figure 5.24 Experimental results to determine the OCV

For the NMC 26650 cell (left) and OCV for all cells (right)

5.7.1.2 Demonstration of Model

To demonstrate the effective behaviour of the cell model the cells are tested under charge and discharge at different C-rates, using the constant current method for both charge and discharge between the cell cut off voltages shown in Table 5.3. The cells are charged at 1C and then discharged at 3C, 2C and 1C with a 10 minute rest between each step with the results being shown in Figure 5.25. All graphs in Figure 5.25 have been created using the values for c_p and R_{in} given in Table 5.4 and modelled using Equation 5.27.

The tests shown in Figure 5.25a and Figure 5.25b are conducted in the same conditions as the experiments to determine the heat capacity and so the values of R_{out} shown in Table 5.6 are used. The test shown in Figure 5.25c is conducted in a freezer meaning the ambient temperature is lowered however the value of R_{out} is also taken from Table 5.6 as the heat transfer from the cell to ambient is still the same as previous experiments because the cell is simply resting on blu tack on the floor of the freezer. The heat transfer from the cell to the ambient has been changed for Figure 5.25d by wrapping the cell in 25 mm Armaflex insulation. A value of 15 K W^{-1} is obtained for R_{out} for the cell wrapped in insulation using the same methodology described in Section 5.4.2.

The method to create the figures in Figure 5.25 is described in detail below Equation 5.27. In summary, at each second, the measured voltage and current are taken from the battery analyser, the SoC of the cell is then calculated using Equation 5.25. This SoC is then used to look up the OCV in Figure 5.24b. The surface temperature at that instant is then calculated using Equation 5.27 and the model then moves to the next second and the process is repeated. The MATALB model used to calculate the temperature can be seen in Appendix B.

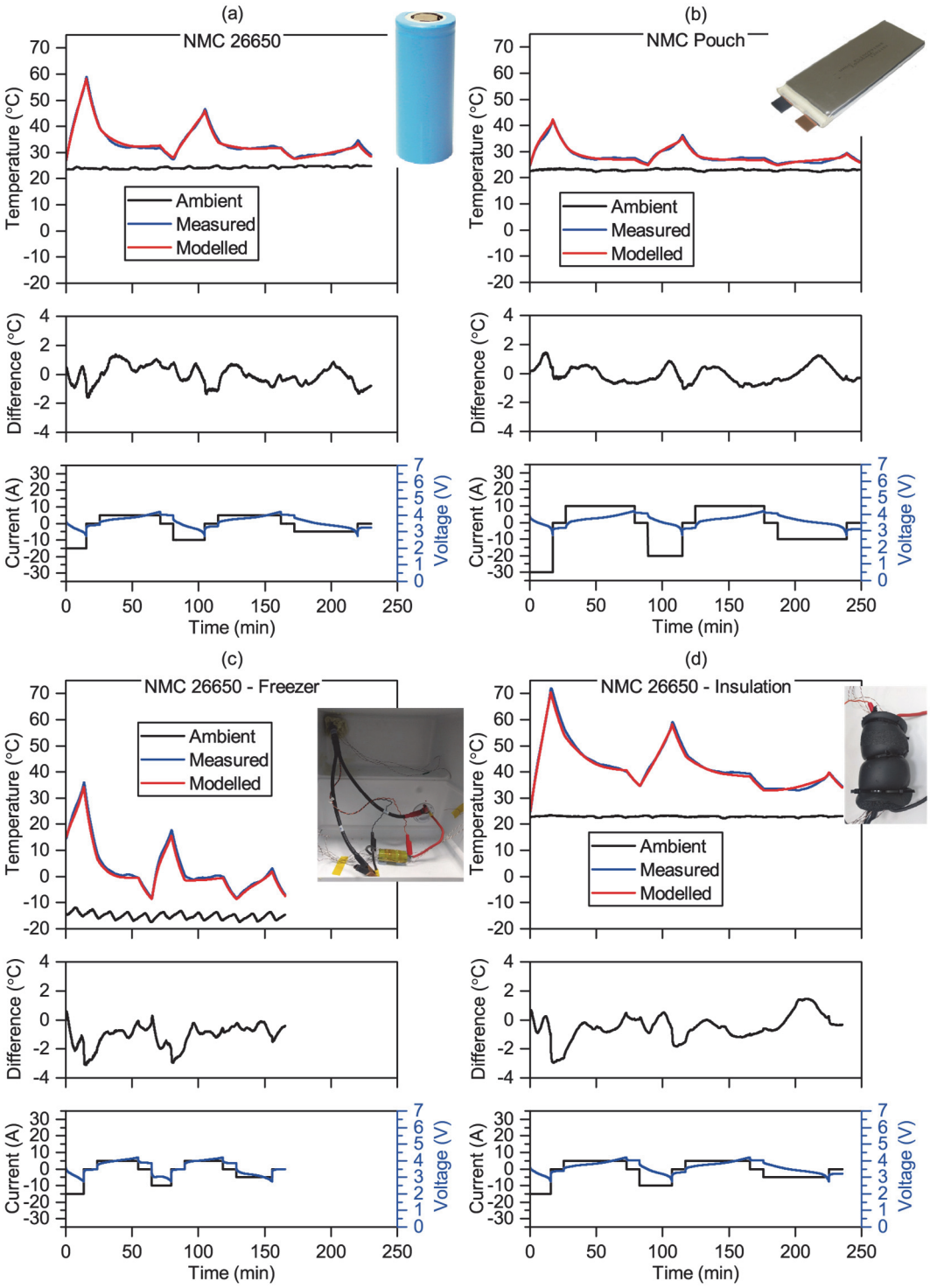

Figure 5.25 Modelled versus measured temperatures for the cells tested

NMC 26650 cell (top left), NMC Pouch cell (top right), NMC 26650 cell in freezer (bottom left) and NMC 26650 cell wrapped in insulation (bottom right)

It is clear from the results in Figure 5.25 that the modelled temperature closely matches that of the temperature obtained during the thermal experiments hence providing further evidence of the modelling methodology and the accuracy of the approach described in this chapter. For the

conditions tested the maximum error is 3.1°C after the 3C discharge of the NMC 26650 in the freezer.

Figure 5.25d is perhaps the most interesting result as it shows that once the methodology described in this chapter has been utilised to obtain the specific heat capacity and internal thermal resistance of the cells, the values obtained can be used to model the cell under significantly different conditions. For this case the cell has been wrapped in insulation, however the cell could also be placed in a model of a battery module or pack. If the cell is modelled in a battery module, finite element modelling would likely be required as the heat transfer to and from the cell becomes more complicated due to heat generated by nearby cells. The thermal model of the module or pack could however use the specific heat capacity and internal thermal resistance of the cells determined using the method described in Section 5.4 as inputs.

5.8 Discussion of Thermal Modelling Results

In general, the modelled surface temperatures match the measured temperatures well, for all cases within 3.1 °C. Differences between the measured and modelled temperatures may arise as a result of variations in temperature and heat transfer within the cell, for example the different materials within the cell which are lumped together in this model. Differences could also arise as a result of other modes of heat generation or consumption not included in this model, such as the entropic heat generation or consumption. It can be seen that even though only three points (cell inside, cell surface and ambient) and only one mode of heat generation are considered, the model accurately predicts the surface temperature with a maximum error of 3.1 °C.

5.8.1 Heat Generation Discussion

Considering only ohmic heat generation is a valid assumption in this work because the examples given are at high rates, over 1C, and so the ohmic heating generation is the dominant mode of heat generation. If the temperature response at lower rates is required it is likely additional modes of heat generation would need to be considered. At lower rates however, less heat will be generated and so the thermal response of the cell is less critical.

All the heat generation being a result of ohmic heat generation means that it is possible to relate the energy lost during charging and discharging to the heat energy leaving the cell calculated using the model. The energy lost during charge and discharge (E_{loss}) is calculated as per Equation 5.40, netting the energy supplied to charge the cell (E_{charge}) with the energy delivered whilst discharging the cell ($E_{discharge}$), both of which are recorded by the battery analyser.

$$E_{loss} = E_{charge} - E_{discharge}$$

Equation 5.40

The heating power (P_{cool} *(W)*) calculated using the model is equal to the rate heat flows away from the cell, which is defined as the right hand side of Equation 5.10, and is defined in Equation 5.41.

$$P_{cool}(t) = \frac{1}{R_{out}}(T_s(t) - T_a)$$

Equation 5.41

To calculate the heat energy leaving the cell this power is integrated over the required time period as per Equation 5.42.

$$E_{heat} = \int \frac{1}{R_{out}}(T_s(t) - T_a)\, dt$$

Equation 5.42

To test the hypothesis, the cycles shown in Figure 5.25a are used, with an initial 1C charge also included to ensure three charge and three discharge steps are used. The test started and finished with the cell at ambient temperature after a rest period. Using Equation 5.40 and Equation 5.42, E_{loss} and E_{heat} are calculated as 23,800 J and 23,000J respectively. This good match means that Equation 5.42 could be used to estimate the energy to be removed by a battery cooling system if the cell was in a battery module or pack. The calculation is only an estimate as, if a cooling system kept the cell temperature lower or higher, the internal cell resistance would change, thereby changing the heat generation and cooling required.

If the NMC 26650 cell is placed in a battery pack and cycled as per Figure 5.25a, the cooling power required to keep the cell at the same temperature as Figure 5.25a can be seen in Figure 5.26, calculated using Equation 5.41. This is the cooling power for one cell and so could be multiplied by the number of cells in the battery pack to obtain the total cooling power required for the battery pack. In reality however this is oversimplified as the battery pack will consist of other items such as metal enclosures, connecting wires, coolant and other items, which will all have heat capacities that will change the cooling power required.

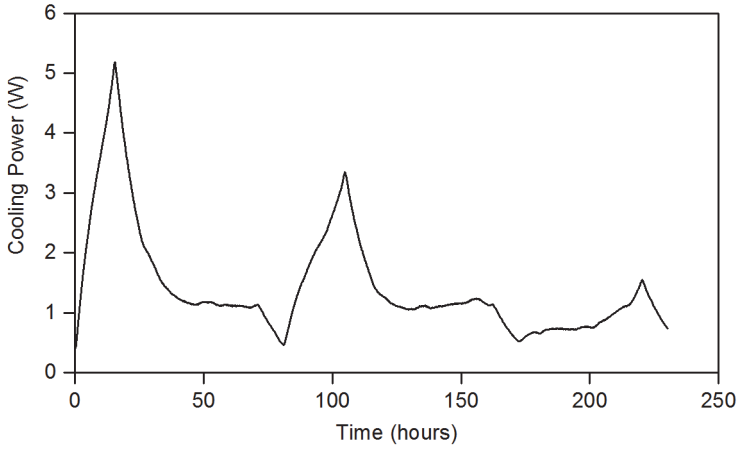

Figure 5.26 Cooling power for the NMC 26650 cell

Calculated using Equation 5.41 and the same experiment seen in Figure 5.25a

5.8.2 Variations in Temperature Across the Cells

The author's model described in this chapter does not take into account variations of temperature across the surface of the cells. The variation in temperature across cells can be significant, especially on larger cells and other researchers [210], found variations across a Lithium-ion 20 Ah pouch cell of 3.8°C after a 5C discharge. In the work in this thesis, the close match of the results obtained using the model and the results obtained from separate calorimeter tests indicate that not taking into account temperature variations is a reasonable assumption in this case. During the experiments to determine the specific heat capacity the maximum variation in temperature across the surface of the cells is observed to be 2.7°C, when a surface thermocouple at the centre of the NMC Prismatic cell is hotter than a thermocouple near the corner of the cell.

To examine the effect of surface temperature variations further, the same experiments to determine the specific heat capacity were repeated with only one thermocouple (thermocouple 5) for the cylindrical cells and two thermocouples (thermocouples 3 and 8) for the pouch and prismatic cells. Thermocouple placement is shown in Figure 5.17 and these thermocouples are chosen such that they are in the centre of the cells. The mean results for specific heat capacity are within 1.8%, 2.9%, 2.6% and 3.6% respectively different to those obtained from the calorimeter experiments for the NMC 26650, LFP 26650, NMC Pouch and NMC Prismatic respectively. This result indicates that in future the author's method could be conducted with only one or two surface thermocouples and one ambient thermocouple if a small error, <4%, in heat capacity is acceptable.

The cell surface temperature variations are greater during the charging and discharging of the cells at various C-rates as shown in Figure 5.25. In these experiments the NMC 26650 cell in the

freezer had a maximum surface temperature variation of 6.7°C, when a surface thermocouple at the centre of cell was reading 38.4°C and a thermocouple near the negative electrode reading 31.7°C. Although, the maximum temperature difference across the surface is 6.7°C, when average values are used it is clear from Figure 5.25c that the maximum difference between the modelled and average surface temperature is less than 2°C.

Not taking into account surface variations is a limitation of the model described in this chapter. However, as described in Section 5.2.1, other thermal models that do take into account temperature variations across cell surfaces often still only use a single value for the specific heat capacity for the entire cell. This means that even if a more complicated thermal model involving surface temperature variations is required, the author's method to determine the specific heat capacity described in this chapter is still useful.

5.9 Other Energy Storage Thermal Modelling

With the success of the author's thermal model for lithium-ion cells the model was then extended to lead-acid and supercapacitor cells. The principles are the same for lead-acid and supercapacitor cells, which are both also electrochemical devices and may be used as the stationary energy store, which may also be required to operate at high rates. At the time of writing a journal paper associated with this section is currently under preparation: Thomas S. Bryden, Borislav Dimitrov, George Hilton, Carlos Ponce de León, Peter Bugryniec, Solomon Brown, Denis Cumming, Andrew Cruden, "Generic Thermal Model Applicable to Lithium-ion, Lead-acid and Supercapacitor Cells".

5.9.1 Details of Lead-acid and Supercapacitor Cells Tested

One lead-acid cell and one supercapacitor cell were tested using the author's method and details of the cells are shown in Table 5.7. The lead-acid cell is a cell which is specifically designed for high rate applications, as shown in the table it can be charged at 11.25 A or 2.5C. This is a high value for lead-acid cells, which can often take 20 hours to charge. The lead-acid cell is also a cylindrical geometry, which is unusual for lead-acid cells, which are often a cuboid geometry. Pictures of the devices under testing are shown in Figure 5.27.

The thermocouple placement for each of the cells is the same as that shown for the cylindrical cells in Figure 5.17, for the vertically oriented lead-acid cell, thermocouples 1, 2 and 3 are at the cell base. The cell tab connections include soldering for the lead-acid cell and a mechanical connection for the supercapacitor, shown in Figure 5.28.

Table 5.7 Details of the lead-acid and supercapacitor cells

	Lead acid	Supercapacitor
Manufacturer	Enersys	Maxwell
Geometry	Cylindrical	Cylindrical
Dimensions	Ø34.3 mm × 96 mm	Ø60.7 mm × 51.5 mm
Name	Cyclon DT	BCAP0650
Nominal Voltage	2 V	2.7 V (Rated)
Capacity	4.5 Ah	650 F
Mass	274.4 g	220 g
Energy density	33 Wh kg^{-1}	4.1 Wh kg^{-1}
Charge cut-off voltage	2.5 V	2.7 V
Discharge cut-off voltage	1.67 V	0 V
Maximum continuous charge current	11.25 A	680 A
Maximum continuous discharge current	22.5 A	680 A

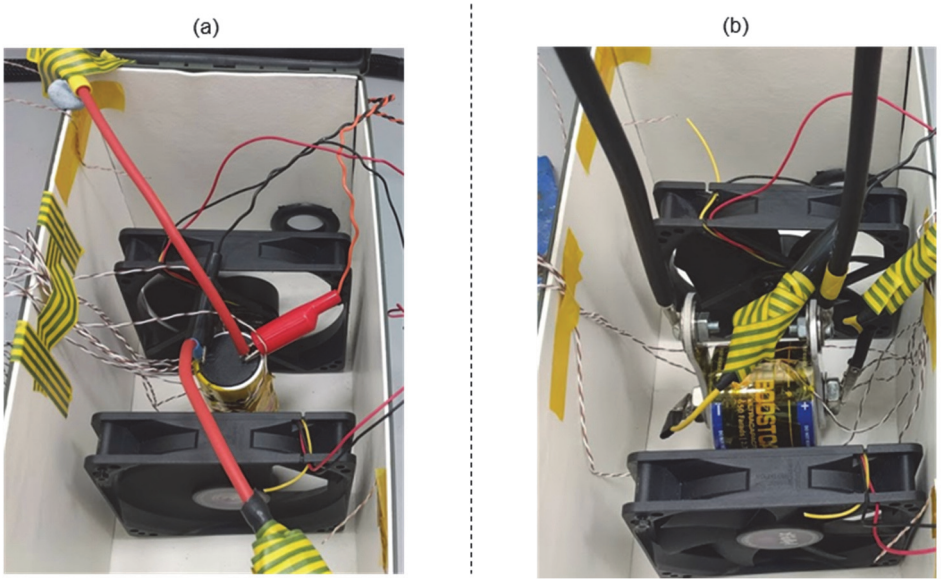

Figure 5.27 Picture of other energy store cells under testing

Lead-acid cell (left) and supercapacitor cell (right)

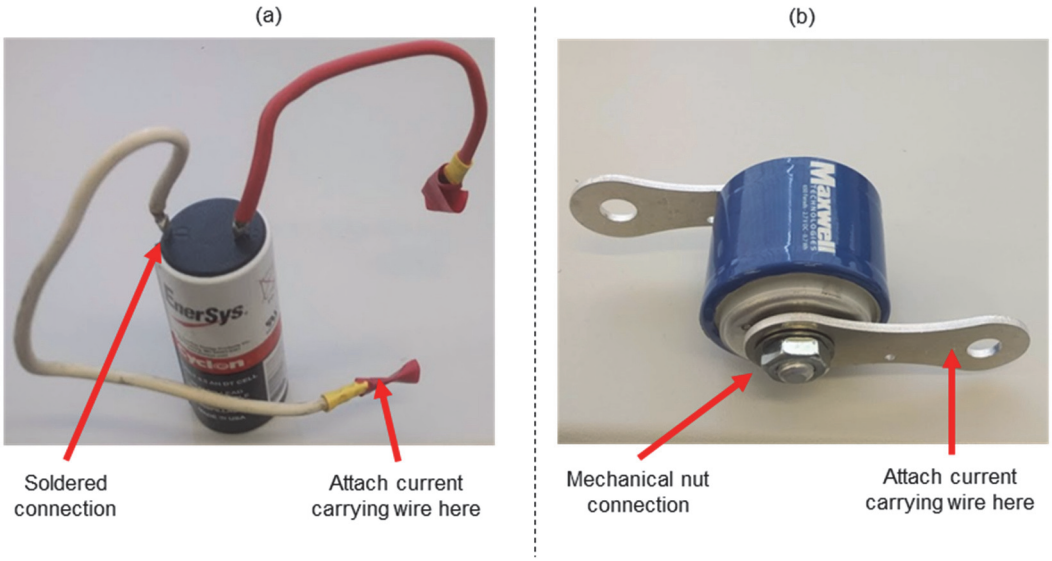

Figure 5.28 Connections of other energy store cells

Lead-acid cell (left) and supercapacitor cell (right)

Although most of the principles are the same when modelling the lead-acid and supercapacitor cells, the required variations are detailed in the following section.

5.9.1.1 Variations Required for Lead-acid Cell

The main difference when operating a lead-acid cell compared to a lithium-ion cell is that the coulombic efficiency of lead-acid cells is much lower, often around 80-90% [109]. This means that the simple coulomb counting seen in Equation 5.25 cannot be used to estimate the SoC. For this work, where electrical modelling is not the focus, the SoC is estimated from the recorded voltage. After a constant current charge or discharge step the cell is left to relax and the relaxation voltage used to estimate the SoC, as shown in Figure 5.29. The manufacturer provides this plot of SoC versus OCV. As constant current is used, the SoC throughout the experiment is estimated simply by interpolating between the initial and final SoC.

Similar to the previously described lithium-ion model, if the model is to be made truly predictive it would need to be combined with an electrical model, which models the voltage and current profile for a given input charge and discharge regime.

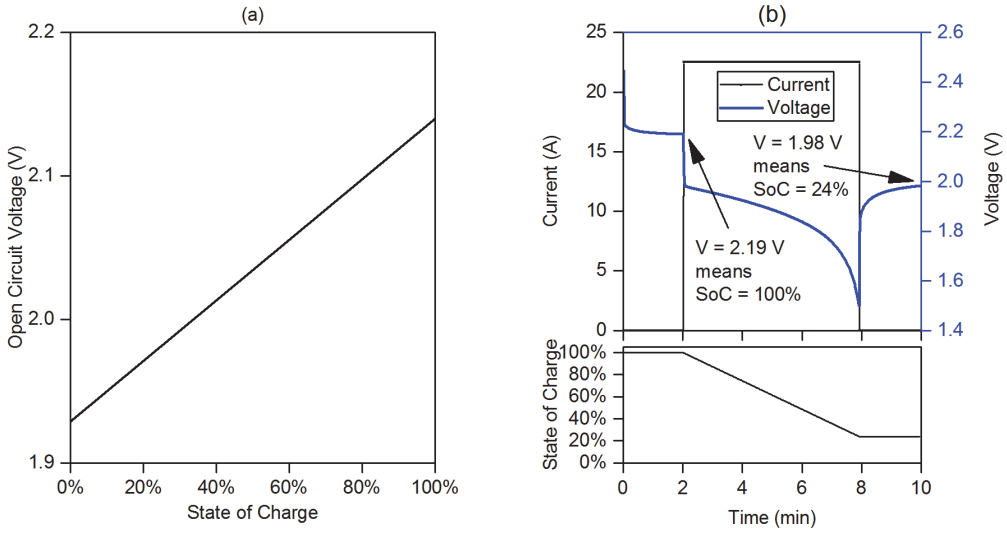

Figure 5.29 Lead-acid cell variations in OCV

Lead-acid OCV [211] (left) and estimating the SoC of the lead-acid cell during discharge (right)

5.9.1.2 Variations Required for Supercapacitor Cell

The challenge when using the method to determine the heat capacity of the supercapacitor cells is that the supercapacitors have a low internal resistance (<0.001 Ω), while for the Lithium-ion NMC tested previously the average internal resistance calculated during the experiment seen in Figure 5.25a is 0.035 Ω, calculated using Equation 2.7. This means that high currents (around 60 A) are required to heat the supercapacitor cell up sufficiently to be able to use the method shown in Figure 5.18. If lower currents are used, the cell heats up less meaning that variations in ambient temperature create errors in the results.

As the supercapacitors have a small energy capacity (0.7 Wh), applying a current of 60 A at 50% SoC for 6 seconds, as per the previously described method, changes the SoC of the supercapacitor by around 14%. This results in a change in OCV of 0.6 V, which is significant compared to the OCV at 50% SoC of 1.35 V. Therefore, the assumption used in the method that during the rapid charge and discharge cycles, shown in Figure 5.18a, the OCV is constant, is therefore not valid for the supercapacitor cells.

Instead, during the rapid charge and discharge cycles the heat generated ($\dot{Q}_{gen}$ *(W)*) is calculated using Equation 5.43, along with the current (*I (A)*), the average voltage during the 6 seconds of charge ($V_{av,cha}$ *(V)*) and the average voltage during the 6 seconds of discharge ($V_{av,dis}$ *(V)*). Using this equation assumes that the coulombic efficiency of the supercapacitor is 100% and also that the OCV lies in the middle of the charge and discharge curves, as illustrated in Figure 5.30.

$$\dot{Q}_{gen} = \frac{I\left(V_{av,cha} - V_{av,dis}\right)}{2}$$

Equation 5.43

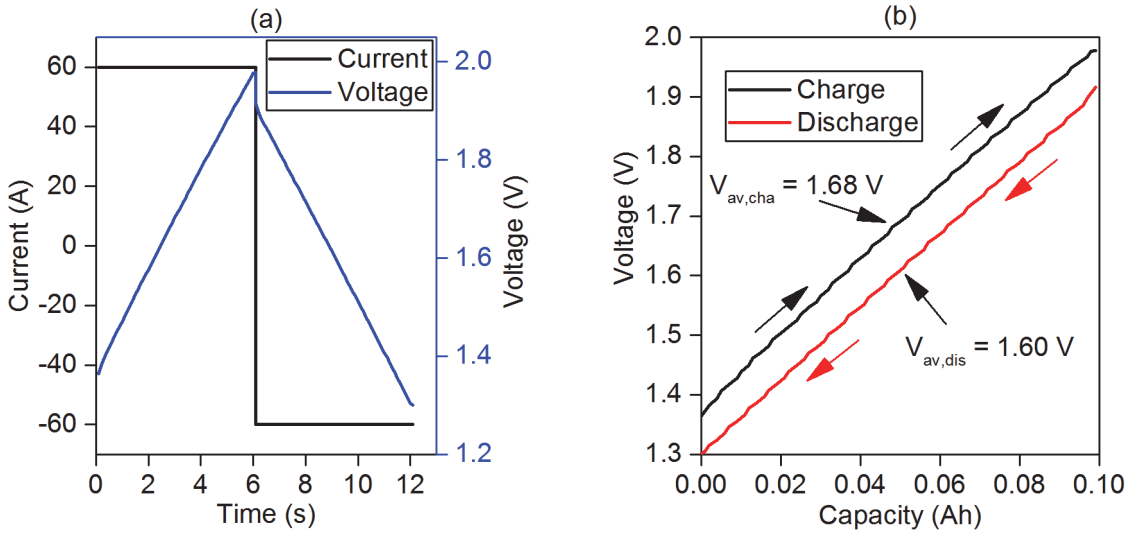

Figure 5.30 Supercapacitor charging and discharging

Plotted versus time (left) and capacity (right)

A second difference when operating the supercapacitor cell is that supercapacitors have significantly more self discharge than lithium-ion cells. Figure 5.31 shows a plot of the OCV versus time for the supercapacitor, it can be seen that the OCV does not level off and continues towards zero, indicating that self discharge is occurring.

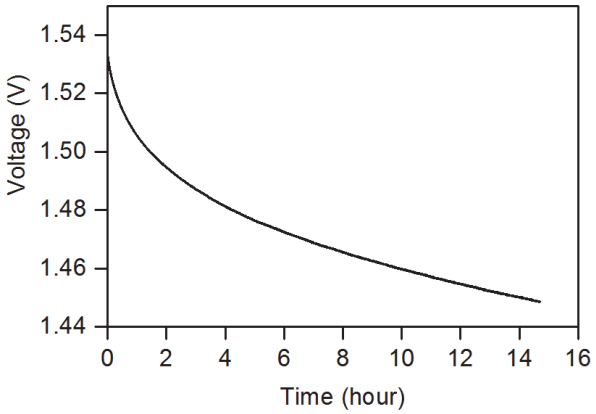

Figure 5.31 Supercapacitor OCV while at rest

Adding the low internal resistance to this self discharge it is very hard to obtain the OCV versus time required for the supercapacitor. For the supercapacitor cells therefore a single value is used for the internal resistance (R_{sup} *(Ω)*) at all times and the heat generation simply calculated using Equation 5.44 and the current (*I (A)*). The internal resistance of the supercapacitor cell is

calculated by dividing the heat generation, calculated in Equation 5.43, by the current squared, giving an average internal resistance of 0.00069 Ω. This value is reasonable as the datasheet gives a maximum equivalent series resistance of 0.0008 Ω.

$$\dot{Q}_{gen(t)} = {I_{(t)}}^2 R_{sup}$$

Equation 5.44

It should be noted that using a single value for the internal resistance was attempted for the lithium-ion cells shown earlier in this chapter however the temperature errors increased significantly. For the Lithium-ion NMC cell seen in Figure 5.25a the maximum temperature error increased from 1.7°C to 5.8°C when using a single value for the internal resistance.

5.9.2 Specific Heat Capacity and Internal Thermal Resistance Results for Other Energy Stores

The same method described in Section 5.4 was applied to both the lead-acid and supercapacitor cells. Again, calorimetry was conducted at the University of Sheffield for both cells and the results as shown in Table 5.8.

Table 5.8 Results for specific heat capacities and the internal thermal resistances of the other energy store cells
The values shown for the author's method are the mean values obtained

	Lead-acid	Supercapacitor
c_p – New method	783 J kg^{-1} K^{-1}	783 J kg^{-1} K^{-1}
c_p – Calorimetry	839 J kg^{-1} K^{-1}	1473 J kg^{-1} K^{-1}
Difference	- 9.0 %	- 36.3 %
R_{in}	1.6 K W^{-1}	0.80 K W^{-1}

From Table 5.8 it is clear that the heat capacity results for the lead-acid cell match the calorimetry within 10% however for the supercapacitor cell there is a large discrepancy between the results found using the new method and the calorimetry, which is discussed in more detail below. The external thermal resistances for the lead-acid and supercapacitor cells are found to be 5.0 K W^{-1} and 5.9 K W^{-1} respectively.

Similar to the lithium-ion cells, the thermal model is verified by cycling the cells. The results are obtained using the same method as the lithium-ion cells along with the variations described in Section 5.9.1.1 and 5.9.1.2 and are shown in Figure 5.32. The lead-acid cell is discharged at 22.5 A

(5C), 18 A (4C), 13.5 A (3C), 9A (2C) and 4.5 A (1C) with 40 minute CC – CV charges in between at 11.25 A (2.5C). The supercapacitor is charged and discharged at 100 A, 80 A, 60 A, 40 A and 20 A each for 40 cycles.

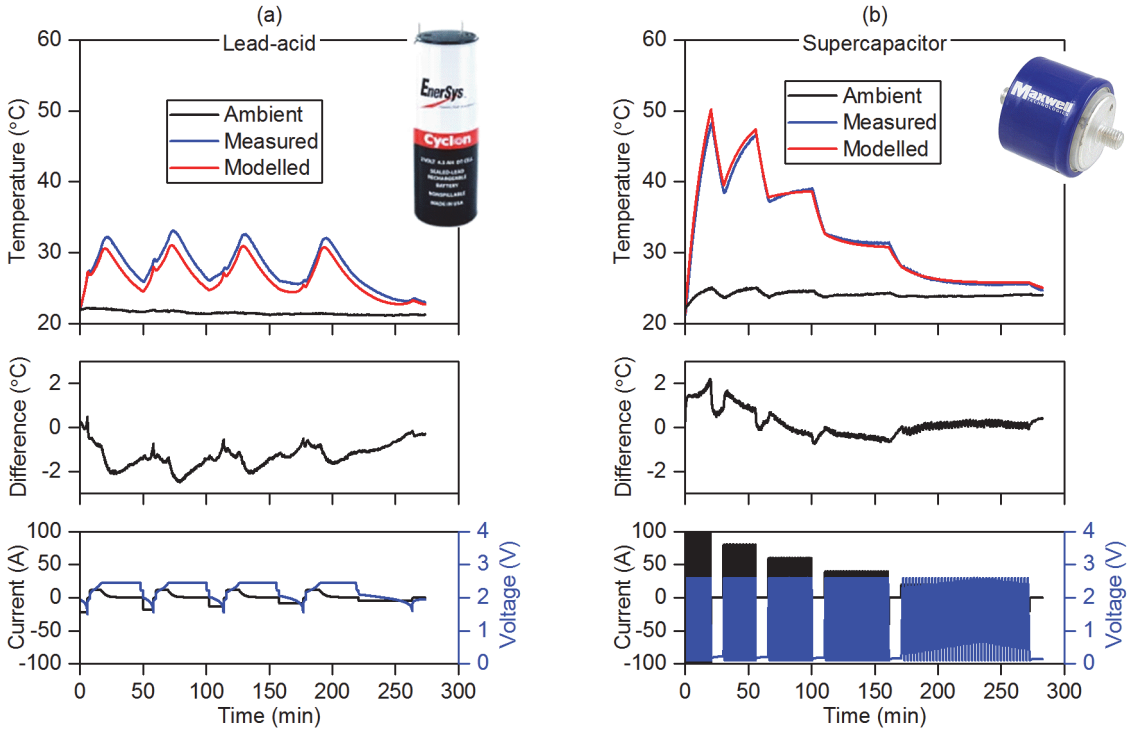

Figure 5.32 Cycling results for the other energy store cells
Lead-acid cell (left) and supercapacitor cell (right)

It is clear from Figure 5.32a the lead-acid cell temperature modelled results match the measured results fairly well although the modelled results are continually lower than the measured results, often between 1°C and 2°C lower. The supercapacitor cell modelled results appear to match the measured results well.

5.9.3 Discussion of Other Energy Storage Thermal Modelling Results

The largest issue with the results is the discrepancy between the supercapacitor heat capacity found using the new method and the measured value during calorimetry. The potential reasons for the discrepancy include:

- A more complicated thermal model is required to model supercapacitors, for example heat transfer in different directions or the different heat capacities within the cell need to be modelled.
- Additional heat generation terms may need to be considered for supercapacitor cells, as currently only the ohmic heat generation term is considered and this term is proportional

to the internal resistance, which as stated above is much smaller than in the lithium-ion cells, therefore other heat generation terms may need to be considered.

- The supercapacitor has large bolts to connect high current wires and as shown in Figure 5.28b metal connectors were used, these large bolts and metal connectors may act as cooling fins and increase transfer heat away from the supercapacitor cells.
- Something may have gone wrong with the calorimetry, unlike for the lithium-ion cells the author of this thesis was not present for the calorimetry experiments for the lead-acid and supercapacitor cells. Further investigation in the University of Sheffield found that during the lead-acid and supercapacitor calorimetry the calorimeter thermocouple was placed in the incorrect position and it was placed on the same cell that the heater was attached to when it should have been placed on one of the other two cells involved in the test. A literature review found some variation between the reported values for the specific heat capacity of supercapacitor cells with values varying between 730 – 1259 J^{-1} kg^{-1} K^{-1} [212-214]. It therefore appears that the Sheffield calorimetry value for specific heat capacity of the supercapacitor is too high.

These results indicate that the thermal model has the potential to be used for energy storage devices other than lithium-ion. Future work could be conducted to determine why the supercapacitor heat capacity does not match that from the calorimetry. The thermal model being extended to lead-acid cells relies on the lead-acid cells being the type that can operate at high rates, the lead-acid cell tested can fully recharge in 40 minutes while often lead-acid acid recharge in over 10 hours.

5.10 Conclusions from Thermal Modelling

The two main conclusions from this chapter are:

- A novel method to determine the heat capacity and internal thermal resistance of lithium-ion cells has been proposed by the author and validated
- The simple thermal model developed by the author, including only one mode of heat generation and two points on the cell (cell inside and cell surface) may be sufficient for thermal modelling of cells at high rates over 1C

When 3D finite element models of battery packs are created to design cooling systems, the key thermal parameters are the heat capacity and the thermal conductivity, or internal thermal resistance, of all objects and materials in the battery pack. The battery pack may consist of metal enclosures, connecting wires, coolant and other objects all of which have known heat capacities and internal thermal resistances from data books. The heat capacity and internal thermal

resistances of the cells in the battery pack however are often not known, as they are not given on cell datasheets and the materials that make up the cell likely will not be known. The novel contribution from this chapter is a new method to determine the heat capacity and internal thermal resistance of cells. The equipment required is common to most battery laboratories and no expensive environment chambers or calorimeters are required.

The method has been validated for cylindrical, pouch and prismatic lithium-ion cell types, with capacities between 2.5 Ah and 10 Ah, by comparing the specific heat capacity results obtained from the model to results obtained using a calorimeter. For the cells tested the maximum error in determined specific heat capacity is 8.1% however when the mean values are used, the maximum error reduces to 3.9%.

It has also been shown that, once the method described in this chapter has been used to obtain the thermal parameters, these thermal parameters can be used to model the surface temperature of the cells at C-rates over 1C. For modelling lower current rates or for more detail regarding the temperature variation in and on the surface of the cell, the model may not be sufficient. However, for many cases, this simple model will be sufficient. Even if a more complicated thermal model is required, the method to determine the cell heat capacity and internal thermal resistance will provide useful inputs for these more complicated models.

The motivation for the thermal modelling is to design the cooling system to deal with excess heat generation during fast charging of EVs. This chapter has demonstrated progress towards this final goal. It has been shown how a thermal model, which is relatively easy to parameterise, can be used to model the temperature of cells during high rate applications similar to what would be seen by an EV while fast charging. This easy to parameterise model will enable further work, which could use the method and model proposed in this chapter, to design innovative EV cooling systems to enable the faster charging of EVs.

Chapter 6 Conclusions

EVs have the potential to help in the fight against climate change, by providing transportation without combusting fuels, also providing health benefits to all people living in cities, by not emitting pollution at the point of use. EVs currently however make up a small proportional of cars on the road and one concern preventing the sale of more EVs is the lack of fast charging. Potential EV owners worry that on long distance journeys they will run out of energy in the EV battery and have to wait for hours while the EV recharges. In this thesis the three key limitations to fast charging of EVs have been identified:

1. Cell current and voltage limits: fast charging requires high currents, which if applied to the cell will exceed the manufacturer current limit and degrade the cell,
2. Electricity grid infrastructure: fast charging requires a high power grid connection, which may not be available at the required fast charging station location,
3. Thermal management of the EV battery pack: additional heat is generated in the EV battery during fast charging, this heat must be removed from the EV battery to keep the cells within the required thermal limits.

Improving the cell current and voltage limits is achieved by changing the material and chemical make up of the EV battery cells. This is important for enabling the future fast charging of EVs however it was decided that changing the material and chemical make up of cells was outside the scope of this PhD. Instead, this PhD research focuses on the other two limitations to fast charging, which will remain limitations once the cell current and voltage limitation is overcome.

To overcome the electricity grid infrastructure limitation to fast charging it has been proposed that stationary energy storage be used at the fast charging station. The stationary energy storage buffers the electricity between the grid and the EV, thereby reducing the grid connection power capacity and meaning expensive electricity grid infrastructure costs can be minimised. From the literature review it was determined that, although this is a popular research topic, the majority of prior research focuses on power flow analysis or design of the power electronics, and little of the prior research is focused on optimising the capacity of the stationary energy storage. Optimising the capacity of the stationary energy storage is key, it must be large enough to ensure there is sufficient power available to charge the EVs but as small as possible to reduce costs.

While developing the method to optimise the capacity of the stationary energy storage it was determined that an important parameter is the time of day that EVs use fast charging stations. Other studies simply used gas station usage or questionnaires to estimate fast charging station

usage so a research gap was identified to provide a better estimate of future fast charging station usage. The first novel contribution of this thesis is therefore the estimation of future fast charging station usage in Chapter 3. The future fast charging station usage is estimated using gasoline vehicle GPS journey data and assuming that all the gasoline vehicles are replaced by EVs that can be charged overnight. The outcome is a distribution of forecasted fast charging station usage versus time of day. As well as designing stationary energy storage at fast charging stations, this novel output is also useful to people planning the rollout of fast charging stations and to electricity grid operators to know when power demand from fast charging stations may peak.

Using this forecasted fast charging station daily usage, a method to optimise the capacity of a stationary energy store at a fast charging station based on user waiting times is proposed. This is the second novel contribution of this thesis. The method detailed in Chapter 4 involves statistically modelling when users will arrive at the fast charging station and then relating the capacity of stationary energy storage to average waiting times. An appropriate capacity energy store can then be chosen based on the acceptable waiting time of EVs arriving at the fast charging station. Once the required capacity of the stationary energy store is known, the cost of this energy store can be compared to the grid infrastructure upgrade costs to determine the optimum solution.

To overcome the thermal management limitation to fast charging, new and larger EV battery cooling systems need to be designed. A more radical solution may even involve stationary cooling whereby, during fast charging, coolant is pumped from the fast charging station to the EV, thereby reducing the size of the on-board cooling system. Whatever the chosen solution, thermal modelling is critical to designing future EV cooling systems during fast charging. Thermal modelling has been shown in the thesis to be a fairly well understood topic with all battery thermal models using the first law of thermodynamics, whereby the change in internal energy at a point is equal to the heat generation minus the heat transferred away from the point. Although thermal models of batteries use the same underlying principles they vary greatly in complexity, including different modes of heat generation and varying levels of complexity regarding cell and battery geometries.

The third novel contribution of this thesis is the method to parameterise cells for use in a high rate thermal model, such as a thermal model of fast charging. The method is described in Chapter 5 and involves determining the heat capacity and internal thermal resistance of cells. The method is validated by performing experiments in a calorimeter and by comparing the modelled results to experimental results. The thermal model and parameterisation method proposed in this thesis have the advantage over other thermal models that the model is simpler and requires only

common, inexpensive equipment found in most battery laboratories to parameterise. This simpler thermal model is appropriate because it is primarily for use in high rate applications, such as fast charging, where heat generation is dominated by one term, the ohmic heat generation.

The model provides a relatively simple method to determine the specific heat capacity and the internal thermal resistance. It should be noted that many more complicated thermal models, for example models looking at surface temperature variations, still only use one value for the heat capacity across the entire cell. This means that even if a more complicated thermal model is used the method proposed in this thesis will still be useful to determine the heat capacity of the cell.

Because the thermal model and the parameterisation method proposed in this thesis are simpler than other thermal models it is envisaged that they will enable more people to work on the designing of future EV cooling systems. This in turn will lead to innovative new EV battery cooling systems being designed to overcome the thermal management limitation to fast EV charging.

This thesis has resulted in two journal publications already published, one regarding lithium-ion thermal modelling [27] and one regarding the fast charging station usage [28]. At the time of submission, one further journal paper has been submitted regarding the method to size the stationary energy storage and one journal paper is being prepared for submission regarding the thermal modelling of lead-acid and supercapacitor cells. These are detailed in Section 1.3.

Two conference papers have also been published and presented at conferences, one regarding the analysis of the Tesla supercharger charging profile [85], and one regarding degradation of lithium-ion cells [215]. In addition the author is co-author on three published journal papers [216-218] and one conference paper.

Through these papers and the research detailed in this thesis significant contributions to knowledge of future fast charging of EVs have been achieved. It is clear how the two fast charging limitations that were the focus of this thesis can be overcome in the future. First using stationary energy storage can overcome the electricity grid infrastructure limitation and the method described in this thesis can be used to optimise the capacity of the stationary energy storage. The next steps will be to use the method in an actual location where the costs of grid infrastructure upgrade are known and determine whether using the stationary energy storage makes sense economically. Secondly the thermal modelling developed in this thesis can be used to design innovative EV battery cooling systems and the method described in this thesis can be used to obtain the required thermal parameters of the cells and also model the cell thermally at high rates, such as fast charging. The next steps will be to use the thermal model to design innovative cooling systems for EVs.

Chapter 7 Further Work

Throughout the work conducted in the thesis several areas of further work have been identified and these are discussed in the following chapter.

7.1 Further work arising from Chapter 3

The analysis in Chapter 3 was conducted using one GPS driving survey from the Northwest USA. It would be interesting to conduct the same analysis with GPS driving surveys from other parts of the world. For example, people from the USA have the reputation of driving longer distances than people living in the UK or Japan and it would be interesting to see how this would affect the results of the analysis.

One limitation of the analysis in Chapter 3 was that the exact GPS traces were not available due to privacy constraints and so the only data available was the vehicle identifier, trip time, trip distance and some basic data regarding whether the trip started or ended at home or work. If instead similar data with the GPS traces of every vehicle were available the analysis could be improved. Having a GPS trace would give additional confidence that the driver was on a long distance journey and therefore required a fast charge. GPS traces would also enable analysis of potential fast charging station locations, for example knowing how the potential usage of fast charging would vary with location. GPS traces would also be useful when estimating the required fast charger power as instances where the driver actually stopped at a service station could be found. The distance travelled after the service station and length of time could then be examined in a similar fashion to that demonstrated in Chapter 3.

There are also other potential applications for the GPS driving data that could be examined in further work. For example for slow charging overnight at home, the GPS driving data could be used to determine what time people park the vehicles at home overnight and how far they drive in the subsequent day. This data could be used to estimate grid electricity requirements from slow charging EVs and design smart charge algorithms that ensure drivers are supplied with enough energy with the minimum impact on the electricity grid. A similar study could be conducted for slow charging at work locations.

7.2 Further work arising from Chapter 4

The model developed in Chapter 4 was a good starting point for a of a fast charging station and the underlying structure could be used for more detailed models of fast charging stations with

stationary energy storage in further work. To develop a detailed model of a fast charging station requires many model modules, which are listed below. These modules were included in simplified form in the model in Chapter 4, for example simply assuming the power electronic convertors were 95% efficient, however in future work any of these modules could be improved in accuracy:

- Model of how long EVs using the fast charging station will have to wait, which was created in detail in Chapter 4
- Forecasting future EV fast charging station usage, which was conducted in detail in Chapter 3
- Model of the local grid infrastructure
- Power electronic models for the AC/DC and DC/DC convertors
- Model for the stationary energy store, including operation and degradation
- Models of the EV batteries charging profiles
    - Forecasts of how EV battery capacities and charging profiles will change in the future
- Model of electricity prices varying at different times
    - Forecasts of how future electricity prices will vary with time
- Economic model of the entire system

7.3 Further work arising from Chapter 5

In Chapter 5, it was mentioned that testing only one of each type of cell could be considered poor experimental planning and so in further work more cells could be tested to ensure that the results are representative of the cells as a whole.

In terms of the method proposed in Chapter 5, the next step in further work would be to take the parameters determined using the method and put them in a 3D CAD model of a battery module or battery pack. The battery module or pack could then be charged and discharged and it could be determined how accurate the model was at predicting the battery module or pack temperature. In further work the 3D CAD model created using the characterisation method proposed in this thesis could then be used to design innovative cooling systems to deal with the excess heat generated during fast charging of the EVs.

The thermal modelling of lead-acid and supercapacitor cells produced promising initial results however more tests are required to validate the model. The calorimetry of the lead-acid and supercapacitor cells had errors and so the calorimetry should be repeated in further work along with the testing of more lead-acid and supercapacitor cells. If this further work produced positive

results the next steps could be to thermally model a hybrid energy storage device during operation using the thermal model proposed in this thesis.

The final proposed further work comes about as a result of ideas generated during the literature review in Chapter 2 and the thermal modelling in Chapter 5. It is proposed that a fast charging station with off-board stationary cooling is investigated. Currently, on-board cooling systems designed to cool the EV during driving are suitable to cool the battery during fast charging events. If however fast charging powers increase, the cooling requirements for fast charging may become larger than the cooling requirements for driving. As fast charges may only be required a few times a year the EV will be driving around with an oversized cooling system. To save space and weight on-board the EV the additional cooling to deal with fast charge events could be placed off-board at the fast charging station and cooled coolant transferred to the EV during the fast charge events. This idea is still in its infancy and so further work could include a feasibility study to determine if the idea is possible, looking at various cooling configurations, types of coolant to use and the economics of the system.

Appendix A Conference and Co-author Papers

The following additional novel contributions and associated journal and conference papers are included in the thesis:

- Applying the same generic thermal model to lead-acid, supercapacitor and lithium-ion cells, Section 5.9 page 135
    - Journal paper, in preparation
    - Thomas S. Bryden, Borislav Dimitrov, George Hilton, Carlos Ponce de León, Peter Bugryniec, Solomon Brown, Denis Cumming, Andrew Cruden, “Generic Thermal Model Applicable to Lithium-ion, Lead-acid and Supercapacitor Cells”
- Analysis of Tesla EV fast charging profiles, Section 2.2.2.2 page 24
    - Conference paper
    - T. S. Bryden, A. J. Cruden, G. Hilton, B. H. Dimitrov, C. P. de León and A. Mortimer, "Off-vehicle energy store selection for high rate EV charging station“, 6th Hybrid and Electric Vehicles Conference (HEVC 2016), London, 2016, 10.1049/cp.2016.0986 [85]
    - Also included an oral presentation at the IET 6th Hybrid and Electric Vehicles Conference (HEVC 2016) in London, UK, November 2016
- Results from lithium-ion cell cycling at standard and high discharge rates
    - Conference paper
    - T. S. Bryden, A. Holland, G. Hilton, B. Dimitrov, C. Ponce de León Albarrán, A. Cruden “Lithium-ion degradation at varying discharge rates”, 3rd Annual Conference in Energy Storage and Its Applications, 3rd CDT-ESA-AC, 11-12 September 2018, Sheffield UK [215]
    - Also included an oral presentation at the 3rd Annual Conference in Energy Storage and Its Applications in Sheffield, UK, September 2018

Additional novel contributions are included in co-authored papers include:

- A method to predict the power demand of fast charging stations, complementing the work in Chapter 3
    - Journal paper
    - G. Hilton, M. Kiaee, T. Bryden, B. Dimitrov, A. Cruden, A. Mortimer “A stochastic method for prediction of the power demand at high rate EV chargers“, IEEE Transactions on Transportation Electrification, 10.1109/TTE.2018.2831003 [216]

- Assessing the economic case for using stationary energy storage with renewable electricity generation and fast charging stations, complementing the work in Chapter 4
    - Journal paper
    - G. Hilton, M. Kiaee, T. Bryden, A. Cruden, A. Mortimer “The case for energy storage installations at high rate EV chargers to enable renewable energy integration in the UK – an optimised approach”, Journal of Energy Storage, [218]
- Investigating the control strategy of a stationary energy store at a fast charging station with renewable solar energy, complementing the work in Chapter 4
    - Conference paper
    - G. Hilton, T. S. Bryden, C. Ponce de León Albarrán, A. Cruden “Dynamic energy store charging of for integration of solar energy with high rate EV demand”, 3rd Annual Conference in Energy Storage and Its Applications, 3rd CDT-ESA-AC, 11-12 September 2018, Sheffield UK [219]
- Designing the power electronics at a charging station, complementing the work in Chapter 2
    - Journal paper
    - B. Dimitrov, A. Cruden, S. Sharkh, C. Ponce-de-Leon, T. Bryden, G. Hilton, “Design Process for a Parallel LLC Resonant Converter for Powered Electric Vehicle Charging Systems”, International Journal of Science and Research (IJSR), 10.21275/ART20172296 [217]

Appendix B MATLAB Scripts

MATLAB scripts for all chapters can be found at the following location:

Bryden, Thomas, Samuel (2019) MATLAB codes for predicting fast charging station usage, user waiting times and a battery thermal model. University of Southampton doi:10.5258/SOTON/D0768 [Dataset]

References

[1] IPCC, Climate Change 2014: Synthesis Report. Contribution of Working Groups I, II and III to the Fifth Assessment Report of the Intergovernmental Panel on Climate Change [Core Writing Team, R.K. Pachauri and L.A. Meyer (eds.)]. 151 pp., Intergovernmental Panel on Climate Change, Geneva, Switzerland, 2014. Accessed on 31 May 2018, http://www.ipcc.ch/report/ar5/syr/

[2] IEA, CO2 Emissions from Fuel Combustion Highlights (2016 Edition), International Energy Agency, Paris, France, 2016. Accessed on 5 May 2017, https://emis.vito.be/sites/emis.vito.be/files/articles/3331/2016/CO2EmissionsfromFuelCombustion_Highlights_2016.pdf

[3] WHO, Reducing Global Health Risks Through mitigation of short-lived climate pollutants Scoping report for policymakers, World Health Organisation, Geneva, Switzerland, 2015. Accessed on 31 May 2018, http://www.who.int/phe/publications/climate-reducing-health-risks/en/

[4] H. Walton, D. Dajnak, S. Beevers, M. Williams, P. Watkiss, and A. Hunt, Understanding the Health Impacts of Air Pollution in London, King's College London, London, United Kingdom, 2015. Accessed on 31 May 2018, https://www.london.gov.uk/sites/default/files/HIAinLondon_KingsReport_14072015_final_0.pdf

[5] A. Mahmoudzadeh Andwari, A. Pesiridis, S. Rajoo, R. Martinez-Botas, and V. Esfahanian, A review of Battery Electric Vehicle technology and readiness levels, *Renewable and Sustainable Energy Reviews,* vol. 78, pp. 414-430, 2017. doi: 10.1016/j.rser.2017.03.138

[6] IEA, Global EV Outlook 2017 Two million and counting, International Energy Agency, 2017. Accessed on 31 May 2018, https://www.iea.org/publications/freepublications/publication/GlobalEVOutlook2017.pdf

[7] G. Crabtree, Energy Storage at the Threshold, presented at NaatBatt Global Charge 2016 Annual Conference, Indian Wells, California, 2016. Accessed on 31 May 2018, http://naatbatt.org/wp-content/uploads/2016/03/JCESR.pdf

[8] J. Neubauer and E. Wood, The impact of range anxiety and home, workplace, and public charging infrastructure on simulated battery electric vehicle lifetime utility, *Journal of Power Sources,* vol. 257, pp. 12-20, 2014. doi: 10.1016/j.jpowsour.2014.01.075

[9] H. Shareef, M. M. Islam, and A. Mohamed, A review of the stage-of-the-art charging technologies, placement methodologies, and impacts of electric vehicles, *Renewable and Sustainable Energy Reviews,* vol. 64, pp. 403-420, 2016. doi: 10.1016/j.rser.2016.06.033

[10] S. Hardman, E. Shiu, and R. Steinberger-Wilckens, Changing the fate of Fuel Cell Vehicles: Can lessons be learnt from Tesla Motors?, *International Journal of Hydrogen Energy,* vol. 40, pp. 1625-1638, 2015. doi: 10.1016/j.ijhydene.2014.11.149

[11] N. S. Pearre, W. Kempton, R. L. Guensler, and V. V. Elango, Electric vehicles: How much range is required for a day's driving?, *Transportation Research Part C: Emerging Technologies,* vol. 19, pp. 1171-1184, 2011. doi: 10.1016/j.trc.2010.12.010

[12] A. Meintz, J. Zhang, R. Vijayagopal, C. Kreutzer, S. Ahmed, I. Bloom*, et al.*, Enabling fast charging – Vehicle considerations, *Journal of Power Sources,* vol. 367, pp. 216-227, 2017. doi: 10.1016/j.jpowsour.2017.07.093

[13] S. Ahmed, I. Bloom, A. N. Jansen, T. Tanim, E. J. Dufek, A. Pesaran*, et al.*, Enabling fast charging – A battery technology gap assessment, *Journal of Power Sources,* vol. 367, pp. 250-262, 2017. doi: 10.1016/j.jpowsour.2017.06.055

[14] ELEVATE Research Project. (2018). *ELEctrochemical Vehicle Advanced TEchnology* [Online, Accessed on 14 May 2018]. Available: http://elevateproject.co.uk/

[15] M. Agostini, S. Brutti, M. A. Navarra, S. Panero, P. Reale, A. Matic*, et al.*, A high-power and fast charging Li-ion battery with outstanding cycle-life, *Scientific Reports,* vol. 7, p. 1104, 2017. doi: 10.1038/s41598-017-01236-y

[16] StoreDot Ltd. (2017). *StoreDot* [Online, Accessed on 23 Jul 2018]. Available: https://www.store-dot.com/

[17] C. Michelbacher, S. Ahmed, I. Bloom, A. Burnham, B. Carlson, F. Dias*, et al.*, Enabling fast charging – Introduction and overview, *Journal of Power Sources,* vol. 367, pp. 214-215, 2017. doi: 10.1016/j.jpowsour.2017.08.008

[18] L. P. Fernandez, T. G. S. Roman, R. Cossent, C. M. Domingo, and P. Frias, Assessment of the Impact of Plug-in Electric Vehicles on Distribution Networks, *IEEE Transactions on Power Systems,* vol. 26, pp. 206-213, 2011. doi: 10.1109/TPWRS.2010.2049133

[19] J. Eyer, Electric Utility Transmission and Distribution Upgrade Deferral Benefits from Modular Electricity Storage Sandia National Laboratories, Albuquerque, USA, 2009. Accessed on 2 Oct 2018, https://prod.sandia.gov/techlib-noauth/access-control.cgi/2009/094070.pdf

[20] DCUSA, Distribution and Connection Use of System Agreement (DCUSA), Wragge & Co LLP, Birmingham, UK, 2017. Accessed on 31 May 2018, https://www.dcusa.co.uk

[21] X. Luo, J. Wang, M. Dooner, and J. Clarke, Overview of current development in electrical energy storage technologies and the application potential in power system operation, *Applied Energy,* vol. 137, pp. 511-536, 2015. doi: 10.1016/j.apenergy.2014.09.081

[22] B. Nykvist and M. Nilsson, Rapidly falling costs of battery packs for electric vehicles, *Nature Climate Change,* vol. 5, 2015. doi: 10.1038/nclimate2564

[23] McKinsey & Company. (2018). *How battery storage can help charge the electric-vehicle market* [Online, Accessed on 9 May 2018]. Available: https://www.mckinsey.com/business-functions/sustainability-and-resource-productivity/our-insights/how-battery-storage-can-help-charge-the-electric-vehicle-market#0

[24] M. Keyser, A. Pesaran, Q. Li, S. Santhanagopalan, K. Smith, E. Wood*, et al.*, Enabling fast charging – Battery thermal considerations, *Journal of Power Sources,* vol. 367, pp. 228-236, 2017. doi: 10.1016/j.jpowsour.2017.07.009

[25] S. Abada, G. Marlair, A. Lecocq, M. Petit, V. Sauvant-Moynot, and F. Huet, Safety focused modeling of lithium-ion batteries: A review, *Journal of Power Sources,* vol. 306, pp. 178-192, 2016. doi: 10.1016/j.jpowsour.2015.11.100

[26] G. Xia, L. Cao, and G. Bi, A review on battery thermal management in electric vehicle application, *Journal of Power Sources,* vol. 367, pp. 90-105, 2017. doi: 10.1016/j.jpowsour.2017.09.046

[27] T. S. Bryden, B. Dimitrov, G. Hilton, C. Ponce de León, P. Bugryniec, S. Brown*, et al.*, Methodology to determine the heat capacity of lithium-ion cells, *Journal of Power Sources,* vol. 395, pp. 369-378, 2018. doi: 10.1016/j.jpowsour.2018.05.084

[28] T. S. Bryden, G. Hilton, A. Cruden, and T. Holton, Electric vehicle fast charging station usage and power requirements, *Energy,* vol. 152, pp. 322-332, 2018. doi: 10.1016/j.energy.2018.03.149

[29] T. B. Reddy and D. Linden, *Linden's handbook of batteries*, 4th ed. New York, NY, USA, McGraw-Hill, 2011, ISBN: 9780071624213

[30] J. T. Warner, *The handbook of lithium-ion battery pack design: chemistry, components, types and terminology*. Amsterdam, Netherlands, Elsevier Inc., 2015, ISBN: 9780128016688

[31] C. Zhao, W. Cao, T. Dong, and F. Jiang, Thermal behavior study of discharging/charging cylindrical lithium-ion battery module cooled by channeled liquid flow, *International Journal of Heat and Mass Transfer,* vol. 120, pp. 751-762, 2018. doi: 10.1016/j.ijheatmasstransfer.2017.12.083

[32] R. Schröder, M. Aydemir, and G. Seliger, Comparatively Assessing different Shapes of Lithium-ion Battery Cells, *Procedia Manufacturing,* vol. 8, pp. 104-111, 2017. doi: 10.1016/j.promfg.2017.02.013

[33] Y. Yin, L. Wan, and Y. Guo, Silicon-based nanomaterials for lithium-ion batteries, *Chinese Science Bulletin,* vol. 57, pp. 4104-4110, 2012. doi: 10.1007/s11434-012-5017-2

[34] Johnson Matthey Battery Systems, Our Guide to Batteries 3rd Edition, Johnson Matthey Battery Systems, Dundee, UK, 2015. Accessed on 31 Mar 2018, http://www.jmbatterysystems.com/technology/our-guide-to-batteries

[35] E. Redondo-Iglesias, P. Venet, and S. Pelissier, Measuring Reversible and Irreversible Capacity Losses on Lithium-Ion Batteries, in *2016 IEEE Vehicle Power and Propulsion Conference (VPPC)*, Hangzhou, China, 2016, doi: 10.1109/VPPC.2016.7791723

[36] Department for Transport. (2018). *Vehicle licensing statistics: July to September 2017* [Online, Accessed on 26 Mar 2018]. Available: https://www.gov.uk/government/statistics/vehicle-licensing-statistics-july-to-september-2017

[37] P. Hummel, D. Lesne, J. Radlinger, C. Golbaz, C. Langan, K. Takahashi*, et al.*, UBS Evidence Lab Electric Car Teardown – Disruption Ahead?, UBS Limited, 2017. Accessed on 31 May 2018, https://neo.ubs.com/shared/d1wkuDlEbYPjF

[38] Citroën. (2018). *Citroën C-Zero* [Online, Accessed on 26 Mar 2018]. Available: http://www.citroen.co.uk/new-cars-and-vans/citroen-range/citroen-c-zero

[39] Tesla. (2018). *Tesla* [Online, Accessed on 25 Feb 2018]. Available: https://www.tesla.com/

[40] Chevrolet. (2018). *Bolt EV* [Online, Accessed on 5 Mar 2018]. Available: http://www.chevrolet.com/bolt-ev-electric-vehicle

[41] Nissan. (2018). *New Nissan Leaf* [Online, Accessed on 8 Jan 2019]. Available: https://www.nissan.co.uk/vehicles/new-vehicles/leaf.html

[42] M. Reuss, General Motors, presented at Bank of America Merrill Lynch Auto Summit, New York City, New York, 2017. Accessed on 31 May 2018, https://www.gm.com/content/dam/gm/events/docs/5253488-666232-2017BAMLAutoSummit

[43] Y. Liu, Q. Sun, W. Li, K. R. Adair, J. Li, and X. Sun, A comprehensive review on recent progress in aluminum–air batteries, *Green Energy & Environment,* vol. 2, pp. 246-277, 2017. doi: 10.1016/j.gee.2017.06.006

[44] P. Tan, H. R. Jiang, X. B. Zhu, L. An, C. Y. Jung, M. C. Wu*, et al.*, Advances and challenges in lithium-air batteries, *Applied Energy,* vol. 204, pp. 780-806, 2017. doi: 10.1016/j.apenergy.2017.07.054

[45] Society of Automotive Engineers. (2012). *Battery guru: Consolidating cell types, materials will take time* [Online, Accessed on 14 Mar 2017]. Available: http://articles.sae.org/10666/

[46] Jaguar Land Rover Limited. (2019). *All-Electric Jaguar I-PACE* [Online, Accessed on 8 Jan 2019]. Available: https://www.jaguar.co.uk/Images/Jaguar-I-PACE-Brochure-1X5901910000BGBEN01P_tcm634-609064.pdf

[47] General Motors. (2017). *2016 Chevrolet Volt Battery System* [Online, Accessed on 14 Mar 2017]. Available: https://media.gm.com/content/dam/Media/microsites/product/Volt_2016/doc/VOLT_BATTERY.pdf

[48] Automotive Energy Supply Corporation. (2013). *Cell, Module, and Pack for EV Applications* [Online, Accessed on 14 Mar 2017]. Available: http://www.eco-aesc-lb.com/en/product/liion_ev/

[49] KIA Motors Europe. (2015). *Advanced battery pack for new Soul EV* [Online, Accessed on 14 Mar 2017]. Available: https://press.kia.com/eu/en/home/media-resouces/press-releases/2014/14_03_04_kia-exhibits-soul-ev-battery-technology.html

[50] Seeking Alpha. (2015). *Tesla Motors (TSLA) Elon Reeve Musk on Q1 2015 Results - Earnings Call Transcript* [Online, Accessed on 14 Mar 2017]. Available: http://seekingalpha.com/article/3151236-tesla-motors-tsla-elon-reeve-musk-on-q1-2015-results-earnings-call-transcript?part=single

[51] Toshiba Corporation. (2011). *Toshiba's SCiB™ Rechargeable Battery Selected by Mitsubishi Motors for New Electric Vehicles* [Online, Accessed on 14 Mar 2017]. Available: https://www.toshiba.co.jp/about/press/2011_06/pr1603.htm

[52] J. Zhu, T. Wierzbicki, and W. Li, A review of safety-focused mechanical modeling of commercial lithium-ion batteries, *Journal of Power Sources,* vol. 378, pp. 153-168, 2018. doi: 10.1016/j.jpowsour.2017.12.034

[53] M. R. Swain, Fuel Leak Simulation, in *DOE Hydrogen Program Review*, 2001, doi: NREL/CP-570-30535

[54] Z. Zeng, B. Wu, L. Xiao, X. Jiang, Y. Chen, X. Ai, *et al.*, Safer lithium ion batteries based on nonflammable electrolyte, *Journal of Power Sources,* vol. 279, pp. 6-12, 2015. doi: 10.1016/j.jpowsour.2014.12.150

[55] Z. Chen, P. Hsu, J. Lopez, Y. Li, J. W. F. To, N. Liu, *et al.*, Fast and reversible thermoresponsive polymer switching materials for safer batteries, *Nature Energy,* vol. 1, 2016. doi: 10.1038/nenergy.2015.9

[56] M. Yilmaz and P. T. Krein, Review of Battery Charger Topologies, Charging Power Levels, and Infrastructure for Plug-In Electric and Hybrid Vehicles, *IEEE Transactions on Power Electronics,* vol. 28, pp. 2151-2169, 2013. doi: 10.1109/TPEL.2012.2212917

[57] International Electrotechnical Commission. (2017). IEC 61851-1:2017 Electric vehicle conductive charging system - Part 1: General requirements

[58] Next Green Car Ltd. (2018). *Zap-Map* [Online, Accessed on Apr 2018]. Available: https://www.zap-map.com/

[59] S. Shokrzadeh, H. Ribberink, I. Rishmawi, and E. Entchev, A simplified control algorithm for utilities to utilize plug-in electric vehicles to reduce distribution transformer overloading, *Energy,* vol. 133, pp. 1121-1131, 2017. doi: 10.1016/j.energy.2017.04.152

[60] Y. Luo, T. Zhu, S. Wan, S. Zhang, and K. Li, Optimal charging scheduling for large-scale EV (electric vehicle) deployment based on the interaction of the smart-grid and intelligent-transport systems, *Energy,* vol. 97, pp. 359-368, 2016. doi: 10.1016/j.energy.2015.12.140

[61] M. C. Falvo, D. Sbordone, I. S. Bayram, and M. Devetsikiotis, EV charging stations and modes: International standards, in *2014 International Symposium on Power Electronics, Electrical Drives, Automation and Motion*, Ischia, Italy, 2014, doi: 10.1109/SPEEDAM.2014.6872107

[62] Advertising Standards Authority Ltd. (2016). *ASA Ruling on Tesla Motors Ltd* [Online, Accessed on 19 Jul 2018]. Available: http://archive.is/MtgpR

[63] ABB. (2013). *ABB Broadens EV Fast Charging Portfolio with Combined Charging System (CCS)* [Online, Accessed on 28 Apr 2016]. Available: http://www.abb.co.uk/cawp/seitp202/f7447f8f559563f6c1257b110038f76e.aspx

[64] CHAdeMO. (2013). *CHAdeMO, Nissan and Volkswagen align on promoting multi-standard fast chargers to accelerate infrastructure deployment and EV adoption* [Online, Accessed on 2 Sep 2018]. Available: https://www.chademo.com/chademo-nissan-and-volkswagen-align-on-promoting-multi-standard-fast-chargers-to-accelerate-infrastructure-deployment-and-ev-adoption/

[65] IHS Markit. (2015). *Global EV Charging Stations to Skyrocket by 2020, IHS Report Says* [Online, Accessed on 28 Apr 2016]. Available: http://press.ihs.com/press-release/automotive/global-ev-charging-stations-skyrocket-2020-ihs-report-says

[66] Ford Motor Company. (2016). *BMW Group, Daimler AG, Ford Motor Company and Volkswagen Group with Audi & Porsche Plan a Joint Venture for Ultra-Fast, High-Power Charging Along Major Highways in Europe* [Online, Accessed on 18 Feb 2017]. Available: https://media.ford.com/content/dam/fordmedia/Europe/en/2016/11/JVFastChargingrelease.pdf

[67] ChargePoint. (2016). *Express Plus Specifications for Power Cube, Power Modules and Station* [Online, Accessed on 18 Feb 2017]. Available: https://www.chargepoint.com/files/datasheets/ds-expressplus.pdf

[68] International Electrotechnical Commission. (2014). IEC 61851-23:2014 Electric vehicle conductive charging system - Part 23: DC electric vehicle charging station

[69] S. Schneider, Combined Charging System 1.0 Specification - CCS 1.0, Coordination Office Charging Interface, c/o Carmeq GmbH, 2015. Accessed on 31 May 2018, http://www.charinev.com/contact/

[70] T. Mitchell. (2015). *China completes Beijing-Shanghai electric car charging route* [Online, Accessed on 20 Oct 2015]. Available: http://www.ft.com/cms/s/0/1b26d892-9d66-11e4-8946-00144feabdc0.html#axzz3p78RGJ7U

[71] Tokyo Electric Power Company. (2010). *Press Release (Mar 15,2010) - Establishment of CHAdeMO Association* [Online, Accessed on 28 Apr 2016]. Available: http://www.tepco.co.jp/en/press/corp-com/release/10031501-e.html

[72] L. Lu, X. Han, J. Li, J. Hua, and M. Ouyang, A review on the key issues for lithium-ion battery management in electric vehicles, *Journal of Power Sources,* vol. 226, pp. 272-288, 2013. doi: 10.1016/j.jpowsour.2012.10.060

[73] R. Chandrasekaran, Quantification of bottlenecks to fast charging of lithium-ion-insertion cells for electric vehicles, *Journal of Power Sources,* vol. 271, pp. 622-632, 2014. doi: 10.1016/j.jpowsour.2014.07.106

[74] T. Waldmann, B. Hogg, and M. Wohlfahrt-Mehrens, Li plating as unwanted side reaction in commercial Li-ion cells – A review, *Journal of Power Sources,* vol. 384, pp. 107-124, 2018. doi: 10.1016/j.jpowsour.2018.02.063

[75] T. Waldmann, M. Kasper, and M. Wohlfahrt-Mehrens, Optimization of Charging Strategy by Prevention of Lithium Deposition on Anodes in high-energy Lithium-ion Batteries – Electrochemical Experiments, *Electrochimica Acta,* vol. 178, pp. 525-532, 2015. doi: 10.1016/j.electacta.2015.08.056

[76] Tesla Motors Club LLC. (2015). *Tesla Motors Club* [Online, Accessed on 9 Dec 2015]. Available: https://teslamotorsclub.com/

[77] L. Somerville. (2018). *Overcoming the impacts of Fast charging on H/EV's, Batteries and Charging Systems* [Online, Accessed on 9 Apr 2018]. Available: https://d3v6gwebjc7bm7.cloudfront.net/event/15/19/43/1/rt/1/documents/resourceList1519735893058/overcomingtheimpactsoffastchargingonhevsbatteriesandchargingsystempresentation1519735908217.pdf

[78] J. Vetter, P. Novák, M. R. Wagner, C. Veit, K. C. Möller, J. O. Besenhard*, et al.*, Ageing mechanisms in lithium-ion batteries, *Journal of Power Sources,* vol. 147, pp. 269-281, 2005. doi: 10.1016/j.jpowsour.2005.01.006

[79] Texas Instruments Incorporated. (2009). *Cell balancing buys extra run time and battery life* [Online, Accessed on 13 Mar 2017]. Available: http://www.ti.com.cn/cn/lit/an/slyt322/slyt322.pdf

[80] J. Liu, Y. Chen, and H. K. Fathy, Nonlinear Model-Predictive Optimal Control of an Active Cell-to-Cell Lithium-Ion Battery Pack Balancing Circuit, in *International Federation of Automatic Control*, 2017, doi: 10.1016/j.ifacol.2017.08.2297

[81] R. Put. (2016). *The first BMW i3 of @dR_nl with a new 33 kWh battery pack charged at @Fastned. From 8% - 80% took just 30 minutes!* [Online, Accessed on 13 Mar 2017]. Available: https://twitter.com/RolandvanderPut/status/758671069477740544

[82] S. Rajagopalan, A. Maitra, J. Halliwell, M. Davis, and M. Duvall, Fast charging: An in-depth look at market penetration, charging characteristics, and advanced technologies, in *2013 World Electric Vehicle Symposium and Exhibition (EVS27)*, Barcelona, Spain, 2013, doi: 10.1109/EVS.2013.6914945

[83] D. Andersson and D. Carlsson, Measurements of ABB's Prototype Fast Charging Station for Electric Vehicles, Master's thesis, Department of Energy and Environment, Chalmers University of Technology, Gothenburg, Sweden, 2012.

[84] T. Bruen and J. Marco, Modelling and experimental evaluation of parallel connected lithium ion cells for an electric vehicle battery system, *Journal of Power Sources,* vol. 310, pp. 91-101, 2016. doi: 10.1016/j.jpowsour.2016.01.001

[85] T. S. Bryden, A. J. Cruden, G. Hilton, B. H. Dimitrov, C. Ponce de León, and A. Mortimer, Off-vehicle energy store selection for high rate EV charging station, in *6th Hybrid and Electric Vehicles Conference (HEVC 2016)*, 2016, doi: 10.1049/cp.2016.0986

[86] World Economic Forum, The Future of Electricity New Technologies Transforming the Grid Edge, World Economic Forum, Geneva, Switzerland, 2017. Accessed on 31 Sep 2018, http://www3.weforum.org/docs/WEF_Future_of_Electricity_2017.pdf

[87] National Grid, Future Energy Sceanrios, National Grid plc, United Kingdom, 2017. Accessed on 31 May 2018, http://fes.nationalgrid.com/media/1253/final-fes-2017-updated-interactive-pdf-44-amended.pdf

[88] S. Leavey. (2012). *The Grid 2025 Challenge* [Online, Accessed on 26 Dec 2018]. Available: http://www.physics.gla.ac.uk/~shild/grid2025challenge/introduction.html

[89] National Grid. (2018). *Historic frequency data* [Online, Accessed on 26 Dec 2018]. Available: https://www.nationalgrideso.com/balancing-services/frequency-response-services/historic-frequency-data

[90] M. A. Gonzalez-Salazar, T. Kirsten, and L. Prchlik, Review of the operational flexibility and emissions of gas- and coal-fired power plants in a future with growing renewables, *Renewable and Sustainable Energy Reviews,* vol. 82, pp. 1497-1513, 2018. doi: 10.1016/j.rser.2017.05.278

[91] UK Department for Business Energy & Industrial Strategy. (2017). *Historical electricity data: 1920 to 2016* [Online, Accessed on 23 Apr 2018]. Available: https://www.gov.uk/government/statistical-data-sets/historical-electricity-data-1920-to-2011

[92] US Department of Energy. (2018). *DOE Global Energy Storage Database* [Online, Accessed on 23 Apr 2018]. Available: https://www.energystorageexchange.org/

[93] National Grid. (2018). *National Grid* [Online, Accessed on 23 Apr 2018]. Available: https://www.nationalgrid.com/uk

[94] International Electrotechnical Commission. (2015). BS 7671:2008+A3:2015 Requirements for Electrical Installations. IET Wiring Regulations

[95] A. A. Akhil, G. Huff, A. B. Currier, B. C. Kaun, D. M. Rastler, S. B. Chen*, et al.*, DOE/EPRI Electricity Storage Handbook in Collaboration with NRECA, Sandia National Laboratories, Albuquerque, USA, 2015. Accessed on 31 May 2018, http://www.sandia.gov/ess/handbook.php

[96] British Gas. (2017). *Tariff information* [Online, Accessed on 14 Mar 2017]. Available: https://www.britishgas.co.uk/products-and-services/gas-and-electricity/our-energy-tariffs/tariff-information.html

[97] N. Jenkins, C. Long, and J. Wu, An Overview of the Smart Grid in Great Britain, *Engineering,* vol. 1, pp. 413-421, 2015. doi: 10.15302/J-ENG-2015112

[98] UK Power Networks, London Power Networks plc Use of System Charging Statement, London Power Networks plc, London, United Kingdom, 2015. Accessed on 31 May 2018, https://www.ukpowernetworks.co.uk/internet/en/about-us/documents/LPN-LC14-Statement-2016-V1.0.pdf

[99] Parliamentary Office of Science and Technology. (2001). *postnote UK Electricity Networks* [Online, Accessed on 24 Apr 2018]. Available: https://www.parliament.uk/documents/post/pn163.pdf

[100] Western Power Distribution. (2018). *Network capacity map* [Online, Accessed on 19 Jul 2018]. Available: https://www.westernpower.co.uk/our-network/network-capacity-map

[101] World Energy Council, World Energy Resources - E-Storage, World Energy Council, 2016. Accessed on 31 May 2018, https://www.worldenergy.org/wp-content/uploads/2017/03/WEResources_E-storage_2016.pdf

[102] L. Richard and M. Petit, Fast charging station with battery storage system for EV: Grid services and battery degradation, in *2018 IEEE International Energy Conference (ENERGYCON)*, Limassol, Cyprus, 2018, doi: 10.1109/ENERGYCON.2018.8398744

[103] S. Bai, D. Yu, and S. Lukic, Optimum design of an EV/PHEV charging station with DC bus and storage system, in *2010 IEEE Energy Conversion Congress and Exposition*, Atlanta, GA, USA, 2010, doi: 10.1109/ECCE.2010.5617834

[104] D. McPhail, Evaluation of ground energy storage assisted electric vehicle DC fast charger for demand charge reduction and providing demand response, *Renewable Energy,* vol. 67, pp. 103-108, 2014. doi: 10.1016/j.renene.2013.11.023

[105] IEC, Electrical Energy Storage, International Electrotechnical Commission, Geneva, Switzerland, 2011. Accessed on 31 May 2018, http://www.iec.ch/whitepaper/pdf/iecWP-energystorage-LR-en.pdf

[106] GS Yuasa. (2016). *GS Yuasa introduces the SLR-1000 Advanced Nano-Carbon Lead Acid battery which provides an unprecedented 5000 cycles at 70% DOD* [Online, Accessed on 17 Sep 2018]. Available: http://www.gs-yuasa.com/webdata/img/gs160310154418/pdf_gs_160310500318.pdf

[107] G. E. Blomgren, The Development and Future of Lithium Ion Batteries, *Journal of The Electrochemical Society,* vol. 164, pp. A5019-A5025, 2017. doi: 10.1149/2.0251701jes

[108] J. Jung, L. Zhang, and J. Zhang, *Lead-acid battery technologies : fundamentals, materials, and applications*, 1st ed. Boca Raton, FL, CRC Press, 2015, ISBN: 9781466592230

[109] S. Sharma, P. Sarma, S. Bordoloi, and P. Barman, Estimation of coulombic efficiency of lead acid battery for range determination of electric vehicle, in *2015 1st Conference on Power, Dielectric and Energy Management at NERIST (ICPDEN)*, 2015, doi: 10.1109/ICPDEN.2015.7084501

[110] A. Yu, V. Chabot, and J. Zhang, *Electrochemical supercapacitors for energy storage and delivery : fundamentals and applications*. Boca Raton, FL, CRC Press, 2013, ISBN: 9781439869901

[111] J. Deng, J. Shi, Y. Liu, and Y. Tang, Application of a hybrid energy storage system in the fast charging station of electric vehicles, *IET Generation, Transmission & Distribution,* vol. 10, pp. 1092-1097, 2016. doi: 10.1049/iet-gtd.2015.0110

[112] B. Sun, T. Dragičević, F. D. Freijedo, J. C. Vasquez, and J. M. Guerrero, A Control Algorithm for Electric Vehicle Fast Charging Stations Equipped With Flywheel Energy Storage Systems, *IEEE Transactions on Power Electronics,* vol. 31, pp. 6674-6685, 2016. doi: 10.1109/TPEL.2015.2500962

[113] M. O. Badawy and Y. Sozer, Power Flow Management of a Grid Tied PV-Battery System for Electric Vehicles Charging, *IEEE Transactions on Industry Applications,* vol. 53, pp. 1347-1357, 2017. doi: 10.1109/TIA.2016.2633526

[114] J. P. Torreglosa, P. García-Triviño, L. M. Fernández-Ramirez, and F. Jurado, Decentralized energy management strategy based on predictive controllers for a medium voltage direct current photovoltaic electric vehicle charging station, *Energy Conversion and Management,* vol. 108, pp. 1-13, 2016. doi: 10.1016/j.enconman.2015.10.074

[115] D. Christen, S. Tschannen, and J. Biela, Highly efficient and compact DC-DC converter for ultra-fast charging of electric vehicles, in *2012 15th International Power Electronics and Motion Control Conference (EPE/PEMC)*, Novi Sad, Serbia, 2012, doi: 10.1109/EPEPEMC.2012.6397481

[116] M. Badawy, N. Arafat, S. Anwar, A. Ahmed, Y. Sozer, and P. Yi, Design and implementation of a 75 KW mobile charging system for electric vehicles, in *2013 IEEE Energy Conversion Congress and Exposition*, Denver, CO, USA, 2013, doi: 10.1109/ECCE.2013.6646898

[117] S. Negarestani, M. Fotuhi-Firuzabad, M. Rastegar, and A. Rajabi-Ghahnavieh, Optimal Sizing of Storage System in a Fast Charging Station for Plug-in Hybrid Electric Vehicles, *IEEE Transactions on Transportation Electrification,* vol. 2, pp. 443-453, 2016. doi: 10.1109/TTE.2016.2559165

[118] H. Höimoja, M. Vasiladiotis, and A. Rufer, Power interfaces and storage selection for an ultrafast EV charging station, in *6th IET International Conference on Power Electronics, Machines and Drives (PEMD 2012)*, Bristol, United Kingdom, 2012, doi: 10.1049/cp.2012.0309

[119] A. Rufer. (2015). *Challenges and Solutions Towards the Ultra Fast Charging of EV's* [Online, Accessed on 18 Feb 2017]. Available: http://ufcev.epfl.ch/files/content/sites/ufcev/files/documents/articles/Rufer_Dubai_2015.pdf

[120] A. Quadrelli, G. Gigliucci, E. Pasca, S. Farnesi, R. Gambuti, F. Flamingo*, et al.*, Power quality conditioning system based on Lithium-Ion Ultracapacitors for Electric Vehicles Quick Charging Stations, in *2015 International Conference on Electrical Systems for Aircraft, Railway, Ship Propulsion and Road Vehicles (ESARS)*, Aachen, Germany, 2015, doi: 10.1109/ESARS.2015.7101492

[121] M. Aziz, T. Oda, and M. Ito, Battery-assisted charging system for simultaneous charging of electric vehicles, *Energy,* vol. 100, pp. 82-90, 2016. doi: 10.1016/j.energy.2016.01.069

[122] M. Triplett. (2016). *EV Charging and Energy Storage* [Online, Accessed on 4 Jan 2018]. Available: http://docketpublic.energy.ca.gov/PublicDocuments/15-MISC-04/TN211251_20160425T164400_EV_Charging_and_Energy_Storage.pdf

[123] Renault. (2017). *Electric vehicle charging on highways with second-life batteries* [Online, Accessed on 8 May 2018]. Available: https://media.group.renault.com/global/en-gb/groupe-renault/media/pressreleases/21194120/les-vehicules-electriques-pourront-se-recharger-sur-lautoroute-grace-aux-batteries-seconde-vie

[124] H. Ding, Z. Hu, and Y. Song, Value of the energy storage system in an electric bus fast charging station, *Applied Energy,* vol. 157, pp. 630-639, 2015. doi: 10.1016/j.apenergy.2015.01.058

[125] ABB. *Taking charge* [Online, Accessed on 4 Jan 2018]. Available: https://library.e.abb.com/public/ba824879a3b6dd2ec1257c5a0041be95/64-69%204m341_EN_72dpi.pdf

[126] Leclanché. (2017). *Leclanché, eCAMION and SGEM to Build and Operate Network of 34 Electric Vehicle Fast-Charging Stations Along Trans-Canada Highway* [Online, Accessed on 8 May 2018]. Available: http://www.leclanche.com/fileadmin/user_upload/20170719_fast_charge_canada_final.pdf

[127] Leclanché. (2017). *Leclanché to develop battery storage solution for Fastned's network of fast charging stations* [Online, Accessed on 8 May 2018]. Available: http://www.leclanche.com/fileadmin/user_upload/190917_leclanche_fastned.pdf

[128] A. A. Pesaran, Battery Thermal Management in EVs and HEVs: Issues and Solutions, presented at Advanced Automotive Battery Conference, Las Vegas, Nevada, 2001. Accessed on 31 May 2018, https://www.nrel.gov/transportation/assets/pdfs/aabc_presentation.pdf

[129] D. T. Adams, G. Berdichevsky, T. E. Colson, A. Hebert, S. Kohn, D. Lyons*, et al.*, Battery pack thermal management system USA Patent US 20090023056 A1, 22 Jan, 2009.

[130] S. Ketkar, P. Laurain, and R. McCormick, Battery system and method for cooling the battery system, USA Patent US 20140322563 A1, 30 Oct, 2014.

[131] Y. Ye, L. H. Saw, Y. Shi, and A. A. O. Tay, Numerical analyses on optimizing a heat pipe thermal management system for lithium-ion batteries during fast charging, *Applied Thermal Engineering,* vol. 86, pp. 281-291, 2015. doi: 10.1016/j.applthermaleng.2015.04.066

[132] J. Mardall and C. H. V. Dyke, Charging station providing thermal conditioning of electric vehicle during charging session, USA Patent US 20170096073 A1, 6 Apr, 2014.

[133] G. Kim, K. Smith, K. Lee, S. Santhanagopalan, and A. Pesaran, Multi-Domain Modeling of Lithium-Ion Batteries Encompassing Multi-Physics in Varied Length Scales, *Journal of The Electrochemical Society,* vol. 158, pp. A955-A969, 2011. doi: 10.1149/1.3597614

[134] K. E. Thomas and J. Newman, Thermal modeling of porous insertion electrodes, *Journal of the Electrochemical Society,* vol. 150, pp. A176-A192, 2003. doi: 10.1149/1.1531194

[135] S. Chacko and Y. M. Chung, Thermal modelling of Li-ion polymer battery for electric vehicle drive cycles, *Journal of Power Sources,* vol. 213, pp. 296-303, 2012. doi: 10.1016/j.jpowsour.2012.04.015

[136] M. Al-Zareer, I. Dincer, and M. A. Rosen, Novel thermal management system using boiling cooling for high-powered lithium-ion battery packs for hybrid electric vehicles, *Journal of Power Sources,* vol. 363, pp. 291-303, 2017. doi: 10.1016/j.jpowsour.2017.07.067

[137] C. Forgez, D. Vinh Do, G. Friedrich, M. Morcrette, and C. Delacourt, Thermal modeling of a cylindrical LiFePO4/graphite lithium-ion battery, *Journal of Power Sources,* vol. 195, pp. 2961-2968, 2010. doi: 10.1016/j.jpowsour.2009.10.105

[138] Electrochem Solutions Inc. *Li-ion Battery Temperature Trends During Charge and Discharge* [Online, Accessed on 29 Jul 2018]. Available: https://directory.qmed.com/sites/default/files/Electrochem%20Li-ion%20Battery%20Temp%20Trends.pdf

[139] J. P. Schmidt, A. Weber, and E. Ivers-Tiffée, A novel and precise measuring method for the entropy of lithium-ion cells: ΔS via electrothermal impedance spectroscopy, *Electrochimica Acta,* vol. 137, pp. 311-319, 2014. doi: 10.1016/j.electacta.2014.05.153

[140] A. A. H. Hussein and I. Batarseh, An overview of generic battery models, in *2011 IEEE Power and Energy Society General Meeting*, 2011, doi: 10.1109/PES.2011.6039674

[141] A. Rahmoun and H. Biechl. (2013). *Modelling of Li-ion batteries using equivalent circuit diagrams* [Online, Accessed on 31 May 2018]. Available: http://www.red.pe.org.pl/articles/2012/7b/40.pdf

[142] C. Liao, H. Li, and L. Wang, A dynamic equivalent circuit model of LiFePO4 cathode material for lithium ion batteries on hybrid electric vehicles, in *2009 IEEE Vehicle Power and Propulsion Conference*, Dearborn, MI, USA, 2009, doi: 10.1109/VPPC.2009.5289681

[143] T. Hu, B. Zanchi, and J. Zhao, Simple Analytical Method for Determining Parameters of Discharging Batteries, *IEEE Transactions on Energy Conversion,* vol. 26, pp. 787-798, 2011. doi: 10.1109/TEC.2011.2129594

[144] L. W. Yao, J. A. Aziz, P. Y. Kong, and N. R. N. Idris, Modeling of lithium-ion battery using MATLAB/simulink, in *IECON 2013 - 39th Annual Conference of the IEEE Industrial Electronics Society*, Vienna, Austria, 2013, doi: 10.1109/IECON.2013.6699393

[145] Y. Kim, S. Mohan, J. B. Siegel, A. G. Stefanopoulou, and Y. Ding, The Estimation of Temperature Distribution in Cylindrical Battery Cells Under Unknown Cooling Conditions, *IEEE Transactions on Control Systems Technology,* vol. 22, pp. 2277-2286, 2014. doi: 10.1109/tcst.2014.2309492

[146] S. Panchal, M. Mathew, R. Fraser, and M. Fowler, Electrochemical thermal modeling and experimental measurements of 18650 cylindrical lithium-ion battery during discharge cycle for an EV, *Applied Thermal Engineering,* vol. 135, pp. 123-132, 2018. doi: 10.1016/j.applthermaleng.2018.02.046

[147] E. Gümüşsu, Ö. Ekici, and M. Köksal, 3-D CFD modeling and experimental testing of thermal behavior of a Li-Ion battery, *Applied Thermal Engineering,* vol. 120, pp. 484-495, 2017. doi: 10.1016/j.applthermaleng.2017.04.017

[148] X. Lin, H. E. Perez, J. B. Siegel, A. G. Stefanopoulou, Y. Li, R. D. Anderson*, et al.*, Online Parameterization of Lumped Thermal Dynamics in Cylindrical Lithium Ion Batteries for Core Temperature Estimation and Health Monitoring, *IEEE Transactions on Control Systems Technology,* vol. 21, pp. 1745-1755, 2013. doi: 10.1109/TCST.2012.2217143

[149] K. A. Murashko, A. V. Mityakov, J. Pyrhönen, V. Y. Mityakov, and S. S. Sapozhnikov, Thermal parameters determination of battery cells by local heat flux measurements, *Journal of Power Sources,* vol. 271, pp. 48-54, 2014. doi: 10.1016/j.jpowsour.2014.07.117

[150] J. Jaguemont, N. Omar, F. Martel, P. Van den Bossche, and J. Van Mierlo, Streamline three-dimensional thermal model of a lithium titanate pouch cell battery in extreme temperature conditions with module simulation, *Journal of Power Sources,* vol. 367, pp. 24-33, 2017. doi: 10.1016/j.jpowsour.2017.09.028

[151] U. S. Kim, J. Yi, C. B. Shin, T. Han, and S. Park, Modelling the thermal behaviour of a lithium-ion battery during charge, *Journal of Power Sources,* vol. 196, pp. 5115-5121, 2011. doi: 10.1016/j.jpowsour.2011.01.103

[152] N. Damay, C. Forgez, M. P. Bichat, G. Friedrich, and A. Ospina, Thermal modeling and experimental validation of a large prismatic Li-ion battery, in *IECON 2013 - 39th Annual Conference of the IEEE Industrial Electronics Society*, Vienna, Austria, 2013, doi: 10.1109/IECON.2013.6699893

[153] W. Allafi, C. Zhang, K. Uddin, D. Worwood, T. Q. Dinh, P. A. Ormeno*, et al.*, A lumped thermal model of lithium-ion battery cells considering radiative heat transfer, *Applied Thermal Engineering,* vol. 143, pp. 472-481, 2018. doi: 10.1016/j.applthermaleng.2018.07.105

[154] M. Farag, H. Sweity, M. Fleckenstein, and S. Habibi, Combined electrochemical, heat generation, and thermal model for large prismatic lithium-ion batteries in real-time applications, *Journal of Power Sources,* vol. 360, pp. 618-633, 2017. doi: 10.1016/j.jpowsour.2017.06.031

[155] Z. Rao, Z. Qian, Y. Kuang, and Y. Li, Thermal performance of liquid cooling based thermal management system for cylindrical lithium-ion battery module with variable contact surface, *Applied Thermal Engineering,* vol. 123, pp. 1514-1522, 2017. doi: 10.1016/j.applthermaleng.2017.06.059

[156] PSRC, Traffic Choices Study – Summary Report, Puget Sound Regional Council, Seattle, WA, 2008. Accessed on 31 May 2018, http://mrsc.org/getmedia/8905d073-65f4-4395-9cff-2090dbf66d68/PSRCtrafficChoicesStudy.aspx

[157] Fastned. *Vehicles & charging tips* [Online, Accessed on 8 Jan 2019]. Available: https://support.fastned.nl/hc/en-gb/sections/115000180588-Vehicles-charging-tips

[158] Audi. *The Audi e-tron* [Online, Accessed on 8 Jan 2019]. Available: https://audimediacenter-a.akamaihd.net/system/production/uploaded_files/13476/file/b50541d05e581819c67a97c8e1fe29f08be42284/en_PressInformation_Audi_e-tron.pdf?1544087493

[159] Hyundai Motor UK Ltd. *KONA Electric* [Online, Accessed on 8 Jan 2019]. Available: https://www.hyundai.co.uk/brochures/brochure_kona_electric.pdf

[160] K. Yunus, H. Z. D. L. Parra, and M. Reza, Distribution grid impact of Plug-In Electric Vehicles charging at fast charging stations using stochastic charging model, presented at 14th European Conference on Power Electronics and Applications, Birmingham, UK, 2011. Accessed on 31 May 2018, https://ieeexplore.ieee.org/abstract/document/6020302/

[161] H. Fathabadi, Novel wind powered electric vehicle charging station with vehicle-to-grid (V2G) connection capability, *Energy Conversion and Management,* vol. 136, pp. 229-239, 2017. doi: 10.1016/j.enconman.2016.12.045

[162] G. Celli, G. G. Soma, F. Pilo, F. Lacu, S. Mocci, and N. Natale, Aggregated electric vehicles load profiles with fast charging stations, in *2014 Power Systems Computation Conference*, Wrocław, Poland, 2014, doi: 10.1109/PSCC.2014.7038402

[163] M. Simpson and T. Markel, Plug-In Electric Vehicle Fast Charge Station Operational Analysis with Integrated Renewables Preprint, presented at International Battery, Hybrid and Fuel Cell Electric Vehicle Symposium 26 (EVS26), Los Angeles, California, 2012. Accessed on 31 May 2018, https://www.nrel.gov/docs/fy12osti/53914.pdf

[164] H. Poincaré, *The foundations of science: science and hypothesis, the value of science, science and method*. New York, USA, Science Press, 1913, ISBN: 1108069495

[165] D. Mohr, H. Kaas, P. Gao, D. Wee, and T. Möller, Automotive revolution – perspective towards 2030, McKinsey & Company, 2016. Accessed on 31 May 2018, https://www.mckinsey.com/~/media/mckinsey/industries/high%20tech/our%20insights/disruptive%20trends%20that%20will%20transform%20the%20auto%20industry/auto%202030%20report%20jan%202016.ashx

[166] D. Uhlir, P. Sedlacek, and J. Hosek, Practial overview of commercial connected cars systems in Europe, in *2017 9th International Congress on Ultra Modern Telecommunications and Control Systems and Workshops (ICUMT)*, Munich, Germany, 2017, doi: 10.1109/ICUMT.2017.8255178

[167] B. Fleming, Advances in Automotive Electronics [Automotive Electronics], *IEEE Vehicular Technology Magazine,* vol. 10, pp. 4-96, 2015. doi: 10.1109/MVT.2015.2481008

[168] SAE International. (2016). J3016_201609: Taxonomy and Definitions for Terms Related to Driving Automation Systems for On-Road Motor Vehicles

[169] F. Ferrero, G. Perboli, M. Rosano, and A. Vesco, Car-sharing services: An annotated review, *Sustainable Cities and Society,* vol. 37, pp. 501-518, 2018. doi: 10.1016/j.scs.2017.09.020

[170] J. Gonder, T. Markel, M. Thornton, and A. Simpson, Using Global Positioning System Travel Data to Assess Real-World Energy Use of Plug-In Hybrid Electric Vehicles, *Transportation Research Record: Journal of the Transportation Research Board,* vol. 2017, pp. 26-32, 2007. doi: 10.3141/2017-04

[171] National Renewable Energy Laboratory. (2017). *Transportation Secure Data Center* [Online, Accessed on 2 Sep 2018]. Available: https://www.nrel.gov/transportation/secure-transportation-data/

[172] I. Staffell and S. Pfenninger, The increasing impact of weather on electricity supply and demand, *Energy,* vol. 145, pp. 65-78, 2018. doi: 10.1016/j.energy.2017.12.051

[173] M. B. Arias and S. Bae, Electric vehicle charging demand forecasting model based on big data technologies, *Applied Energy,* vol. 183, pp. 327-339, 2016. doi: 10.1016/j.apenergy.2016.08.080

[174] J. Martínez-Lao, F. G. Montoya, M. G. Montoya, and F. Manzano-Agugliaro, Electric vehicles in Spain: An overview of charging systems, *Renewable and Sustainable Energy Reviews,* vol. 77, pp. 970-983, 2017. doi: 10.1016/j.rser.2016.11.239

[175] M. Neaimeh, S. D. Salisbury, G. A. Hill, P. T. Blythe, D. R. Scoffield, and J. E. Francfort, Analysing the usage and evidencing the importance of fast chargers for the adoption of battery electric vehicles, *Energy Policy,* vol. 108, pp. 474-486, 2017. doi: 10.1016/j.enpol.2017.06.033

[176] T. Gnann, S. Funke, N. Jakobsson, P. Plötz, F. Sprei, and A. Bennehag, Fast charging infrastructure for electric vehicles: Today's situation and future needs, *Transportation Research Part D: Transport and Environment,* vol. 62, pp. 314-329, 2018. doi: 10.1016/j.trd.2018.03.004

[177] L. Rubino, C. Capasso, and O. Veneri, Review on plug-in electric vehicle charging architectures integrated with distributed energy sources for sustainable mobility, *Applied Energy,* vol. 207, pp. 438-464, 2017. doi: 10.1016/j.apenergy.2017.06.097

[178] N. Jakobsson, T. Gnann, P. Plötz, F. Sprei, and S. Karlsson, Are multi-car households better suited for battery electric vehicles? – Driving patterns and economics in Sweden and Germany, *Transportation Research Part C: Emerging Technologies,* vol. 65, pp. 1-15, 2016. doi: 10.1016/j.trc.2016.01.018

[179] United States Council for Automotive Research LLC. (2018). *U.S. Advanced Battery Consortium LLC* [Online, Accessed on 5 Mar 2018]. Available: http://www.uscar.org/guest/teams/12/U-S-Advanced-Battery-Consortium

[180] J. Neubauer, A. Pesaran, C. Bae, R. Elder, and B. Cunningham, Updating United States Advanced Battery Consortium and Department of Energy battery technology targets for battery electric vehicles, *Journal of Power Sources,* vol. 271, pp. 614-621, 2014. doi: 10.1016/j.jpowsour.2014.06.043

[181] The White House. (2016). *FACT SHEET: Obama Administration Announces Federal and Private Sector Actions to Accelerate Electric Vehicle Adoption in the United States* [Online, Accessed on 5 Mar 2018]. Available: https://obamawhitehouse.archives.gov/the-press-office/2016/07/21/fact-sheet-obama-administration-announces-federal-and-private-sector

[182] BMW. (2018). *The BMW i3* [Online, Accessed on 25 Feb 2018]. Available: https://www.bmw.co.uk/bmw-cars/bmw-i/2017-bmw-i3

[183] Direct Line Insurance Group plc. (2017). *Mind your P's and Q's, leading psychologist and Privilege Insurance reveal the 'Ideal Queue'* [Online, Accessed on 17 Jul 2018]. Available: https://www.directlinegroup.com/media/news/brand/2017/16022017.aspx

[184] statistica. (2018). *Petrol station sites in the United Kingdom (UK) from 2000 to 2017* [Online, Accessed on 4 Jul 2018]. Available: https://www.statista.com/statistics/312331/number-of-petrol-stations-in-the-united-kingdom-uk/

[185] Department for Transport. (2016). *Road Use Statistics Great Britain 2016* [Online, Accessed on 22 Jun 2018]. Available: https://assets.publishing.service.gov.uk/government/uploads/system/uploads/attachment_data/file/514912/road-use-statistics.pdf

[186] Tesla Motors UK Limited. (2016). *Detailed Site Plan for Tesla Supercharger Elveden Inn* [Online, Accessed on 22 Jun 2018]. Available: https://planning.westsuffolk.gov.uk/online-applications/files/1EDDBA5F3AAA5380EBFB21CACD2C0137/pdf/DC_15_2587_FUL-DETAILED_SITE_PLAN-1038992.pdf

[187] Department for Transport. (2016). *Traffic counts - Suffolk* [Online, Accessed on 22 Jun 2018]. Available: https://www.dft.gov.uk/traffic-counts/cp.php?la=Suffolk

[188] IET, Electricity Storage, The Institution of Engineering and Technology, Stevenage, UK, 2012. Accessed on 2 Oct 2018, https://www.theiet.org/factfiles/energy/energy-storage-page.cfm

[189] M. N. Ozisik, *Heat Conduction*, 2nd ed. Hoboken, NJ, USA, John Wiley & Sons. Inc., 1993, ISBN: 0471532568

[190] Z. Gao, C. Chin, W. Woo, and J. Jia, Integrated Equivalent Circuit and Thermal Model for Simulation of Temperature-Dependent LiFePO4 Battery in Actual Embedded Application, *Energies,* vol. 10, p. 85, 2017. doi: 10.3390/en10010085

[191] D. Ren, X. Feng, L. Lu, M. Ouyang, S. Zheng, J. Li*, et al.*, An electrochemical-thermal coupled overcharge-to-thermal-runaway model for lithium ion battery, *Journal of Power Sources,* vol. 364, pp. 328-340, 2017. doi: 10.1016/j.jpowsour.2017.08.035

[192] R. Rizk, H. Louahlia, H. Gualous, and P. Schaetzel, Experimental analysis and transient thermal modelling of a high capacity prismatic lithium-ion battery, *International Communications in Heat and Mass Transfer,* vol. 94, pp. 115-125, 2018. doi: 10.1016/j.icheatmasstransfer.2018.03.018

[193] C. Qi, Y. Zhu, F. Gao, K. Yang, and Q. Jiao, Mathematical model for thermal behavior of lithium ion battery pack under overcharge, *International Journal of Heat and Mass Transfer,* vol. 124, pp. 552-563, 2018. doi: 10.1016/j.ijheatmasstransfer.2018.03.100

[194] J. Jaguemont, A. Nikolian, N. Omar, S. Goutam, J. Van Mierlo, and P. Van den Bossche, Development of a Two-Dimensional-Thermal Model of Three Battery Chemistries, *IEEE Transactions on Energy Conversion,* vol. 32, pp. 1447-1455, 2017. doi: 10.1109/TEC.2017.2697944

[195] Z. Wang, J. Ma, and L. Zhang, Finite Element Thermal Model and Simulation for a Cylindrical Li-Ion Battery, *IEEE Access,* vol. 5, pp. 15372-15379, 2017. doi: 10.1109/ACCESS.2017.2723436

[196] J. Jaguemont, L. Boulon, and Y. Dubé, Characterization and Modeling of a Hybrid-Electric-Vehicle Lithium-Ion Battery Pack at Low Temperatures, *IEEE Transactions on Vehicular Technology,* vol. 65, pp. 1-14, 2016. doi: 10.1109/TVT.2015.2391053

[197] R. Benger, H. Wenzl, H. P. Beck, M. Jiang, D. Ohms, and G. Schaedlich, Electrochemical and thermal modelimh of lithium-ion cells for use in HEV or EV application, in *EVS24*, Stavanger, Norway, 2009

[198] Y. Xiao, Model-Based Virtual Thermal Sensors for Lithium-Ion Battery in EV Applications, *IEEE Transactions on Industrial Electronics,* vol. 62, pp. 3112-3122, 2015. doi: 10.1109/TIE.2014.2386793

[199] H. E. Perez, X. Hu, S. Dey, and S. J. Moura, Optimal Charging of Li-Ion Batteries With Coupled Electro-Thermal-Aging Dynamics, *IEEE Transactions on Vehicular Technology,* vol. 66, pp. 7761-7770, 2017. doi: 10.1109/TVT.2017.2676044

[200] N. S. Spinner, R. Mazurick, A. Brandon, S. L. Rose-Pehrsson, and S. G. Tuttle, Analytical, Numerical and Experimental Determination of Thermophysical Properties of Commercial 18650 LiCoO2 Lithium-Ion Battery, *Journal of the Electrochemical Society,* vol. 162, pp. A2789-A2795, 2015. doi: 10.1149/2.0871514jes

[201] D. Werner, A. Loges, D. J. Becker, and T. Wetzel, Thermal conductivity of Li-ion batteries and their electrode configurations – A novel combination of modelling and experimental approach, *Journal of Power Sources,* vol. 364, pp. 72-83, 2017. doi: 10.1016/j.jpowsour.2017.07.105

[202] S. C. Chen, C. C. Wan, and Y. Y. Wang, Thermal analysis of lithium-ion batteries, *Journal of Power Sources,* vol. 140, pp. 111-124, 2005. doi: 10.1016/j.jpowsour.2004.05.064

[203] K. Shah, S. J. Drake, D. A. Wetz, J. K. Ostanek, S. P. Miller, J. M. Heinzel*, et al.*, Modeling of steady-state convective cooling of cylindrical Li-ion cells, *Journal of Power Sources,* vol. 258, pp. 374-381, 2014. doi: 10.1016/j.jpowsour.2014.01.115

[204] C. Lin, C. Cui, and X. Xu, Lithium-ion battery electro-thermal model and its application in the numerical simulation of short circuit experiment, in *2013 World Electric Vehicle Symposium and Exhibition (EVS27)*, Barcelona, Spain, 2013, doi: 10.1109/EVS.2013.6914959

[205] D. Worwood, Q. Kellner, M. Wojtala, W. D. Widanage, R. Mglen, D. Greenwood*, et al.*, A new approach to the internal thermal management of cylindrical battery cells for automotive applications, *Journal of Power Sources,* vol. 346, pp. 151-166, 2017. doi: 10.1016/j.jpowsour.2017.02.023

[206] M. Salameh, S. Wilke, B. Schweitzer, P. Sveum, S. Al-Hallaj, and M. Krishnamurthy, Thermal State of Charge Estimation in Phase Change Composites for Passively Cooled Lithium-Ion Battery Packs, *IEEE Transactions on Industry Applications,* vol. 54, pp. 426-436, 2018. doi: 10.1109/TIA.2017.2763588

[207] Energizer Holdings. *Battery Interconnections* [Online, Accessed on 21 Feb 2017]. Available: http://data.energizer.com/design_hints/catalog/designhints_interconnect.pdf

[208] D. Doerffel, PhD Thesis - Testing and characterisation of large high-energy lithium-ion batteries for electric and hybrid electric vehicles, School of Engineering Sciences, University of Southampton, Southampton, UK, 2007.

[209] Thermal Hazard Technology. (2018). *Contact us* [Online, Accessed on 19 Jun 2018]. Available: http://www.thermalhazardtechnology.com/contact-us

[210] T. Grandjean, A. Barai, E. Hosseinzadeh, Y. Guo, A. McGordon, and J. Marco, Large format lithium ion pouch cell full thermal characterisation for improved electric vehicle thermal management, *Journal of Power Sources,* vol. 359, pp. 215-225, 2017. doi: 10.1016/j.jpowsour.2017.05.016

[211] EnerSys. (2008). *Cyclon - Application Manual* [Online, Accessed on 9 Oct 2018]. Available: http://www.enersys-emea.com/reserve/pdf/EN-CYC-AM-007_1208.pdf

[212] Y. Parvini, J. B. Siegel, A. G. Stefanopoulou, and A. Vahidi, Supercapacitor Electrical and Thermal Modeling, Identification, and Validation for a Wide Range of Temperature and Power Applications, *IEEE Transactions on Industrial Electronics,* vol. 63, pp. 1574-1585, 2016. doi: 10.1109/TIE.2015.2494868

[213] J. Lee, J. Yi, D. Kim, C. Shin, K. S. Min, J. Choi*, et al.*, Modeling of the Electrical and Thermal Behaviors of an Ultracapacitor, *Energies,* vol. 7, 2014. doi: 10.3390/en7128264

[214] M. Al Sakka, H. Gualous, J. Van Mierlo, and H. Culcu, Thermal modeling and heat management of supercapacitor modules for vehicle applications, *Journal of Power Sources,* vol. 194, pp. 581-587, 2009. doi: 10.1016/j.jpowsour.2009.06.038

[215] T. S. Bryden, A. Holland, G. Hilton, B. Dimitrov, C. P. de León Albarrán, and A. Cruden, Lithium-ion degradation at varying discharge rates, *Energy Procedia,* vol. 151, pp. 194-198, 2018. doi: 10.1016/j.egypro.2018.09.047

[216] G. Hilton, M. Kiaee, T. Bryden, B. Dimitrov, A. Cruden, and A. Mortimer, A Stochastic Method for Prediction of the Power Demand at High Rate EV Chargers, *IEEE Transactions on Transportation Electrification,* vol. 4, pp. 744-756, 2018. doi: 10.1109/TTE.2018.2831003

[217] B. Dimitrov, A. Cruden, S. Sharkh, C. Ponce de León, T. Bryden, and G. Hilton, Design Process for a Parallel LLC Resonant Converter for Powered Electric Vehicle Charging Systems, *International Journal of Science and Research (IJSR),* vol. 6, pp. 2022-2028, 2017. doi: 10.21275/ART20172296

[218] G. Hilton, M. Kiaee, T. Bryden, A. Cruden, and A. Mortimer, The case for energy storage installations at high rate EV chargers to enable solar energy integration in the UK – An optimised approach, *Journal of Energy Storage,* vol. 21, pp. 435-444, 2019. doi: 10.1016/j.est.2018.12.012

[219] G. Hilton, T. Bryden, C. P. de Leon, and A. Cruden, Dynamic charging algorithm for energy storage devices at high rate EV chargers for integration of solar energy, *Energy Procedia,* vol. 151, pp. 2-6, 2018. doi: 10.1016/j.egypro.2018.09.018